



UNIVERSITÀ DEGLI STUDI DI SIENA
DIPARTIMENTO DI BIOTECNOLOGIE, CHIMICA E FARMACIA

DOTTORATO DI RICERCA IN
SCIENZE CHIMICHE E FARMACEUTICHE - CICLO XXXIII
COORDINATORE: **Prof. Maurizio Taddei**

**IDENTIFICATION AND DEVELOPMENT OF ACTIVE
PRINCIPLES FROM PLANT SOURCES**

SETTORE SCIENTIFICO-DISCIPLINARE: CHIM/08

DOTTORANDO:

Paolo Governa

TUTOR:

Prof. Fabrizio Manetti

ANNO ACCADEMICO: 2019/2020

TABLE OF CONTENTS

TABLE OF CONTENTS	i
ABSTRACT	1
CHAPTER 1. Introduction	3
1.1. The use of natural products as pharmaceutical tools.....	3
1.2. The concept of phytocomplex.....	4
1.3. The problem of pharmacokinetics.....	5
1.4. Aim of the study.....	6
1.5. References.....	7
PART 1	11
CHAPTER 2. Comparing the effects of <i>in vitro</i> simulated gastrointestinal digestion on isolated natural products and complex herbal extracts	12
2.1. Introduction.....	12
2.2. Materials and methods.....	13
2.2.1. Chemicals.....	13
2.2.2. Plant material and extraction.....	14
2.2.3. <i>In vitro</i> simulated gastrointestinal digestion.....	14
2.2.4. Chromatographic conditions.....	14
2.2.5. Statistical analysis.....	15
2.3. Results and discussion.....	15
2.3.1. Gastrointestinal stability of different classes of isolated phenolic compounds.....	15
2.3.2. Chemical characterization of the herbal extracts.....	17
2.3.3. The mixture of constituents in herbal extracts protects single compounds from <i>in vitro</i> simulated gastrointestinal digestion.....	20
2.4. Conclusions.....	23
2.5. References.....	24
CHAPTER 3. Stability and bioaccessibility of <i>Cannabis sativa</i> L. extracts under <i>in vitro</i> simulated gastrointestinal digestion	28

3.1. Introduction.....	28
3.2. Materials and methods	30
3.2.1. Chemicals	30
3.2.2. Plant material and extraction	30
3.2.3. <i>In vitro</i> simulated gastrointestinal digestion	31
3.2.4. Chromatographic conditions.....	31
3.2.5. Statistical analysis.....	32
3.3. Results and discussion	32
3.3.1. Quantification of cannabinoids	32
3.3.2. <i>In vitro</i> simulated gastrointestinal digestion and bioaccessibility	34
3.4. Conclusions.....	37
3.5. References.....	38
CHAPTER 4. Effect of <i>in vitro</i> simulated digestion on the anti-<i>Helicobacter pylori</i> activity of different propolis extracts.....	41
4.1. Introduction.....	41
4.2. Materials and methods	44
4.2.1. Sample preparation and chemical analysis	44
4.2.2. <i>In vitro</i> simulated gastric digestion	44
4.2.3. Anti-HP activity	45
4.2.4. Urease inhibition assay	45
4.2.5. Computational details	46
4.2.6. Statistical analysis.....	47
4.3. Results and discussion	47
4.3.1. Chemical analysis	47
4.3.2. Stability of propolis constituents under <i>in vitro</i> simulated gastric digestion.....	49
4.3.3. Anti-HP activity of DPE and its main constituents	50
4.3.4. Urease inhibition	51
4.4. Conclusions.....	53
4.5. References.....	54
CHAPTER 5. Effect of <i>in vitro</i> simulated digestion on the antioxidant activity of different <i>Camellia sinensis</i> (L.) Kuntze leaves extracts	63
5.1. Introduction.....	63

5.2. Materials and methods	64
5.2.1. Sample preparation and chemical analysis	64
5.2.2. <i>In vitro</i> simulated digestion	65
5.2.3. DPPH test.....	65
5.2.4. Cell culture.....	66
5.2.5. Evaluation of the antioxidant activity	66
5.2.6. Measurement of trans-epithelial electric resistance	66
5.2.7. DPPH-HPLC-DAD analysis	67
5.2.8. Statistical analysis.....	67
5.3. Results and discussion	67
5.3.1. Chemical analysis	67
5.3.2. Stability of tea constituents under <i>in vitro</i> simulated digestion	68
5.3.3. The antioxidant activity of teas is reduced by digestion.....	70
5.4. Conclusion	74
5.5. References.....	75
PART 2.....	80
CHAPTER 6. Exploiting the Caco-2 permeability model to study the bioavailability of complex mixtures of compounds.....	81
6.1. Introduction.....	81
6.2. Materials and methods	83
6.2.1. Computational details	83
6.2.2. Chemicals.....	84
6.2.3. Cell culture.....	84
6.2.4. Caco-2 permeability assay.....	85
6.2.5. Chromatographic conditions.....	86
6.2.6. Statistical analysis.....	87
6.3. Results and discussion	87
6.3.1. <i>In silico</i> selection and coupling of compounds	87
6.3.2. Caco-2 permeability assay.....	95
6.4. Conclusions.....	103
6.5. References.....	103

CHAPTER 7. Structure-based identification of P-glycoprotein inhibitors from natural sources	108
7.1. Introduction.....	108
7.2. Materials and methods	113
7.2.1. Computational details	113
7.2.1.1. Protein and ligands preparation.....	113
7.2.1.2. Molecular docking.....	114
7.2.1.3. 3D common pharmacophore generation.....	115
7.2.2. Statistical analysis.....	117
7.3. Results and discussion	117
7.3.1. Validation of the docking protocol.....	117
7.3.1.1. Redocking of zosuquidar.....	117
7.3.1.2. Docking of Validation set 1	119
7.3.1.3. Docking of Validation set 2 and 3D common pharmacophore generation	121
7.3.2. Virtual screening results	124
7.4. Conclusions.....	128
7.5. References.....	129
CHAPTER 8. Conclusions	134
ACKNOWLEDGEMENTS	136
APPENDIX I. List of publications	139
APPENDIX I. Conferences participation	142

ABSTRACT

Plants are the source of wide variety of molecules with potential therapeutic application. More than 80 percent of the world population still relies on traditional medicine systems, which are mostly based on herbal remedies. Furthermore, about 35 percent of the currently available medicines have been developed using natural products as a lead compound. One of the major limitations for the clinical use of natural products, both as isolated compounds and as complex herbal extracts, is represented by the limited knowledge of their pharmacokinetic properties. Indeed, several experimental models, including *in vivo*, cell-free and cell-based, together with *in silico* methods have been developed for the evaluation of pharmacokinetic parameters, such as gastrointestinal stability, intestinal absorption, and hepatic metabolism. However, these methods are barely applied to natural products, particularly to herbal extracts. The main difficulty in the study of pharmacokinetic parameters of herbal products originates from their complex nature: a herbal product, in fact, is composed of hundreds of molecules. As a consequence, the choice of a marker compound for pharmacokinetic studies is crucial but sometimes difficult. Moreover, the mixture of constituents in an herbal extract could potentially modulate the biological properties of single natural products. On this basis, extrapolation of pharmacokinetic parameters of herbal extracts by only relying on data acquired for single compounds could be a challenging issue.

Obtaining pharmacokinetic data on different natural products and herbal extracts is, hence, an urgent task. Particularly, ability to predict at least several of these parameters by using fast and cost-effective computational tools will be of great benefit to the pharmaceutical and food supplement research and industry.

In this study, we used a simple cell-free method to evaluate the effect of *in vitro* simulated gastrointestinal digestion on the stability, bioaccessibility, and biological effects of several natural products, belonging to different classes of polyphenols, and herbal extracts containing them. We also used the Caco-2 cell permeability assay to

evaluate the intestinal absorption of mixtures of compounds administered at the same time.

In most cases, we found that administration of herbal extracts protects its constituents from degradation induced by the digestive processes, while intestinal bioavailability is often reduced when using mixtures of compounds.

Moreover, an *in silico* virtual screening protocol based on molecular docking and pharmacophore modeling was used to identify new putative P-glycoprotein ligands from natural sources. The computational tool was first checked for its ability to discern between known P-gp binders and non-binders, and then used to prioritize compounds from commercial sources of natural compounds. Assays on selected compounds will provide full validation of the virtual screening approach.

The overall aim of this work is to enlarge the knowledge on pharmacokinetic parameters of natural products and herbal extracts to be used for setting up a computational model able to predict the pharmacokinetics parameters of complex mixtures of compounds.

CHAPTER 1

Introduction

1.1. The use of natural products as pharmaceutical tools

Natural products have been used in the traditional medicine systems for millennia. Indeed, traditional Chinese medicine has a history of over 3000 years [1], while ancient Egyptian left traces of natural products use in the Ebers Papyrus, dated 2900 BC [2,3]. In that times, a combination of prayers, magic practices and herbal extracts were used for treating diseases. It was during the Greek civilization, first, and during the Roman Empire, later, that divine intervention in medicine was refused and a new scientific approach to diseases and their management was developed [4]. This revolution opened the way for a more modern medicinal use of natural products.

Until the establishment of synthetic medicinal chemistry, crude plant extracts were the most important sources of therapeutic products. It was in 1816, with the isolation of morphine from *Papaver somniferum* L., that natural products started to be used as the basis for the development of more potent or selective drugs. Other natural products that deeply contributed to the history of drug discovery includes salicin, digitoxin, quinine and pilocarpine [5].

Although synthetic drug discovery contributed to overcome several intrinsic limit of the older plant-based medicine, the World Health Organization estimated that more than 80% of the world population still rely on traditional medicine systems [6]. Moreover, since less than 10% of the world's biodiversity has been investigated for the possible therapeutic application, natural products still represent an invaluable source of chemical entities, which are used for the discovery of novel drugs [3,5].

Currently, the use of herbal extracts and isolated natural products is emerging not only in the pharmaceutical field, but also in the food industry and in cosmetics, making natural products an interesting study topic not only for research purposes, but also from an economical point of view [7].

1.2. The concept of phytocomplex

Plant extracts contains a mixture of several constituents. The ensemble of this constituents is called “phytocomplex”. Not all the constituents of a phytocomplex can exert physiologic or therapeutic activities. Indeed, along with the active principles, a number of other inactive compounds are usually extracted. While these molecules do not have a biological effect themselves, they can modulate the effect of the active principles, by modifying their pharmacodynamics and pharmacokinetics [8].

The interaction between the constituents of a phytocomplex can positively or negatively affect the biological activity of the active principle. When the use of the phytocomplex leads to clinical advantages, i.e. it enhances the pharmacological profile of the active principle alone, herbal extracts are to be preferred, compared to isolated compounds [9]. This effect is sometimes defined as the “entourage effect” [10]. Different scenarios can explain this phenomenon, including synergism, increase of bioavailability, or mechanism of action involving more than one target simultaneously. Also, sometimes, natural products can be chemically instable when purified, while they are more stable in the phytocomplex. A well-known example of synergism is represented by ginkgolides from *Gingko biloba* L. leaves extract, which are platelet-activating factor antagonists. Their activity is strongly enhanced by the presence of ginkgoflavones [11]. An example of the multi-target enhancement of the biological activity is represented by *Matricaria recutita* L.: at the acidic pH of the stomach, matricine is converted to camazulen carboxylate, which inhibits cyclooxygenase 2. Flavonoids in the *M. recutita* extract also have anti-inflammatory activity, which potentiate the effect of camazulen carboxylate [12]. Moreover, bisabolol, another constituent of *M. recutita* extract, exerts gastroprotective activity by activating ATP-sensitive potassium channels and by lowering the degradation of reduced glutathione [13,14]. A similar example is represented by *Glycyrrhiza glabra* L., which exert anti-inflammatory activity through the inhibition of cyclooxygenase-2 and 5-lipoxygenase [15] but is also gastroprotective by increasing the levels of prostaglandin E2, through the inhibition of 15-hydroxyprostaglandin dehydrogenase and delta-13-prostaglandin reductase [16]. Finally, several examples exist of instable purified natural products,

which are instead stabilized by the phytocomplex, including *Valeriana officinalis* L. [17], *Humulus lupulus* L. [18], and *Hypericum perforatum* L. [19].

There are also cases in which a specific therapeutic condition can only be treated by using plant phytocomplexes, as synthetic monomolecular drugs do not exist yet for that particular indication. This is the case of herbal adaptogens, which are drugs able to preserve the homeostasis in response to fatigue and stress stimuli, through the modulation of the hypothalamic-pituitary-adrenal axis and of stress-related mediators, such as heat-shock proteins and mitogen-activated protein kinases [20]. Some examples of herbal drugs with adaptogenic activity include: *Rhodiola rosea* L., *Eleutherococcus senticosus* (Rupr. & Maxim.) Maxim., *Schisandra chinensis* (Turcz.) Baill., and *Panax ginseng* C.A.Mey. [21,22].

The phytocomplex not always positively affects the pharmacological profile of its constituents. Namdar defined this phenomenon as “parasitage effect”, which is the opposite of the entourage effect [23]. There are many examples in which the single natural compounds demonstrated to be more active than the whole phytocomplex, including the anticancer constituents of *Taxus brevifolia* Nutt., the central nervous system stimulants contained in *Camellia sinensis* (L.) Kuntze and *Coffea arabica* L., cocaine from *Erythroxylum coca* Lam., morphine from *Papaver somniferum* L., and the antimalaric constituents of *Artemisia annua* L.

1.3. The problem of pharmacokinetics

Even though their increasing popularity, the pharmaceutical applications of herbal products are limited by the shortage of clinical trials and by the inadequate knowledge of their pharmacokinetics [24]. Some medicinal plants are enlisted in the pharmacopoeia of different countries and in other official documents, such as the European Medicine Agency (EMA) and the World Health Organization monographs. In Europe, the herbal species which are enlisted in the EMA monographs as “well-established use” have been evaluated for their safety and clinical effectiveness, and information on their pharmacokinetics are adequate that they are authorized to be registered as drug [7]. However, among the vast amount of herbal species with potential therapeutic use, only a few are enlisted in these monographs, or have been

investigated for their pharmacokinetic properties. This is mainly due to the difficulties of evaluating the absorption, distribution, metabolism, and excretion (ADME) properties of mixture of compounds administered at one time.

It is known that natural compounds suffer from several pharmacokinetic issues, including poor solubility, metabolism in the gastrointestinal tract, effect of efflux mechanisms, and high first-pass metabolism [25]. In particular, polyphenols, one of the major class of natural compounds found in plants, are characterized by a largely variable bioavailability, which depend on their physico-chemical properties [26,27].

Today, a large number of experimental models is available for investigating the pharmacokinetic properties of a drug candidate [28,29]. ADME parameters can be deeply evaluated with the support of *in vivo* studies [28]. Moreover, together with the development of more efficient analytical techniques (i.e., HPLC, MS, NMR), *in vitro* and *in silico* systems are emerging tools to investigate the bioavailability of novel drug and to support and guide the identification of metabolites with an extremely accurate level of detail [30].

Although being largely utilized for single molecule studies, pharmacokinetic models are barely applied to more complex mixtures of molecules, such as herbal products, due to the necessity of choosing a small number of chemical markers [24]. Indeed, most pharmacokinetic principles of synthetic single molecule drugs are frequently applied to herbal products, even if this has not been validated through experimental studies [31].

1.4. Aim of the study

The main aim of this study was to acquire data on some parameter involved in the bioavailability of natural products, such as stability to gastrointestinal digestion, bioaccessibility, intestinal permeability and effect of efflux protein, evaluating the differences between isolated compounds and herbal products.

The part 1 of the thesis, is focused on the effect of *in vitro* simulated gastrointestinal digestion on the stability of selected polyphenols and herbal extracts containing them. Some practical examples of how digestive process can affect the

bioaccessibility and the biological activity of natural products of interest is also provided.

Part 2 is focused on bioavailability parameters, such as intestinal permeability and efflux mechanisms. In particular, the cell-based Caco-2 permeability model was used for evaluating the changes in intestinal permeability using isolated compounds and couples of molecules. Moreover, a computational protocol was set up for the evaluation of P-glycoprotein binders from natural sources, with the aim of discerning among possible substrates and inhibitors.

This work represents the first step of a broader project aimed at setting up an experimental model which, by combining *in vitro* cell-free and cell-based models to computational techniques, will be able to predict the ADME properties of complex mixture of molecules, focusing on natural products.

1.5. References

1. Gu, S.; Pei, J. Innovating Chinese Herbal Medicine: from traditional health practice to scientific drug discovery. *Front. Pharmacol.* **2017**, *8*, 381.
2. Lemonnier, N.; Zhou, G.-B.; Prasher, B.; Mukerji, M.; Chen, Z.; Brahmachari, S. K.; Noble, D.; Auffray, C.; Sagner, M. Traditional knowledge-based medicine: a review of history, principles, and relevance in the present context of p4 systems medicine. *Prog. Prev. Med.* **2017**, *2*.
3. Cragg, G. M.; Newman, D. J. Biodiversity: a continuing source of novel drug leads. *Pure Appl. Chem.* *77*, 7–24.
4. Tipton, C. M. The history of “exercise is medicine” in ancient civilizations. *Adv. Physiol. Educ.* **2014**, *38*, 109–117.
5. Dias, D. A.; Urban, S.; Roessner, U. A historical overview of natural products in drug discovery. *Metabolites* **2012**, *2*, 303–336.
6. World Health Organization. *WHO global report on traditional and complementary medicine*; 2019.

7. Biagi, M.; Pecorari, R.; Appendino, G.; Miraldi, E.; Magnano, A. R.; Governa, P.; Cettolin, G.; Giachetti, D. Herbal products in Italy: the thin line between phytotherapy, nutrition and parapharmaceuticals; a normative overview of the fastest growing market in Europe. *Pharmaceuticals* **2016**, *9*, E65.
8. Williamson, E. M. Synergy and other interactions in phytomedicines. *Phytomedicine* **2001**, *8*, 401–409.
9. Gilbert, B.; Alves, L. F. Synergy in plant medicines. *Curr. Med. Chem.* **2003**, *10*, 13–20.
10. Ribeiro, S. Whole organisms or pure compounds? entourage effect versus drug specificity. In *Plant medicines, healing and psychedelic science: cultural perspectives*; labate, B. C.; Cavnar, C., Eds.; Springer International Publishing: Cham, 2018; pp. 133–149.
11. European Medicine Agency. Assessment report on *Ginkgo biloba* L., folium https://www.ema.europa.eu/en/documents/herbal-report/final-assessment-report-ginkgo-biloba-l-folium_en.pdf.
12. European Medicine Agency. Assessment report on *Matricaria recutita* L. flos and *Matricaria recutita* L. aetheroleum http://www.ema.europa.eu/docs/en_GB/document_library/Herbal_-_HMPC_assessment_report/2014/07/WC500170079.pdf.
13. Moura Rocha, N. F.; Venâncio, E. T.; Moura, B. A.; Gomes Silva, M. I.; Aquino Neto, M. R.; Vasconcelos Rios, E. R.; de Sousa, D. P.; Mendes Vasconcelos, S. M.; de França Fonteles, M. M.; de Sousa, F. C. F. Gastroprotection of (-)-alpha-bisabolol on acute gastric mucosal lesions in mice: the possible involved pharmacological mechanisms. *Fundam. Clin. Pharmacol.* **2010**, *24*, 63–71.
14. Bezerra, S. B.; Leal, L. K. A. M.; Nogueira, N. A. P.; Campos, A. R. Bisabolol-induced gastroprotection against acute gastric lesions: role of prostaglandins, nitric oxide, and KATP+ channels. *J. Med. Food* **2009**, *12*, 1403–1406.
15. Chandrasekaran, C. V; Deepak, H. B.; Thiyagarajan, P.; Kathiresan, S.; Sangli, G. K.; Deepak, M.; Agarwal, A. Dual inhibitory effect of *Glycyrrhiza glabra* (GutGard™)

on COX and LOX products. *Phytomedicine* **2011**, *18*, 278–284.

16. Baker, M. E. Licorice and enzymes other than 11 beta-hydroxysteroid dehydrogenase: an evolutionary perspective. *Steroids* **1994**, *59*, 136–141.

17. European Medicine Agency. Assessment report on *Valeriana officinalis* L., radix and *Valeriana officinalis* L. aetheroleum https://www.ema.europa.eu/en/documents/herbal-report/final-assessment-report-valeriana-officinalis-l-radix-valeriana-officinalis-l-aetheroleum_en.pdf.

18. European Medicine Agency. Assessment report on *Humulus lupulus* L., flos https://www.ema.europa.eu/en/documents/herbal-report/final-assessment-report-humulus-lupulus-l-flos_en.pdf.

19. European Medicine Agency. Assessment report on *Hypericum perforatum* L., herba https://www.ema.europa.eu/en/documents/herbal-report/assessment-report-hypericum-perforatum-l-herba_en.pdf.

20. Panossian, A.; Wikman, G. Effects of Adaptogens on the central nervous system and the molecular mechanisms associated with their stress-protective activity. *Pharmaceuticals (Basel)*. **2010**, *3*, 188–224.

21. Borgonetti, V.; Governa, P.; Biagi, M.; Dalia, P.; Corsi, L. *Rhodiola rosea* L. modulates inflammatory processes in a CRH-activated BV2 cell model. *Phytomedicine* **2020**, *68*, 153143.

22. Panossian, A. G. Adaptogens: tonic herbs for fatigue and stress. *Altern. Complement. Ther.* **2003**, *9*, 327–331.

23. Namdar, D.; Anis, O.; Poulin, P.; Koltai, H. Chronological review and rational and future prospects of cannabis-based drug development. *Molecules* **2020**, *25*, 4821.

24. He, S.; Chan, E.; Zhou, S. ADME properties of herbal medicines in humans: evidence, challenges and strategies. *Curr. Pharm. Des.* **2011**, *17*, 357–407.

25. Mukherjee, P. K.; Harwansh, R. K.; Bhattacharyya, S. Bioavailability of herbal products: approach toward improved pharmacokinetics. In *Evidence-based validation of herbal medicine*; Mukherjee, P. K., Ed.; Elsevier: Boston, 2015; pp. 217–245.

-
26. Manach, C.; Williamson, G.; Morand, C.; Scalbert, A.; Rémésy, C. Bioavailability and bioefficacy of polyphenols in humans. I. Review of 97 bioavailability studies. *Am. J. Clin. Nutr.* **2005**, *81*, 230S-242S.
27. Manach, C.; Scalbert, A.; Morand, C.; Rémésy, C.; Jiménez, L. Polyphenols: food sources and bioavailability. *Am. J. Clin. Nutr.* **2004**, *79*, 727–747.
28. Pelkonen, O.; Turpeinen, M.; Raunio, H. *In vivo-in vitro-in silico* pharmacokinetic modelling in drug development - current status and future directions. *Clin. Pharmacokinet.* **2011**, *50*, 483–491.
29. Sager, J. E.; Yu, J.; Ragueneau-majlessi, I.; Isoherranen, N. Physiologically based pharmacokinetic (PBPK) modeling and simulation approaches: a systematic review of published models, applications, and model verification. *Drug Metab. Dispos.* **2015**, *43*, 1823–1837.
30. Kirchmair, J.; Göller, A. H.; Lang, D.; Kunze, J.; Testa, B.; Wilson, I. D.; Glen, R. C.; Schneider, G. Predicting drug metabolism: experiment and/or computation? *Nat. Rev. Drug Discov.* **2015**, *14*, 387–404.
31. Kirchmair, J.; Williamson, M. J.; Tyzack, J. D.; Tan, L.; Bond, P. J.; Bender, A.; Glen, R. C. Computational prediction of metabolism: sites, products, SAR, P450 enzyme dynamics, and mechanisms. **2012**, *52*, 617-648.

PART 1

CHAPTER 2

Comparing the effects of *in vitro* simulated gastrointestinal digestion on isolated natural products and complex herbal extracts

2.1. Introduction

To exert their nutritional and/or pharmacological effect, orally administered natural products have to overcome the possible degradation occurring during gastrointestinal digestion and to be absorbed by the intestine. The bioavailability differs critically from one polyphenol to another [1]. Several factors, including polarity, molecular weight, different association with the plant matrix, and the effect of transport protein, can influence their bioavailability. Particularly, structural changes of natural compounds during digestion can lead to the maintenance or modification of their biological activity, by influencing their bioavailability [2].

The experimental evaluation of natural products digestion can be achieved using different models. Human and animal studies are expensive and limited by ethical issues, thus, *in vitro* and *in silico* methods are emerging [3]. In particular, cell-free methods can be used for simulating gastrointestinal digestion [4], while cell-based methods are more useful to evaluate the intestinal absorption [5].

Several models have been developed for simulating gastrointestinal digestion *in vitro*, and they can be classified into two main categories: static and dynamic models. Static models define fixed parameters, such (pH, temperature, and the period of time) to independently simulate the oral, gastric and intestinal environment. They are generally simpler and are useful for screening of several samples. Differently, dynamic models take into account the continuous changes of the physicochemical conditions and include mechanical simulation of peristaltic forces [3]. These are more complex models, which are less likely to be used for evaluating large number of samples but can provide experimental conditions more similar to physiological conditions, which

better resemble *in vivo* digestion. Moreover, they are usually automated and paired with computational management of different digestive phases [6,7].

These methods have been successfully used for the analysis of the stability to digestion and bioaccessibility of plant extracts, particularly in the field of food science. Nevertheless, when developing novel drugs from natural sources, information about the bioavailability of the active principle is often derived from data obtained using a single molecule. If the active principle consists of a complex mixture of molecules, such as in the case of herbal extracts, translation of the data obtained on single molecules are not always straightforward. Indeed, the presence of other constituents in the extract can alter the digestion process of the active principle, leading to increased or reduced stability, thus, influencing the final bioavailability.

In this work, we set up a simple method for the analysis of the stability to *in vitro* simulated gastrointestinal digestion of 10 natural compounds, belonging to different classes of polyphenols. We focused on these classes of compounds because they are among the most studied natural products, being the chemical marker of several medicinal plants, and have been reported to possess controversial bioavailability [8]. The same method was also applied to different herbal products containing mixtures of selected phenolic constituents from the previous 10 compounds, to verify whether the compound stability may differ in complex mixtures.

2.2. Materials and methods

2.2.1. Chemicals

All solvents used in this work were purchased from Sigma-Aldrich (Milan, Italy). Apigenin, apigenin-7-glucoside, chlorogenic acid, bisdemethoxycurcumin (BMC), curcumin (CUR), demethoxycurcumin (DMC), resveratrol and resveratrol-3-O-glucoside were purchased from Sigma-Aldrich. Cyanidin chloride and cyanidin-3-O-glucoside were purchased from Extrasynthese (Genay, France). NaCl, pepsin from porcine gastric mucosa, pancreatin from porcine pancreas, and bile salts mixture were

purchased from Sigma Aldrich. Na₂CO₃ was purchased from Sodalco S.p.A. (Corsico, Italy).

2.2.2. Plant material and extraction

Curcuma longa L. dried rhizomes, *Matricaria recutita* L. flowers, and *Cynara scolimus* L. leaves were purchased from Erbamea (San Giustino, Perugia, Italy). Powdered *C. longa* rhizomes were extracted in methanol. Comminuted *M. recutita* flowers were extracted for 24 h using 70% v/v ethanol, 70% v/v methanol and pure methanol, with a 1:6 drug-extract ratio (DER). Comminuted *C. scolimus* leaves were extracted for 24 h using 80% v/v methanol and double distilled water (ddH₂O), with a 1:6 DER.

2.2.3. In vitro simulated gastrointestinal digestion

In vitro simulated digestion was carried out as previously described [3], with slight modifications. Briefly, extracts and reference standards were suspended in 20 mL simulated gastric juice that contained pepsin from porcine gastric mucosa (300 UI/mL) and NaCl (10 mg/mL), obtaining a final 1:20 dilution for the extracts and a concentration of 1 mg/mL for the reference standards. The pH of the solution was adjusted to 1.7 using HCl. Samples were incubated for 2 h at 37 °C with shaking. Then, pancreatin from porcine pancreas (10 mg/mL) and bile salts mixture (20 mg/mL) were added and the pH was increased by adding Na₂CO₃ (15 mg/mL) to simulate the intestinal environment. Intestinal digestion was carried out for 2 h at 37 °C with shaking. Samples were then centrifuged, filtered and immediately used for further analysis.

2.2.4. Chromatographic conditions

Samples (10 µL) were injected into a HPLC-DAD system, consisting of a Shimadzu Prominence LC 2030 3D instrument, equipped with a Bondpak® C18 column (10 µm, 125 Å, 3.9 mm, Waters Corporation, Milford, MA). The mobile phase consisted of ddH₂O + 0.1% v/v formic acid (A) and acetonitrile + 0.1% v/v formic acid (B). The following method was applied: B from 10% at 0 min to 25% at 15 min and

then from 25% to 35% at 18 min and from 35% to 50% at 25 min. Flow rate was set to 0.8 mL/min and column temperature to 28 °C. Chromatograms were recorded at 320 nm for resveratrol and resveratrol-3-O-glucoside, 330 nm for chlorogenic acid, 366 nm for apigenin and apigenin-7-glucoside, and 520 nm for cyanidin and cyanidin-3-O-glucoside. A different method was used for *C. longa* and curcuminoids [9]: A from 50% at 0 min to 45% at 8 min, then isocratic until 10 min. Flow rate was set to 0.9 mL/min and column temperature to 28 °C. Calibration curves were set up using reference standards at concentration ranging from 0.008 to 0.500 mg/mL, with correlation coefficients (R^2) > 0.99.

2.2.5. Statistical analysis

The statistical differences between the results were determined by the analysis of the variance (ANOVA) or by using the Student's t-test. Values are expressed in the range of +/- standard deviation and $p < 0.05$ was considered statistically significant. Graphs and calculations were performed using GraphPad Prism.

2.3. Results and discussion

2.3.1. Gastrointestinal stability of different classes of isolated phenolic compounds

The analyzed phenolic compounds were found to be differently affected by *in vitro* simulated gastrointestinal digestion. Indeed, stilbenes and flavones showed higher stability, compared to the other classes of polyphenols, with anthocyanins being the less stable (table 2.1).

Simulated gastric digestion has been reported to have little effect on flavones recovery, which is, however, deeply affected by intestinal digestion [10]. Interestingly, we observed that glycosylation doubled the stability of apigenin to gastrointestinal digestion, thus suggesting a protective role of the sugar moiety. This result is similar to the increased recovery of quercetin-3-glucoside, compared to quercetin, observed by

Boyer and co-workers [11] and is consistent with the higher bioavailability of glycosides, compared to that of aglycones, observed in humans [12–14].

Table 2.1. relative gastrointestinal stability of reference standards. Values (%) are expressed as mean \pm standard deviation.

Chemical classification	Sample	Gastrointestinal stability
Flavones	apigenin	21.80 \pm 10.54
	apigenin-7-glucoside	43.95 \pm 5.67
Caffeoylquinic derivarives	chlorogenic acid	1.48 \pm 0.86
Anthocyanins	cyanidin chloride	< 0.10
	cyanidin-3-O-glucoside	2.48 \pm 1.28
Curcuminoids	BMC	17.50 \pm 6.43
	CUR	0.25 \pm 0.09
	DMC	0.90 \pm 0.33
Stilbenes	resveratrol	26.98 \pm 0.13
	resveratrol-3-O-glucoside	59.88 \pm 13.26

Caffeoylquinic acids, such as chlorogenic acid, are known to be instable in aqueous solution [15], especially at non-acidic pH. The degradation of chlorogenic acid after simulated digestion is consistent with previously published studies [16,17] and may be due to the precipitation of insoluble bile salts complex.

The very low recovery of anthocyanins after simulated digestion has been already reported in the past, using raspberry [18], pomegranate [19], and strawberry [20] extracts, as well as red wine [21]. Indeed, in aqueous solutions, antocyanins exist in a dynamic equilibrium between a variety of different molecular forms. These forms are highly unstable to oxygen, temperature, light, enzymes and, particularly pH changes. Although being mostly stable at low pH, such as in the stomach, the increase

of pH in the intestine causes the conversion of the red flavylum cation to the blue quinonoidal structure, through a rapid loss of proton, or to the colorless hemiketal form, through a slower hydration process. This last form can further tautomerize to generate the *cis*- and *trans* chalcones. Moreover, anthocyanins can bind to components of the pancreatine/bile salts mixtures, generating insoluble complexes [18]. Thus, digestive processes have a huge impact on the bioavailability of anthocyanins. In a similar way to flavones, glycosylation increased the recovery of cyanidin.

Due to its high lipophilicity, CUR is not soluble in water, thus, its recovery in simulated gastrointestinal fluids was very low. This is consistent with the work of Ubeyitogullari, who reported the bioaccessibility of crude CUR, physically mixed with empty nanoporous starch aerogels, to be 0.4% [22]. Similar results were also obtained by Park, who studied nanostructured lipid carrier to improve the bioaccessibility of CUR [23]. Intriguingly, even if CUR represents the most abundant curcuminoid in turmeric, demethoxylated forms have been reported to have a better intestinal absorption in humans, compared to CUR [24].

Stilbenes were found to be the most stable group tested. Also in this case, glycosilation caused a marked increase in the stability of resveratrol to simulated *in vitro* digestion, suggesting that the hydroxyl groups of resveratrol can undergo metabolic conversion during digestion. This was confirmed by Hu, who synthesized resveratrol esters with caprylic acid, to improve its stability during simulated gastrointestinal digestion [25].

2.3.2. Chemical characterization of the herbal extracts

Based on these results, we decided to repeat the experiments by using herbal extracts containing selected constituents from table 2.1. In particular, we selected constituents belonging to the classes of flavones, caffeoylquinic derivatives and curcuminoids. We decided to exclude stilbenes as they resulted the most stable among the tested compounds and anthocyanins as their gastrointestinal stability as single constituents, as well as herbal extracts, is already detailed in literature.

The HPLC-DAD chromatograms of *M. recutita*, *C. scolimus*, and *C. longa* extracts are shown in figure 2.1.

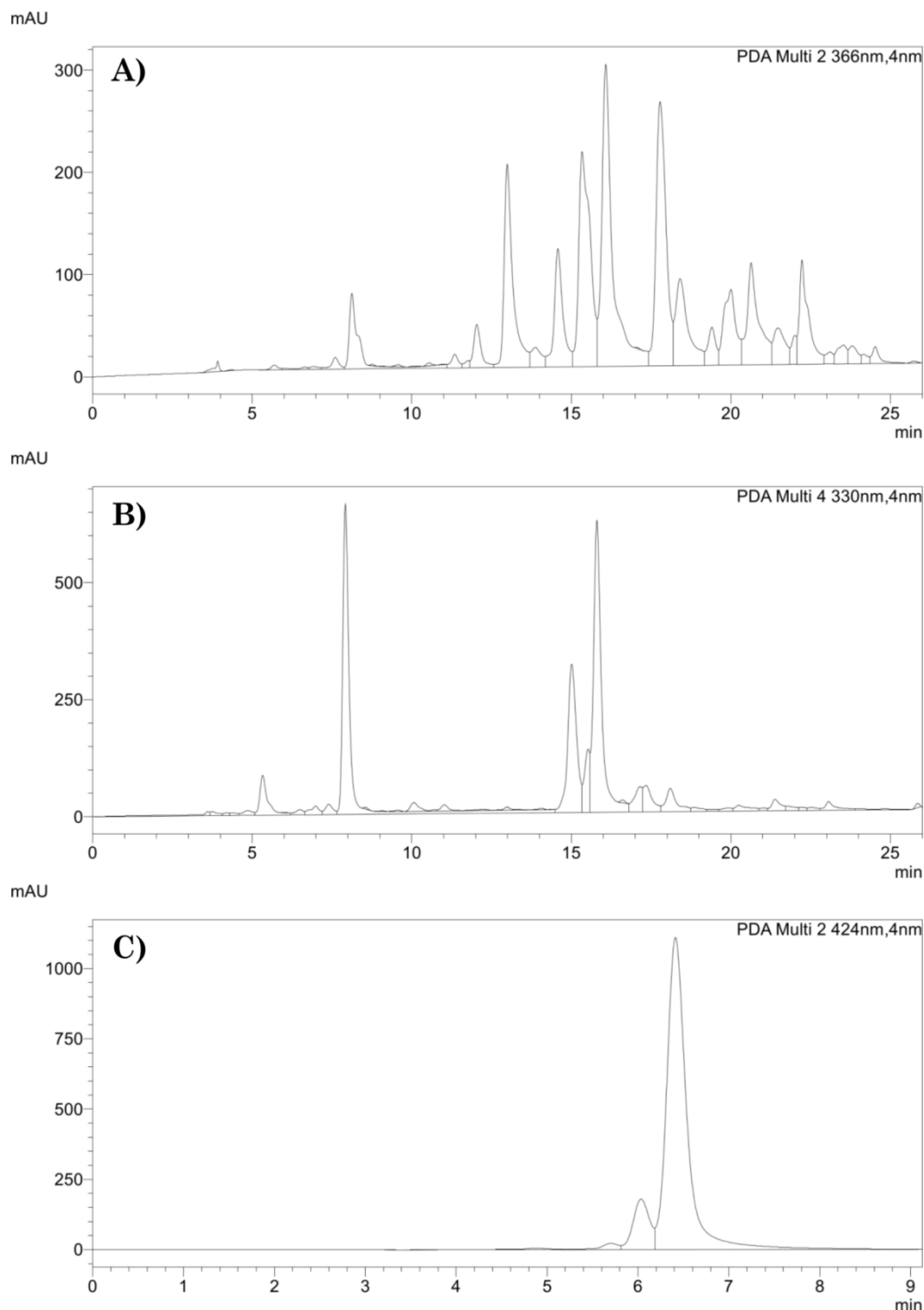


Figure 2.1. HPLC-DAD chromatograms of the selected herbal extracts. (A) *M. recutita*, recorded at 366 nm. Apigenin-7-glucoside RT = 17.8 min; apigenin RT = 23.8 min. (B) *C. scolimus*, recorded at 330 nm. Chlorogenic acid RT = 7.9 min. (C) *C. longa*, recorded at 424 nm. BMC RT = 5.7 min; DMC RT = 6.0 min; CUR RT = 6.4 min.

M. recutita flowers were used as a source of apigenin and apigenin-7-glucoside [26]. We used three different solvents to maximize the flavones extraction. The chemical characterization of each extract is reported in table 2.2. Consistently with the work by Haghi, we obtained higher amount of apigenin and apigenin-7-glucoside in the 70% v/v ethanol extract, with apigenin-7-glucoside being more abundant than apigenin [27]. Thus, we chose this extract to perform the digestion experiments.

Table 2.2. Chemical characterization of *M. recutita* extracts.

Sample	Extraction method	Main constituents (%)	
		apigenin	apigenin-7-glucoside
<i>M. recutita</i> flowers	70% v/v ethanol	1.06 ± 0.28	8.11 ± 0.35
	70% v/v methanol	0.81 ± 0.17	7.87 ± 0.22
	methanol	0.57 ± 0.23	5.50 ± 0.31

Artichoke leave extracts are usually standardized for their content in caffeoylquinic acids, expressed as chlorogenic acid. Song reported that methanol has the highest extraction efficiency on polyphenols and chlorogenic acid, compared to ethanol or water [28]. Indeed, we confirmed that 80% v/v methanol is much more effective in extracting chlorogenic acid, compared to ddH₂O (table 2.3), hence, we performed *in vitro* simulated digestion experiments on the 80% v/v methanol extract.

Table 2.3. Chemical characterization of *C. scolimus* extracts.

Sample	Extraction method	Chlorogenic acid (%)
<i>C. scolimus</i> leaves	80% v/v methanol	5.04 ± 0.21
	ddH ₂ O	<0.1

Finally, a *C. longa* rhizome extract containing 48.07% total curcuminoids was obtained using methanol as a solvent. CUR was the most abundant constituent, representing 67.63% of total curcuminoids, followed by DMC and BMC, representing

22.95% and 9.42% of total curcuminoids, respectively (table 2.4). This phytochemical profile is coherent with that of commonly available *C. longa* extract.

Table 2.4. Chemical characterization of *C. longa* extract.

Sample	Extraction method	Main constituents (%)		
		BMC	CUR	DMC
<i>C. longa</i> rhizomes	Methanol	4.53 ± 0.54	32.51 ± 0.32	11.03 ± 0.28

2.3.3. The mixture of constituents in herbal extracts protects single compounds from in vitro simulated gastrointestinal digestion

The effect of food matrix on the stability of food constituents has been widely studied [29]. A plethora of examples can be found in literature regarding the effects of food matrix on polyphenols digestion and bioaccessibility [17,20,30–32]. Herbal extracts contain a mixture of several constituents, which can influence the bioavailability of each other. One of the mechanisms by which this may occur is the modulation of the stability to gastrointestinal digestion. In the examples reported in this chapter, it is evident that the gastrointestinal stability of single constituents is different when they are used as isolated compounds, compared to their stability when they are enclosed in the complex mixture of the herbal extract. Indeed, figure 2.2 shows that both apigenin and apigenin-7-glucoside recovery after simulated digestion are significantly increased (+68% and +120%, respectively), compared to the reference standards alone.

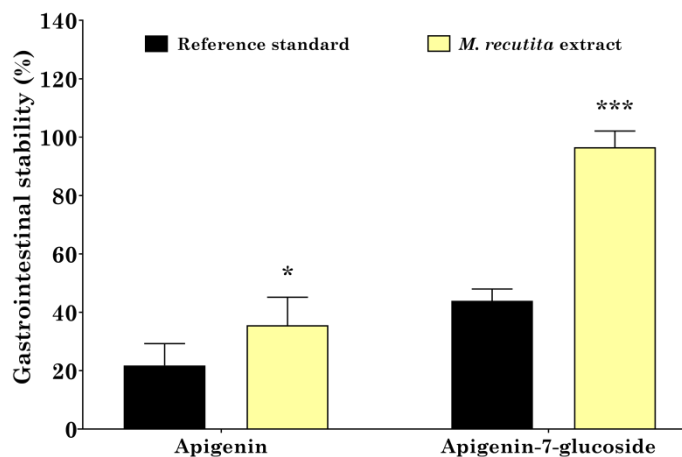


Figure 2.2. Stability of *M. recutita* flavones after *in vitro* simulated gastrointestinal digestion. * $p < 0.05$ vs reference standard; * $p < 0.001$ vs reference standard, two-way ANOVA followed by Tuckey's post-hoc.**

Noticeably, also in the case of *M. recutita* extract, glycosylation improved the stability of apigenin. Indeed, apigenin-7-glucoside was completely recovered, suggesting that other constituents of the extract may act by protecting this compound from degradation during digestion.

Similarly, chlorogenic acid stability upon simulated digestion was significantly affected by *C. scolymus* phytocomplex. Indeed, its recovery increased from 1.48%, using the reference standard alone, to 55.08%, when using the herbal extract (figure 2.3).

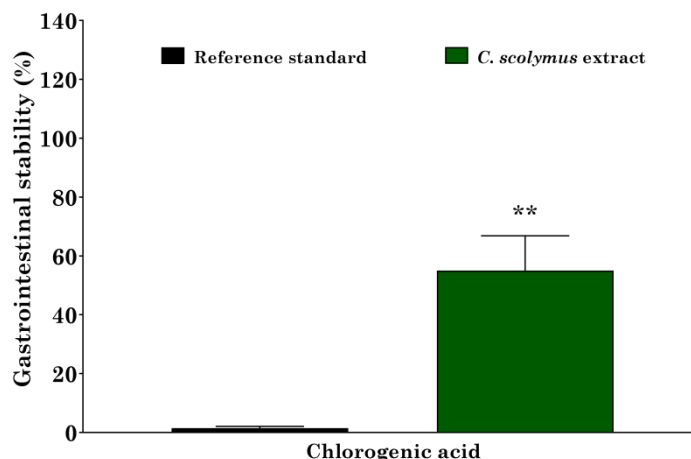


Figure 2.3. Stability of chlorogenic acid in *C. scolymus* extract after *in vitro* simulated gastrointestinal digestion. ** $p < 0.01$ vs reference standard, paired t test.

In 2015, D’Antuono and colleagues investigated the *in vitro* bioaccessibility, intestinal uptake and bioavailability of *Cynara cardunculus* (L.) subsp. *scolymus* Hayek polyphenols. Consistently with our results, they observed a much higher stability of chlorogenic acid in the herbal extract, compared to the reference standard, after simulated gastrointestinal digestion [33]. One possible explanation for this marked difference may be related to the ability of artichoke extracts to inhibit digestive enzymes [34].

Regarding curcuminoids, CUR stability to gastrointestinal digestion remained very low when using the herbal extract, even if a not statistically significant increase from 0.25% to 3.79% was observed. A much more evident effect was observed for DMC, whose stability increased from 0.90% when tested as single compound to 17.79% when in herbal matrix, and for BMC from 17.5% when tested as single compound to 104.78% in turmeric extract (figure 2.4).

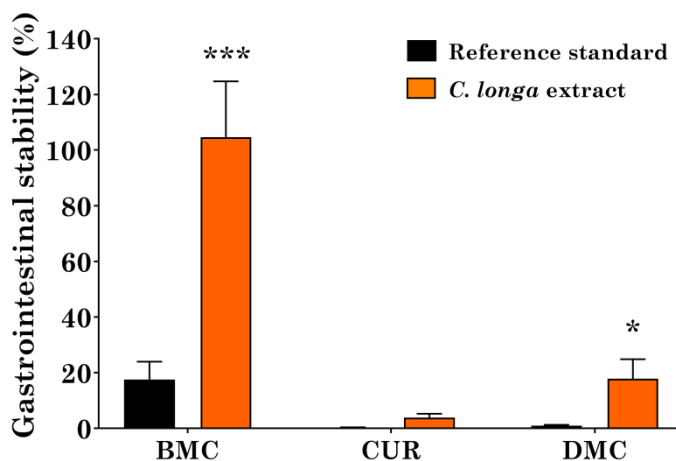


Figure 2.4. Stability of *C. longa* curcuminoids after *in vitro* simulated gastrointestinal digestion. * $p < 0.05$ vs reference standard; * $p < 0.001$ vs reference standard, two-way ANOVA followed by Tuckey's post-hoc.**

Despite being present in lower concentration in the extract, BMC can potentially reach the intestine at a concentration three-fold higher than that of CUR and DMC, which partially explains the higher bioavailability of BMC observed in humans, compared to CUR [24].

2.4. Conclusions

Oral bioavailability is one of the main factors that limit the clinical use of natural products. To reach the site of absorption, an orally-administered drug has to overcome the digestion process without being extensively metabolized. In this work we evaluated the effect of *in vitro* simulated gastrointestinal digestion on different classes of polyphenols. Moreover, we investigated the changes in the gastrointestinal stability of these compounds when used as a complex mixture of molecules, such as in the case of herbal extracts. Using *M. recutita*, *C. scolymus*, and *C. longa* as simple examples, we found that the phytocomplex significantly influenced the recovery of single constituents. In particular, we found a protective role of the phytocomplex, resulting in higher stability of the compounds to the digestive process. There might also be cases in which the phytocomplex may reduce, or leave unaltered, the stability of single constituents. These results provide evidence that it is extremely important to take into

account the effect of gastrointestinal digestion when evaluating the biological effectiveness of an herbal extract, as this cannot be extrapolated from data obtained using single compounds.

2.5. References

1. Manach, C.; Williamson, G.; Morand, C.; Scalbert, A.; Rémésy, C. Bioavailability and bioefficacy of polyphenols in humans. I. Review of 97 bioavailability studies. *Am. J. Clin. Nutr.* **2005**, *81*, 230S-242S.
2. Wojtunik-Kulesza, K.; Oniszczyk, A.; Oniszczyk, T.; Combrzyński, M.; Nowakowska, D.; Matwijczuk, A. Influence of *in vitro* digestion on composition, bioaccessibility and antioxidant activity of food polyphenols - a non-systematic review. *Nutrients* **2020**, *12*, 1401.
3. Alminger, M.; Aura, A. M.; Bohn, T.; Dufour, C.; El, S. N.; Gomes, A.; Karakaya, S.; Martínez-Cuesta, M. C.; McDougall, G. J.; Requena, T.; Santos, C. N. *In vitro* models for studying secondary plant metabolite digestion and bioaccessibility. *Compr. Rev. Food Sci. Food Saf.* **2014**, *13*, 413–436.
4. Stewart, R. J. C.; Morton, H.; Coad, J.; Pedley, K. C. *In vitro* digestion for assessing micronutrient bioavailability: the importance of digestion duration. *Int. J. Food Sci. Nutr.* **2019**, *70*, 71–77.
5. Hubatsch, I.; Ragnarsson, E. G. E.; Artursson, P. Determination of drug permeability and prediction of drug absorption in Caco-2 monolayers. *Nat. Protoc.* **2007**, *2*, 2111–2119.
6. Kong, F.; Singh, R. P. A human gastric simulator (HGS) to study food digestion in human stomach. *J. Food Sci.* **2010**, *75*, E627-35.
7. Minekus, M.; Marteau, P.; Havenaar, R.; Veld, J. H. J. H. in't A multicompartmental dynamic computer-controlled model simulating the stomach and small intestine. *Altern. to Lab. Anim.* **1995**, *23*, 197–209.

8. Manach, C.; Scalbert, A.; Morand, C.; Rémésy, C.; Jiménez, L. Polyphenols: food sources and bioavailability. *Am. J. Clin. Nutr.* **2004**, *79*, 727–747.
9. Governa, P.; Marchi, M.; Cocetta, V.; Leo, B. De; Saunders, P. T. K.; Catanzaro, D.; Miraldi, E.; Montopoli, M.; Biagi, M. Effects of *Boswellia serrata* Roxb. and *Curcuma longa* L. in an *in vitro* intestinal inflammation model using immune cells and Caco-2. *Pharmaceuticals* **2018**, *11*, 126.
10. Vallejo, F.; Gil-Izquierdo, A.; Pérez-Vicente, A.; García-Viguera, C. In Vitro Gastrointestinal Digestion Study of broccoli inflorescence phenolic compounds, glucosinolates, and vitamin C. *J. Agric. Food Chem.* **2004**, *52*, 135–138.
11. Boyer, J.; Brown, D.; Liu, R. H. *In vitro* digestion and lactase treatment influence uptake of quercetin and quercetin glucoside by the Caco-2 cell monolayer. *Nutr. J.* **2005**, *4*, 1.
12. Ross, J. A.; Kasum, C. M. Dietary flavonoids: bioavailability, metabolic effects, and safety. *Annu. Rev. Nutr.* **2002**, *22*, 19–34.
13. Hollman, P. C.; Katan, M. B. Dietary flavonoids: intake, health effects and bioavailability. *Food Chem. Toxicol.* **1999**, *37*, 937–942.
14. Hollman, P. C.; Katan, M. B. Absorption, metabolism and health effects of dietary flavonoids in man. *Biomed. Pharmacother.* **1997**, *51*, 305–310.
15. Clifford, M. N. Chlorogenic acids and other cinnamates - nature, occurrence and dietary burden. *J. Sci. Food Agric.* **1999**, *79*, 362–372.
16. Liu, G.; Ying, D.; Guo, B.; Cheng, L. J.; May, B.; Bird, T.; Sanguansri, L.; Cao, Y.; Augustin, M. Extrusion of apple pomace increases antioxidant activity upon *in vitro* digestion. *Food Funct.* **2019**, *10*, 951–963.
17. Kamiloglu, S.; Ozkan, G.; Isik, H.; Horoz, O.; Van Camp, J.; Capanoglu, E. Black carrot pomace as a source of polyphenols for enhancing the nutritional value of cake: an *in vitro* digestion study with a standardized static model. *LWT* **2017**, *77*, 475–481.
18. McDougall, G. J.; Dobson, P.; Smith, P.; Blake, A.; Stewart, D. Assessing potential bioavailability of raspberry anthocyanins using an *in vitro* digestion system. *J. Agric.*

Food Chem. **2005**, *53*, 5896–5904.

19. Pérez-Vicente, A.; Gil-Izquierdo, A.; García-Viguera, C. *In vitro* gastrointestinal digestion study of pomegranate juice phenolic compounds, anthocyanins, and vitamin C. *J. Agric. Food Chem.* **2002**, *50*, 2308–2312.

20. Gil-Izquierdo, A.; Zafrilla, P.; Tomás-Barberán, F. A. An *in vitro* method to simulate phenolic compound release from the food matrix in the gastrointestinal tract. *Eur. Food Res. Technol.* **2002**, *214*, 155–159.

21. McDougall, G. J.; Fyffe, S.; Dobson, P.; Stewart, D. Anthocyanins from red wine - their stability under simulated gastrointestinal digestion. *Phytochemistry* **2005**, *66*, 2540–2548.

22. Ubeyitogullari, A.; Ciftci, O. N. A novel and green nanoparticle formation approach to forming low-crystallinity curcumin nanoparticles to improve curcumin's bioaccessibility. *Sci. Rep.* **2019**, *9*, 19112.

23. Park, S. J.; Garcia, C. V.; Shin, G. H.; Kim, J. T. Improvement of curcuminoid bioaccessibility from turmeric by a nanostructured lipid carrier system. *Food Chem.* **2018**, *251*, 51–57.

24. Cuomo, J.; Appendino, G.; Dern, A. S.; Schneider, E.; McKinnon, T. P.; Brown, M. J.; Togni, S.; Dixon, B. M. Comparative absorption of a standardized curcuminoid mixture and its lecithin formulation. *J. Nat. Prod.* **2011**, *74*, 664–669.

25. Hu, X.-P.; Yin, F.-W.; Zhou, D.-Y.; Xie, H.-K.; Zhu, B.-W.; Ma, X.-C.; Tian, X.-G.; Wang, C.; Shahidi, F. Stability of resveratrol esters with caprylic acid during simulated *in vitro* gastrointestinal digestion. *Food Chem.* **2019**, *276*, 675–679.

26. European Medicine Agency. Assessment report on *Matricaria recutita* L. flos and *Matricaria recutita* L. aetheroleum
http://www.ema.europa.eu/docs/en_GB/document_library/Herbal_-_HMPC_assessment_report/2014/07/WC500170079.pdf.

27. Haghi, G.; Hatami, A.; Safaei, A.; Mehran, M. Analysis of phenolic compounds in *Matricaria chamomilla* and its extracts by UPLC-UV. *Res. Pharm. Sci.* **2014**, *9*, 31–37.

28. Shuhui Song; Hongju He; Xiaowei Tang; Wenqi Wang Determination of polyphenols and chlorogenic acid in artichoke (*Cynara scolymus* L.). In *Acta horticulturae*; International Society for Horticultural Science (ISHS), Leuven, Belgium, 2010; pp. 167–172.
29. Wojtunik-Kulesza, K.; Oniszczyk, A.; Oniszczyk, T.; Combrzyński, M.; Nowakowska, D.; Matwijczuk, A. Influence of *in vitro* digestion on composition, bioaccessibility and antioxidant activity of food polyphenols - a non-systematic review. *Nutrients* **2020**, *12*, 1401.
30. Tarko, T.; Duda-Chodak, A. Influence of food matrix on the bioaccessibility of fruit polyphenolic compounds. *J. Agric. Food Chem.* **2020**, *68*, 1315–1325.
31. Pineda-Vadillo, C.; Nau, F.; Dubiard, C. G.; Cheynier, V.; Meudec, E.; Sanz-Buenhombre, M.; Guadarrama, A.; Tóth, T.; Csavajda, É.; Hingyi, H.; Karakaya, S.; Sibakov, J.; Capozzi, F.; Bordoni, A.; Dupont, D. *In vitro* digestion of dairy and egg products enriched with grape extracts: effect of the food matrix on polyphenol bioaccessibility and antioxidant activity. *Food Res. Int.* **2016**, *88*, 284–292.
32. Mandalari, G.; Vardakou, M.; Faulks, R.; Bisignano, C.; Martorana, M.; Smeriglio, A.; Trombetta, D. Food matrix effects of polyphenol bioaccessibility from almond skin during simulated human digestion. *Nutrients* **2016**, *8*, 568.
33. D'Antuono, I.; Garbetta, A.; Linsalata, V.; Minervini, F.; Cardinali, A. Polyphenols from artichoke heads (*Cynara cardunculus* (L.) subsp. *scolymus* Hayek): *in vitro* bioaccessibility, intestinal uptake and bioavailability. *Food Funct.* **2015**, *6*, 1268–1277.
34. Mahboubi, M. *Cynara scolymus* (artichoke) and its efficacy in management of obesity. *Bull. Fac. Pharmacy, Cairo Univ.* **2018**, *56*, 115–120.

CHAPTER 3

Stability and bioaccessibility of *Cannabis sativa* L. extracts under *in vitro* simulated gastrointestinal digestion

3.1. Introduction

Cannabis sativa L. (Cannabaceae) has been used since ancient times as a medicinal tool and as a source of textile fiber and, more recently, as a psychoactive drug for recreational uses [1,2]. Thanks to the discovery of the endocannabinoid system as a regulator of several physiologic functions, *C. sativa* is attracting the interest of the pharmaceutical industry, because of the intriguing therapeutic potential of its constituents [3].

Indeed, a wide variety of molecules are produced by *C. sativa*, the more characteristic being represented by a class of terpenophenolic compounds, known as cannabinoids [4]. Among the over 400 compounds found in *C. sativa* [5], more than 90 different cannabinoids, including their breakdown products, have been reported [6]. Two other main classes of constituents, terpenes and flavonoids, are present in the *C. sativa* phytocomplex, even if their pharmacological role is still under evaluation [5].

Cannabinoids in *C. sativa* are typically present as acidic precursors [5]. However, their decarboxylated derivatives are responsible for the most therapeutic effects, thus, several decarboxylation methods have been proposed [7].

Δ^9 -tetrahydrocannabinol (THC) is the major psychotropic constituent of *C. sativa*. It is a partial agonist at cannabinoid receptor 1 (CB1) and 2 (CB2) [8]. The higher affinity for CB1 is responsible for the insurgence of psychotropic effects [4]. THC, and its synthetic version dronabinol, have been investigated for their analgesic, antispasmodic and antiemetic activity [9].

Cannabidiol (CBD), on the other hand, is the major non-psychotropic cannabinoid in *C. sativa*. It is a weak inverse agonist at CB2 and it has been approved

by the FDA for the treatment of intractable childhood-onset seizures [10]. Other than its anti-epileptic effect, CBD has been studied for its potential therapeutic role in mood disorders [11], multiple sclerosis [12], and in a number of diseases associated with oxidative stress, and inflammation [3,13].

THC levels in cannabis dramatically increased from 1970 to 2017, increasing the risk of addiction and mental health disorders [14]. However, CBD seems to be able to moderate the toxic effects of THC [15,16].

Apart from the pharmacological properties of isolated cannabinoids, in the last decade, many efforts have been made to investigate the clinical effectiveness of the whole *C. sativa* extract [12,17–19]. Despite the growing scientific interest, however, only one standardized extract with a fixed THC:CBD ratio (1:1) has been registered as a medicinal product so far [20]. In Italy, eight variety of medical cannabis with different content of THC and CBD and cultivated indoor in The Netherlands, Canada and Italy, are authorized. These can be dispensed as herbal substance, used by patients for self-medication by vaporization, as an herbal tea or as galenic herbal preparations, such as oil or other standardized extracts [21]. However, information on the pharmacodynamics and pharmacokinetics of these preparations are lacking.

Moreover, the controversial, unregulated growing market of the so-called “cannabis light” products, i.e. *C. sativa* herbal material or derived preparations with THC content lower than 0.2%, complicated the situation by increasing the availability of products which have not been clinically evaluated for their pharmaco-toxicological profile.

Thus, there is the need for the development of efficient analysis methods to characterize the chemical and biological properties of different *C. sativa* products. In particular, information about the stability of these products after oral ingestion would be of great use for guiding the development of novel cannabis-based drugs.

Recently, we analyzed the chemical composition, the microbial contamination, and the levels of heavy metals of 12 non-psychoactive *C. sativa* products, finding that most of the cannabis light products do not comply with the Italian food legislation, or have different amount of THC and CBD than the quantity declared on the label [22].

In this study, we aimed at evaluating the stability to digestion of different non-psychoactive *C. sativa* products. We used three different extraction methods, namely decoction, oleolite and hydroalcoholic extraction, to extract two different *C. sativa* varieties with THC level lower than 0.2%, before and after heat-induced decarboxylation of cannabinoids. CBD, THC, and their relative acidic forms (CBDA and THCA) were quantified by HPLC-DAD and their stability and bioaccessibility under *in vitro* simulated gastrointestinal digestion were evaluated.

3.2. Materials and methods

3.2.1. Chemicals

All solvents used in this work were purchased from Sigma-Aldrich. NaCl, pepsin from porcine gastric mucosa, pancreatin from porcine pancreas, and bile salts mixture were from Sigma Aldrich. Na₂CO₃ was purchased from Sodafco S.p.A. CBD was purchased from Linnea SA (Riazzino, TI, Switzerland).

3.2.2. Plant material and extraction

The dried inflorescences of a commercially available product from indoor cultivation named “Mary-light” and of a field-grown *C. sativa* var. *carmagnole*, with different CBD content, were extracted for 4 h, using ddH₂O, 96% v/v ethanol or extravirgin olive oil (EVO), with (d) or without heat decarboxylation of cannabinoids. We obtained four different extracts, namely non-decarboxylated Mary-light (M), decarboxylated Mary-light (dM), non-decarboxylated *C. sativa* var. *carmagnole* (C) and decarboxylated *C. sativa* var. *carmagnole* (dC) extracts. The drug-extract ratio (DER) of each extract was 1:10. Heat decarboxylation of cannabinoids was performed following the method of Romano and Hazekamp [23], by heating plant material in an oven at 145 °C for 30 min.

3.2.3. *In vitro simulated gastrointestinal digestion*

In vitro simulated digestion was carried out as previously described [24], with slight modifications. Briefly, extracts (1 mL) and CBD were suspended in 20 mL of simulated gastric juice that contained pepsin from porcine gastric mucosa (300 UI/mL) and NaCl (10 mg/mL), obtaining a final 1:20 dilution for the extracts and a concentration of 1 mg/mL for CBD. The pH of the solution was adjusted to 1.7 using HCl. Samples were incubated for 2 h at 37 °C with shaking. One mL gastric solution was sampled and stored at -80 °C for further analysis. Then, pancreatin from porcine pancreas (10 mg/mL) and bile salts mixture (20 mg/mL) were added to the solutions to simulate the intestinal environment. To evaluate the bioaccessibility of the samples, semi-permeable cellulose dialysis tubes (Sigma Aldrich), with a molecular cut-off of 12 kDa, containing 19 mL of NaHCO₃ (15 mg/mL) in ddH₂O, were inserted into the solutions. Intestinal digestion was carried out for 2 h at 37 °C with shaking. The fraction of the samples able to permeate into the dialysis tubes was considered “bioaccessible” or “serum available”, while the fraction which remained out of the dialysis tubes was considered “not bioaccessible” or “colon available”. Samples were then centrifuged, filtered, and immediately used for further analysis.

3.2.4. *Chromatographic conditions*

Samples (20 µL) were injected into a HPLC-DAD system, consisting of a Shimadzu Prominence LC 2030 3D instrument, equipped with a Bondpak® C18 column (10 µm, 125 Å, 3.9 mm, Waters Corporation). The mobile phase consisted of ddH₂O + 0.1% v/v formic acid (A) and acetonitrile + 0.1% v/v formic acid (B). The following method was applied: A 35% at 0 min for 3 min, then from 35% to 10% at 10 min, A 10% for 2 min and from 10% to 35% at 14 min, then A 35% for 1 min. Flow rate was set to 1.2 mL/min and column temperature to 28 °C. Chromatograms were recorded at 225 nm. The calibration curve of CBD was set up using concentrations ranging from 0.008 to 0.500 mg/mL, with R² > 0.99. The quantification of CBDA, THC and THCA was performed using CBD as a reference standard, by conversion according to the Dutch office for Medicinal Cannabis analytic monograph for *Cannabis Flos* Version 7.1 (November 28, 2014).

3.2.5. Statistical analysis

The statistical differences between the results were determined by ANOVA or by using the Student's t-test. Values are expressed in the range of +/- standard deviation and $p < 0.05$ was considered statistically significant. Graphs and calculations were performed using GraphPad Prism.

3.3. Results and discussion

3.3.1. Quantification of cannabinoids

The HPLC-DAD chromatograms of the extracts (figure 3.1) show that, despite being suggested by several therapeutic systems, water extraction by decoction is not a suitable method for the extraction of cannabinoids, while ethanol and EVO gave higher yields, with ethanol being significantly better. In nature, cannabinoids occur mostly as acidic precursors, while their decarboxylated derivatives are usually produced by manufacturing processes or smoking [25].

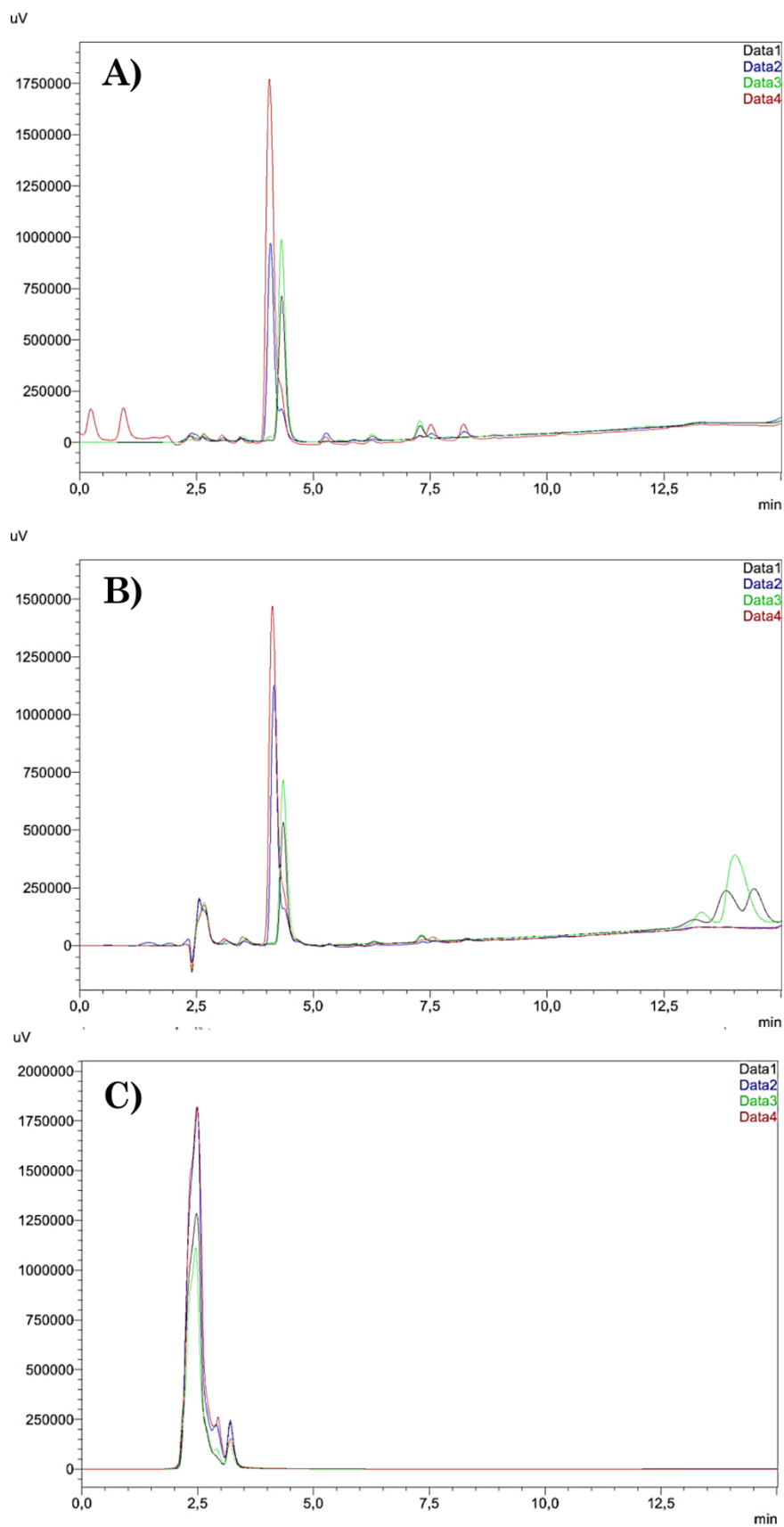


Figure 3.1. HPLC-DAD chromatograms recorded at 225 nm of the (A) ethanol, (B) olive oil and (C) water extracts. M (red), dM (green), C (blue) and dC (black). CBDA RT = 4.1 min; CBD RT = 4.4 min; THCA RT = 7.3 min; THC RT = 7.5 min.

Consistently, CBD and THC were not detected neither in M ethanol and EVO extracts, nor in C EVO extract. Small amounts of CBD were found in C ethanol extract. On the contrary, the acidic form of cannabinoids was much more present in the non-decarboxylated extracts, with CBDA being 63% higher in M, compared to C. THC content was always below the Italian legal limit of 0.2 %. The quantification of the cannabinoids in the extracts is reported in table 3.1.

Table 1. Cannabinoids content of the extracts (% w/v). Data are expressed as mean \pm standard deviation. n.d. = not determined.

Solvent	Sample	CBDA	CBD	THCA	THC
EtOH	M	0.60 \pm 0.03	n.d.	0.05 \pm 0.04	n.d.
	dM	0.06 \pm 0.07	0.53 \pm 0.09	n.d.	0.05 \pm 0.02
	C	0.38 \pm 0.06	0.08 \pm 0.01	0.01 \pm 0.01	n.d.
	dC	n.d.	0.36 \pm 0.02	n.d.	0.04 \pm 0.03
EVO	M	0.42 \pm 0.04	n.d.	0.01 \pm 0.01	n.d.
	dM	0.07 \pm 0.02	0.34 \pm 0.02	n.d.	n.d.
	C	0.26 \pm 0.03	n.d.	n.d.	n.d.
	dC	0.06 \pm 0.02	0.25 \pm 0.07	n.d.	n.d.
ddH ₂ O	M	n.d.	n.d.	n.d.	n.d.
	dM	n.d.	n.d.	n.d.	n.d.
	C	n.d.	n.d.	n.d.	n.d.
	dC	n.d.	n.d.	n.d.	n.d.

3.3.2. *In vitro* simulated gastrointestinal digestion and bioaccessibility

The stability of isolated CBD after gastrointestinal digestion resulted to be approximately 75%, and a large part (60%) of the initial amount of CBD was able to permeate across the dialysis tube, reaching the serum available fraction, thus showing a good bioaccessibility (figure 3.2).

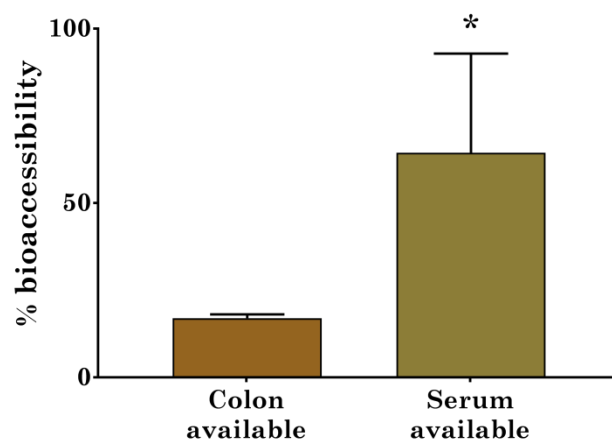


Figure 3.2. CBD bioaccessibility after *in vitro* simulated gastrointestinal digestion.
* $p < 0.001$ vs colon available, unpaired t test.

Differences in cannabinoids recovery and bioaccessibility were found when comparing the different *C. sativa* preparations (figure 3.3).

Indeed, the total recovery of CBDA was approximately 30% and 60% in M and C ethanol extracts, respectively, with the colon available to serum available ratio (CSR) being almost identical. Interestingly, the stability of CBDA to *in vitro* simulated digestion resulted to be significantly higher when using the EVO extracts. The total recovery of CBDA was almost 100% for M and C, respectively. 87% of CBDA was found in the colon available fraction for both M and C, while a small, yet significant, difference was found in the serum available, with a CSR of 6.4 and 8.9 for M and C, respectively. Small amount of CBDA were also present in the decarboxylated EVO extracts, with its stability to simulated digestion being lower (approximately 42% and 37% in dM and dC, respectively) and only colon available, compared to the non-decarboxylated one.

CBD recovery was comparable in each ethanol extract, with an average total recovery of 42%. A similar value was obtained for dC EVO extract, while dM EVO extract showed a protective effect on CBD stability, with the colon available recovery being approximately 47% and 90%, respectively. Similarly to CBDA, the CBD colon available fraction was higher than the serum available fraction, with an average CSR of 10 in the ethanol extracts, while no CBD was detected in the serum available

fractions of EVO extracts. While the absence of CBD in the serum available fraction of the EVO extracts may be due to a limitation of the experimental procedure, as the formation of micelles may interfere with the permeation through the dialysis tube, a lower bioaccessibility of CBD when using *C. sativa* extracts, compared to the reference standard alone, can be speculated.

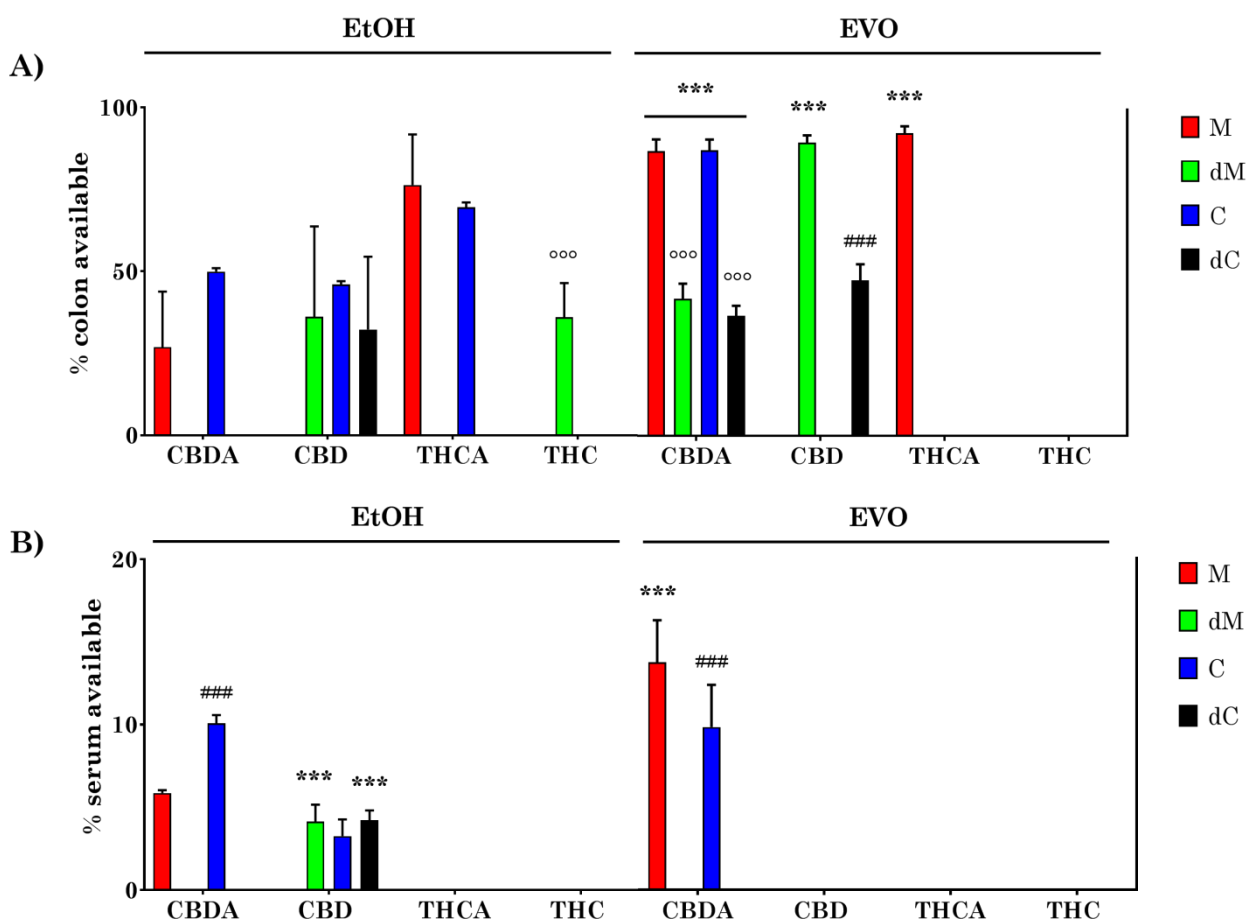


Figure 3.3. (A) Colon and (B) serum available fractions of different *C. sativa* extracts after *in vitro* simulated gastrointestinal digestion. * $p < 0.001$ EtOH vs EVO; ### $p < 0.001$ field-grown vs indoor cultivation; °°° $p < 0.001$ non-decarboxylated vs decarboxylated**

The THCA and THC content of the analyzed extracts was very low, thus, the measurement of their stability and bioaccessibility after *in vitro* simulated gastrointestinal digestion was not the aim of this work. However, it is interesting to note that, the presence of THCA and THC was not detected in the serum available

fractions of each extract. The colon available recovery of THCA was 76% and 70% for M and C ethanol extracts and 92% for M EVO extract, respectively. A significant difference was found when comparing the stability of THC in dM and dC ethanol extracts. Indeed, the colon available recovery of THC was approximately 36% in dM, while no trace of THC was detected in dC. Even if additional experiments are required to confirm this hypothesis, these data may suggest that a higher CBD:THC ratio in the initial extract may lead to an increased stability of THC after *in vitro* simulated digestion.

3.4. Conclusions

The stability and bioaccessibility of the main cannabinoids in different non-psychoactive *C. sativa* extracts were evaluated in an *in vitro* model of simulated gastrointestinal digestion.

Differently from the observation on *M. recutita*, *C. scolymsus* and *C. longa* reported in chapter 2, where the use of the herbal extract increased the gastrointestinal stability of the constituents, we found that the bioaccessibility of CBD was lower when using the *C. sativa* extracts, compared to the use of the single reference standard. These different results even more strengthen the hypothesis that pharmacokinetic data obtained with single natural compounds cannot be translated to herbal extracts containing such compounds, as the complex mixture of constituents in the extract may positively or negatively influence the way these compounds are digested and absorbed.

Although the initial content in the extracts was low, we also found that THC is not orally bioaccessible, thus, its bioavailability after oral administration of *C. sativa* extracts is expected to be very low, supporting the use of vaporization as a different administration route.

Even if the bioaccessibility of cannabinoids was reduced when using the herbal extracts, their overall stability to gastrointestinal digestion could suggest a possible therapeutic application in gastrointestinal disorders, such as inflammatory bowel

disease, where a local accumulation of anti-inflammatory cannabinoids in the intestine is desirable, compared to a systemic distribution after absorption.

Notably, we found that the overall gastrointestinal stability and bioaccessibility were strongly influenced by the extraction solvent used, and that, despite being a suggested dispensation method in Italy, water extraction by decoction is not an effective method for extracting cannabinoids.

In conclusion, our study demonstrated the need to standardize cannabis preparations, not only to obtain the maximum yield of constituents, but also taking into account the effect of the extraction method and of the whole phytocomplex on their gastrointestinal digestion.

3.5. References

1. Lal, S.; Shekher, A.; Puneet; Narula, A. S.; Abrahamse, H.; Gupta, S. C. Cannabis and its constituents for cancer: history, biogenesis, chemistry and pharmacological activities. *Pharmacol. Res.* **2020**, *163*, 105302.
2. Pertwee, R. G. *Handbook of Cannabis*; Oxford University Press: USA, 2014.
3. Pellati, F.; Borgonetti, V.; Brighenti, V.; Biagi, M.; Benvenuti, S.; Corsi, L. *Cannabis sativa* L. and nonpsychoactive cannabinoids: their chemistry and role against oxidative stress, inflammation, and cancer. *Biomed Res. Int.* **2018**, *2018*, 1691428.
4. Appendino, G.; Chianese, G.; Taglialatela-Scafati, O. Cannabinoids: occurrence and medicinal chemistry. *Curr. Med. Chem.* 2011, *18*, 1085–1099.
5. Andre, C. M.; Hausman, J.-F.; Guerriero, G. *Cannabis sativa*: the plant of the thousand and one molecules. *Front. Plant Sci.* **2016**, *7*, 19.
6. Brenneisen, R. Chemistry and analysis of phytocannabinoids and other cannabis constituents. In *Marijuana and the Cannabinoid*; Springer Science & Business Media, 2007; p. pp 17-49.
7. Wang, M.; Wang, Y.-H.; Avula, B.; Radwan, M. M.; Wanas, A. S.; van Antwerp, J.;

Parcher, J. F.; ElSohly, M. A.; Khan, I. A. Decarboxylation study of acidic cannabinoids: a novel approach using ultra-high-performance supercritical fluid chromatography/photodiode array-mass spectrometry. *Cannabis cannabinoid Res.* **2016**, *1*, 262–271.

8. Pertwee, R. G. The diverse CB1 and CB2 receptor pharmacology of three plant cannabinoids: delta9-tetrahydrocannabinol, cannabidiol and delta9-tetrahydrocannabivarin. *Br. J. Pharmacol.* **2008**, *153*, 199–215.

9. Balter, R. E.; Haney, M. The synthetic analog of Δ^9 -tetrahydrocannabinol (THC): nabilone. Pharmacology and clinical application. In *Handbook of Cannabis and related pathologies – biology, pharmacology, diagnosis and treatment*; Preedy, V. R., Ed.; Academic Press: San Diego, 2017; pp. 821–827.

10. Britch, S. C.; Babalonis, S.; Walsh, S. L. Cannabidiol: pharmacology and therapeutic targets. *Psychopharmacology.* **2020**. DOI: 10.1007/s00213-020-05712-8.

11. García-Gutiérrez, S.; Navarrete, F.; Gasparyan, A.; Austrich-Olivares, A.; Sala, F.; Manzanares, J. Cannabidiol: a potential new alternative for the treatment of anxiety, depression, and psychotic disorders. *Biomolecules* **2020**, *10*, 1575.

12. Jones, É.; Vlachou, S. A critical review of the role of the cannabinoid compounds Δ^9 -tetrahydrocannabinol (Δ^9 -THC) and cannabidiol (CBD) and their combination in multiple sclerosis treatment. *Molecules* **2020**, *25*, 4930.

13. Borgonetti, V.; Governa, P.; Montopoli, M.; Biagi, M. *Cannabis sativa* L. Constituents and Their Role in Neuroinflammation. *Curr. Bioact. Compd.* **2019**, *15*, 147–158.

14. Freeman, T. P.; Craft, S.; Wilson, J.; Stylianou, S.; ElSohly, M.; Di Forti, M.; Lynskey, M. T. Changes in delta-9-tetrahydrocannabinol (THC) and cannabidiol (CBD) concentrations in cannabis over time: systematic review and meta-analysis. *Addiction* **2020**. DOI: 10.1111/add.15253.

15. Morgan, C. J. A.; Freeman, T. P.; Schafer, G. L.; Curran, H. V. Cannabidiol attenuates the appetitive effects of delta 9-tetrahydrocannabinol in humans smoking their chosen cannabis. *Neuropsychopharmacol.* **2010**, *35*, 1879–1885.

16. Morgan, C. J. A.; Schafer, G.; Freeman, T. P.; Curran, H. V. Impact of cannabidiol on the acute memory and psychotomimetic effects of smoked cannabis: naturalistic study: naturalistic study [corrected]. *Br. J. Psychiatry* **2010**, *197*, 285–290.
17. Patten, S. B. Cannabis and non-psychotic mental disorders. *Curr. Opin. Psychol.* **2021**, *38*, 61–66.
18. Chung, M.; Kim, H. K.; Abdi, S. Update on cannabis and cannabinoids for cancer pain. *Curr. Opin. Anesthesiol.* **2020**, *33*, 825–831.
19. Gressler, L. E.; Baltz, A. P.; Costantino, R. C.; Slejko, J. F.; Onukwugha, E. Exploring the use of state medical cannabis legislation as a proxy for medical cannabis use among patients receiving chemotherapy. *Curr. Treat. Options Oncol.* **2020**, *22*, 1.
20. Namdar, D.; Anis, O.; Poulin, P.; Koltai, H. Chronological review and rational and future prospects of cannabis-based drug development. *Molecules* **2020**, *25*, 4821.
21. Minghetti, P.; Marini, V.; Zaccara, V.; Casiraghi, A. Regulation for prescribing and dispensing system of cannabis: the Italian case. *Curr. Bioact. Compd.* **2019**, *15*, 196–200.
22. Musa, P. Canapa light: dalla moda del momento alle indagini scientifiche, University of Siena, 2019.
23. Romano, L. L.; Hazekamp, A. Cannabis oil: chemical evaluation of an upcoming cannabis-based medicine. *Cannabinoids* **2013**, *1*, 1–11.
24. Alming, M.; Aura, A. M.; Bohn, T.; Dufour, C.; El, S. N.; Gomes, A.; Karakaya, S.; Martínez-Cuesta, M. C.; McDougall, G. J.; Requena, T.; Santos, C. N. *In vitro* models for studying secondary plant metabolite digestion and bioaccessibility. *Compr. Rev. Food Sci. Food Saf.* **2014**, *13*, 413–436.
25. Ramirez, C. L.; Fanovich, M. A.; Churio, M. S. Cannabinoids: extraction methods, analysis, and physicochemical characterization. In *Studies in natural products chemistry*; Atta-ur-Rahman, Ed.; Elsevier, 2019; Vol. 61, pp. 143–173.

CHAPTER 4

Effect of *in vitro* simulated digestion on the anti-*Helicobacter pylori* activity of different propolis extracts

4.1. Introduction

Helicobacter pylori (HP), a spiral-shaped Gram-negative microaerophilic bacterium, which colonizes the stomach, is among the most common pathogens causing infection in human worldwide [1,2]. The ability of HP to overthrow the host physiology and to evade the immune response, contribute to complicate the clinical management of the infection [3]. Indeed, the inability of the immune system to eradicate HP may lead to a progressive clinical course, characterized by the appearance of gastritis, atrophy, intestinal metaplasia and dysplasia, eventually leading to gastric/duodenal ulcer and gastric cancer [4].

To colonize the host stomach, HP needs to adapt to the gastric environment, by surviving to the acidic pH, penetrating and growing into the mucus layer [5].

Different virulence factors participate in HP colonization phase. Urease is the enzyme involved in the acid acclimation, by catalyzing the hydrolysis of urea into ammonia and carbon dioxide, thus, increasing the environment pH [6]. The spiral morphology and the presence of flagella are pivotal for penetrating the mucus layer and reaching the gastric epithelium, where specific proteins promote the adhesion process [7–9]. Moreover, a number of other virulence factors are involved in the clinical manifestation of HP infection. The vacuolating cytotoxin A (VacA) and the cytotoxin-associated gene (CagA) are among the most studied. VacA is known to cause the formation of pore in the cell membrane and vacuole, as well as the induction of apoptosis in the mitochondria and the modulation of the host immune response by interacting with the proliferation of T cells [10]. Differently, CagA is an oncogenic toxin, which interacts with the intracellular signaling pathways of the host, reducing

cell adhesion and stimulating cell migration and proliferation, as well as stimulating the production of the pro-inflammatory cytokine IL-8 by gastric epithelial cells [11,12].

The current clinical management of HP infection is based on the use of proton pump inhibitors in combination with at least two antibiotic drugs, such as amoxicillin, metronidazole, clarithromycin, tetracycline, and levofloxacin [13]. Several issues arise with the use of these therapeutic approaches, including the rapid development of bacterial resistance to the antibiotic, particularly to clarithromycin [14] and levofloxacin [15], the low stability of antibiotic in the acidic environment of the stomach, and the scarce compliance of the patients [16].

Moreover, oxidative stress and gastric inflammation are strictly involved in the progression of HP-related gastric diseases [17–20] and are not targeted by the conventional antibiotic therapy.

To overcome the limit of the conventional antibiotic therapy, natural products with anti-HP activity have been widely investigated [21]. Some examples include *Allium sativum* L. [22], sulforaphane isothiocyanate from *Brassica oleracea* L. [23,24], *Glycyrrhiza glabra* L. [25–27], red wine [28], and green tea [29,30], as well as some flavonoids such as quercetin and naringenin [31].

Propolis is a resinous product made by honeybees to repair and protect the hives, preventing the microbial infection of larvae [32]. Its chemical composition varies depending on the vegetal origin and geographical region where it was produced, affecting the physical properties, such as color, smell, taste, and consistency [33,34]. Flavonoids are widely present in most of the propolis, independently from the origin. Flavones, such as chrysin and acacetin, are mostly present in the temperate region-native propolis, while flavonols, such as galangin and quercetin, are mostly present in Eurasian propolis. Pinocembrin, a flavanone, is commonly found in different propolis, independently from the origin [34]. Other frequently found constituents include caffeic acid phenethyl ester (CAPE) [35], phenolic acids, such as benzoic acid, gallic acid, caffeic acid, cinnamic acid and chlorogenic acid, and terpenes [34].

Traditionally, propolis has been used for century as an antimicrobial agent [36]. More recently, indeed, this activity has been demonstrated *in vitro*, *in vivo*, and in

clinical trials as well, against Gram-positive and Gram-negative bacteria, including drug-resistant species, such as methicillin-resistant *Staphylococcus aureus*, vancomycin-resistant *Enterococcus*, and several *Streptococcus* strains, with minimum inhibitory concentration (MIC) varying based on the chemical composition [37–39]. Antifungal activity was also reported against different *Candida* species [40,41]. The most widely-accepted antimicrobial mechanism of action of propolis is related to its effect on the membrane permeability, which may lead to cell lysis and may participate in reducing the development of resistance to antibiotic and antifungal drugs [42]. Also, inhibition of bacterial RNA-polymerase was observed for some of the propolis constituents [43].

Other important biological effect of propolis consists in its ability to modulate the immune response, leading to a pronounced anti-inflammatory activity [37], and its antioxidant properties [44,45], which make it a promising candidate for the management of the complex pathological situation related to HP infection. The anti-inflammatory activity is mainly related to the content in CAPE and galangin. Both of them, in fact, were reported to inhibit the nuclear translocation of NF- κ B [46–50], which is a key pathway by which CagA promote gastric inflammation [51,52]. On the other hand, the antioxidant and radical scavenging activity of propolis was found to depend mostly on the presence of pinocembrin, chrysin and pinobanksin [53].

Information on the *in vitro* anti-HP effect of propolis are emerging and were also evaluated by our group in the past, even if the actual clinical effectiveness is still to be validated [54–56].

In this work we have characterized from a chemical point of view three different propolis extracts and for the first time, we evaluated their stability under *in vitro* simulated gastric digestion, compared to their main constituents alone. The extract showing higher stability to digestion was tested for its anti-HP activity. Finally, we evaluated the possible inhibition of urease by using *in vitro* colorimetric assay and molecular docking simulations.

4.2. Materials and methods

4.2.1. Sample preparation and chemical analysis

All solvents were from Sigma-Aldrich.

Raw green baccharis-type propolis (Bnatural, Corbetta, Milan, Italy) and dark poplar-type propolis (Selerbe, Tavarnelle Val di Pesa, Florence, Italy) were extracted using 80% v/v ethanol for 2 h in an ultrasound bath. A commercial propolis-based extract (Propolfenol®), standardized to contain 50% w/w total phenolic compounds, kindly provided by Erba Vita Group S.p.A. (Chiesanuova, Republic of San Marino) was dissolved in 80% v/v ethanol. Three different propolis extract were, hence, obtained: green propolis extract (GPE), dark propolis extract (DPE) and Propolfenol® extract (PPF). The final propolis concentration was adjusted to 400 mg/mL for each extract.

For the chemical characterization by HPLC-DAD, samples were further diluted to obtain a propolis concentration of 2.5 mg/mL and then filtered. A Shimadzu Prominence LC 2030 3D instrument, equipped with a Bondpak® C18 column, 10 µm, 125 Å, 3.9 mm x 300 mm (Waters Corporation) was used. The mobile phase was composed of water with 0.1% v/v formic acid (A) and methanol with 0.1% v/v formic acid (B), using the following gradient phases, as previously described [37], with a few modifications: A from 0 % at 0 min to 50% at 6 min, from 50% to 70% at 12 min and from 70% to 50% at 16 min. The flux was set to 0.75 mL/min and the injected volume was 20 µL. Absorbance was recorded at 280 nm and 366 nm and calibration curves obtained using galangin and pinocembrin (Sigma-Aldrich) as reference standards, ranging from 0.008 to 0.5 mg/mL ($R^2 > 0.99$), were used for quantification.

4.2.2. *In vitro* simulated gastric digestion

In vitro simulated gastric digestion was carried out as previously described [57], with slight modifications. Briefly, extracts (125 µL, corresponding to 50 mg of dry propolis) and reference standards (1 mg/mL) were suspended in 20 mL of simulated gastric juice that contained pepsin from porcine gastric mucosa (300 UI/mL, Sigma-Aldrich) and NaCl (10 mg/mL). The pH of the solution was adjusted to 1.7 using HCl.

Samples were incubated for 4 h at 37 °C with shaking. Samples were then filtered and immediately used for further analysis.

4.2.3. Anti-HP activity

A multiwell suspension test was performed, as previously published [58], with a few modifications, for determining the anti-HP activity of the samples. The VacA+ CagA+ HP clinical isolate 10K was kindly provided by Professor Natale Figura (Department of Internal Medicine, Endocrine-Metabolic Sciences and Biochemistry, University of Siena). Columbia-blood agar (CBA), Brucella broth bovine serum (BBS) were purchased from Biomerieux, Florence. Microaerophilic sachets for HP culturing were from Oxoid (Milan, Italy). DPE (13575 – 212 mg/L), galangin (300 – 5 mg/L) and pinocembrin (300 – 5 mg/L) were diluted in BBS and added to the appropriate well of 96-well plates (Sarstedt, Verona, Italy). BBS was used as negative control. Microbial suspension (1×10^5) was added to each well and plates were incubated at 37 °C for 4 h, in microaerobic condition. 5 μ L of solution were transferred to CBA plates and incubated for 24 h.

The MIC and the minimum bactericidal concentration (MBC) were extrapolated from the multiwell assay and CBA plates, respectively.

The strains susceptibility of the tested HP strains to antimicrobial drugs were confirmed using amoxicillin, clarithromycin, and levofloxacin and comparing MICs with European Committee on Antimicrobial Susceptibility Testing (EUCAST) breakpoint tables (www.eucast.org).

4.2.4. Urease inhibition assay

The colorimetric urease activity assay kit (Sigma-Aldrich) was used to measure the inhibition of urease activity by DPE, galangin and pinocembrin. This assay is based on the quantification of urease-produced ammonia, using the Berthelot method [59]. Briefly, a suspension (1×10^6 CFU/mL) of the 10K clinical isolate was centrifuged (10000 x g for 3 min) and the pellet was used as the source of urease. DPE, galangin, and pinocembrin were used at the MBC found in the previous experiment. 90 μ L of DPE (848.4 mg/L), galangin (37.5 mg/L), and pinocembrin (18.8 mg/L), diluted in the

assay buffer (10 mM Na₃PO₄, pH 7.2) containing the 10K suspension pellet (1 x 10⁶ CFU/mL), were added to the appropriate well in a 96-well plate. A standard curve was created by using decreasing NH₄Cl concentration (final ammonia concentration 500 – 0 μM). Assay buffer was used as blank control, while the 10K suspension pellet (1 x 10⁶ CFU/mL) in assay buffer was used as positive control. 10 μL of urea were added to each well and incubated for 15 min at 37 °C. Then, 100 μL of reagent A were added to stop the urease reaction. After mixing, 50 μL of reagent B were added and incubated for 30 min in the dark. Finally, absorbance was measured at 670 nm using a Victor® Nivo™ plate reader (PerkinElmer, Waltham, MA). Urease activity was calculated using the following formula (Eq. 4.1):

$$Urease\ activity\ (units/L) = \frac{(Abs_{670})_{sample} - (Abs_{670})_{blank}}{Slope \times t} \times n$$

where Abs_{670} is the absorbance at 670 nm, n is the dilution factor, $Slope$ is the slope obtained by linear regression fitting of the standard curve, and t is the incubation time (15 min).

The percent inhibition of urease was then calculated using the following formula (Eq. 4.2):

$$Urease\ \% \ inhibition = \frac{(Urease\ activity)_{positive} - (Urease\ activity)_{sample}}{Urease\ activity_{positive}} \times 100$$

where $(Urease\ activity)_{positive}$ is the urease activity (units/L) of the positive control.

4.2.5. Computational details

The X-ray 3D structure of the HP urease with acetohydroxamic acid bound in the active site (PDBID: 1e9y) was obtained from the Protein Data Bank (PDB) [60].

The protein was prepared using AutoDock Tools [61], following the standard preparation protocol [62]: adding polar hydrogens, assigning Gasteiger-Marsili atomic charges [63], then merging non-polar hydrogens.

The tridimensional coordinates of galangin and pinocembrin were downloaded from the ZINC database [643] in Mol2 format and converted to PDBQT format using OpenBabel [64].

The protein was treated as rigid, and the grid box was centered on the co-crystallized ligand (box center: x:127.99, y:129.092, z:86.811) and sized to be 14×14×14 Å.

AutoDock Vina (v1.1.2) was used to perform the molecular docking simulations, setting the exhaustiveness to default [62].

4.2.6. Statistical analysis

The statistical differences between the biological results were determined by ANOVA. Values are expressed in the range of +/- standard deviation and $p < 0.05$ was considered statistically significant. Graphs and calculations were performed using GraphPad Prism.

4.3. Results and discussion

4.3.1. Chemical analysis

By comparison with reference standards retention time (RT) and UV spectra, we identified pinocembrin (RT = 10.6 min) and galangin (RT = 12.8 min), which are the two typical chemical markers of propolis, in each sample (figure 4.1).

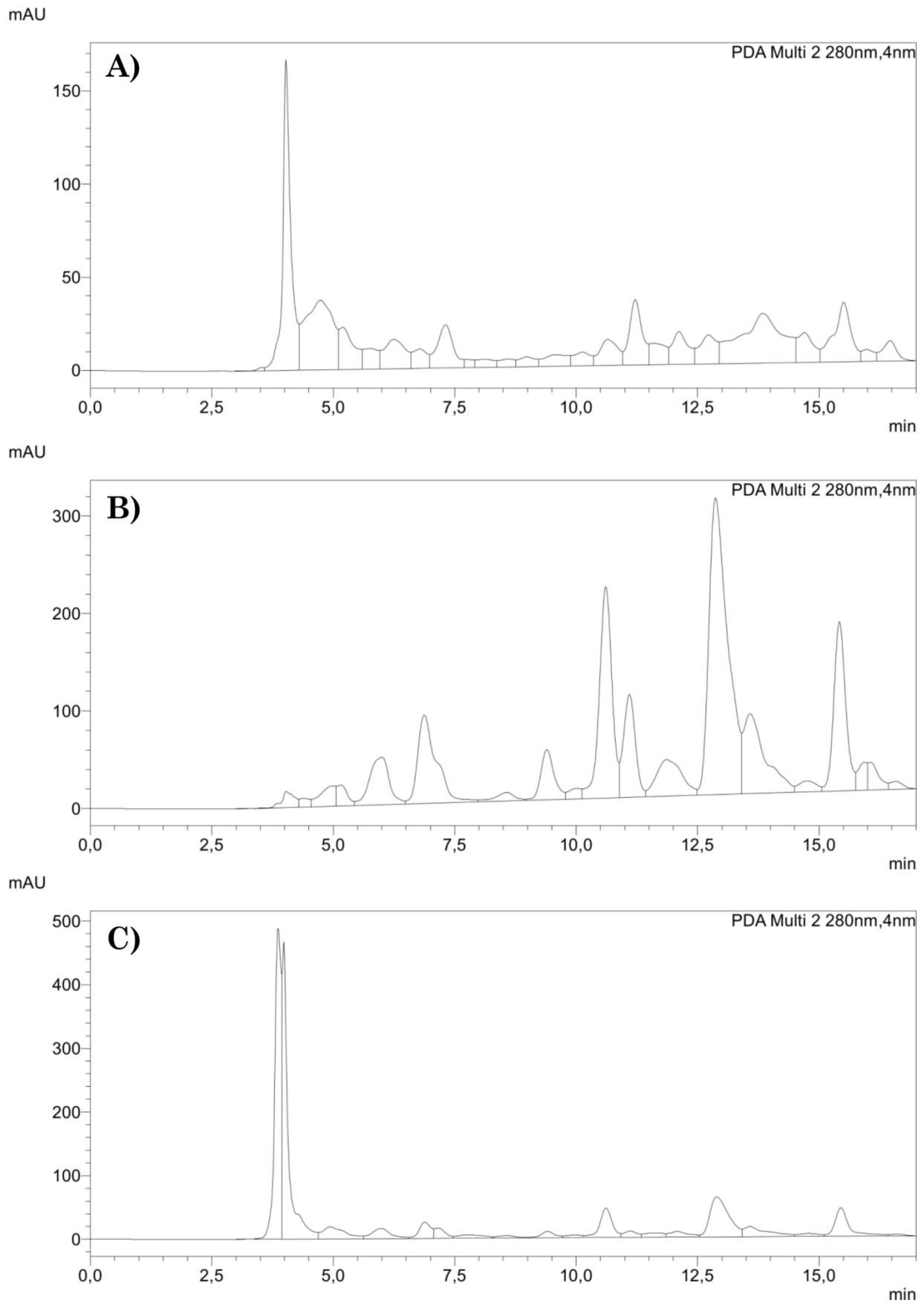


Figure 4.1. HPLC-DAD chromatograms of (A) GPE, (B) DPE and (C) PPF, registered at 280 nm. Pinocembrin RT = 10.6; galangin RT = 12.9.

The chemical characterization of the samples is reported in table 4.1. Galangin was found to be the main flavonoid of each propolis sample, while pinocembrin was found to be 2-5-fold lower in comparison to galangin, depending on the sample. DPE contained the higher amount of both galangin and pinocembrin, followed by PPF and GPE, respectively.

Table 4.1. Chemical characterization of the extracts. Values (mg/g dry propolis) are expressed as mean \pm standard deviation.

Sample	galangin	pinocembrin
GPE	12.65 \pm 0.63	1.64 \pm 0.15
DPE	83.46 \pm 0.59	27.42 \pm 0.29
PPF	13.84 \pm 0.23	3.11 \pm 0.21

4.3.2. Stability of propolis constituents under *in vitro* simulated gastric digestion

When used as a single reference standard, galangin showed a high stability to simulated gastric digestion, with a recovery 6-fold higher than pinocembrin (table 4.2).

Table 4.2. Relative gastric stability of reference standards. Values (%) are expressed as mean \pm standard deviation.

Sample	Gastric stability
galangin	73.97 \pm 8.26
pinocembrin	12.31 \pm 1.15

Different recoveries were obtained when using the three propolis extracts (figure 4.1). Indeed, when using GPE and PPF, galangin stability was approximately 5% and 0.5%, respectively, which is significantly lower, compared to the reference standard alone. Conversely, while being slightly lower than the reference standard, DPE had a protective effect on galangin stability, which resulted to be 63% and significantly higher than GPE and PPF. On the other hand, each propolis extract was able to significantly protect pinocembrin from gastric digestion-induced degradation. Indeed, pinocembrin recovery was 26%, 94% and 40% when using GPE, DPE and PPF,

respectively. Similarly to galangin, the stability of pinocembrin in DPE was significantly higher than that of GPE and PPF.

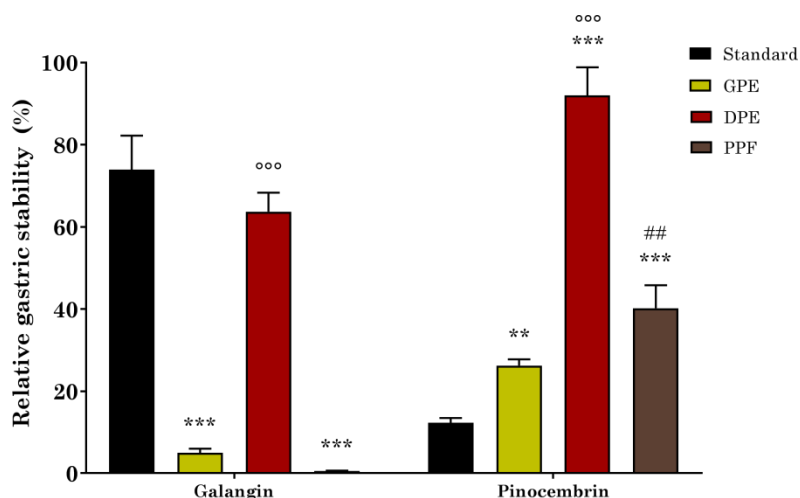


Figure 4.1. Relative gastric stability of GPE, DPE and PPF flavonoids. * $p < 0.001$ vs reference standard; $^{\circ\circ\circ}p < 0.001$ DPE vs GPE and PPF; $^{\#\#}p < 0.01$ PPF vs GPE.**

These data suggest that galangin stability to simulated gastric digestion is not dependent from its quantity in the initial extract, while this seems to be likely for pinocembrin. More importantly, even if more data are required to fully understand the reasons why DPE is more effective than GPE and PPF in protecting its main constituents from degradation during gastric digestion, it is evident that dissimilarities in the chemical composition (i.e., in the presence and quantity of minor constituents, other than galangin and pinocembrin) of propolis extracts from diverse sources may modulate differently the gastric stability of their constituents. In the future, a more detailed phytochemical analysis of the initial propolis samples may be helpful to find out the role of each constituent during the digestive process.

4.3.3. Anti-HP activity of DPE and its main constituents

DPE resulted to be the most stable propolis extract after simulated gastric digestion, thus, possessing an important characteristic to be exploited for evaluating its anti-HP effectiveness. Interestingly, MIC and MBC values obtained against the 10K clinical isolate, matched, and suggested that DPE and its flavonoids may act mainly with a bactericidal mechanism. Consistently, it has been speculated that the

antimicrobial activity of propolis is due to its ability to bind to the cell wall, leading to the lysis of the microbial cell [66]. A similar observation was reported for several flavonoids too [67]. Although interesting MIC and MBC values, lower than 1000 mg/L, were obtained with DPE, galangin and pinocembrin gave better results, with MIC and MBC values being 37.5 mg/L for galangin and 18.8 mg/L for pinocembrin, respectively.

Table 4.3. Anti-HP activity of DPE and its constituents against the 10K clinical isolate. MIC and MBC are expressed as mg/L

Sample	MIC	MBC
DPE	848.4	848.4
galangin	37.5	37.5
pinocembrin	18.8	18.8

The 10K clinical isolate used in this work is both VacA+ and CagA+, thus representing an ideal model for evaluating the anti-HP activity of a drug candidate. The activity of DPE and its constituents on the 10K clinical isolate suggest a possible role in the prevention of the VacA-induced immune response and may help in reducing the risk of CagA-induced gastric ulcer and cancer.

The gastric localization of HP is one of the main factors limiting the success of the drug discovery process. Indeed, to overcome the limited persistence in the stomach due to turnover and emptying time, a compound must be rapidly effective. The bactericidal effect of propolis and its constituents was already evident after 4 h of treatment, thus, suggesting a quick anti-HP activity. Moreover, as observed in the *in vitro* simulated gastric digestion experiment, DPE was able to protect galangin and pinocembrin from degradation. Hence, DPE could be considered as an encouraging candidate for the management of HP infection.

4.3.4. Urease inhibition

Urease is a virulence factor involved in the colonization phase of the HP infection [68]. By using a simple colorimetric method, we determined the *in vitro* inhibition of urease from the 10k clinical isolate of DPE, galangin, and pinocembrin at their respective MIC.

DPE showed a weak anti-urease activity at the tested concentration, with a % inhibition lower than 30%. Conversely, both galangin and pinocembrin resulted particularly active, with the % inhibition being more than double, compared to DPE (Table 4.4). While galangin gave a higher % inhibition, compared to pinocembrin, it has to be stressed that samples were tested at their respective MIC. Galangin MIC is twofold higher than that of pinocembrin, thus, urease inhibition by pinocembrin is expected to be higher than that of galangin at the same concentration. A future perspective of this work involves the determination of the IC₅₀ of DPE, galangin, and pinocembrin, to clarify this aspect. In 2012, Xiao and colleagues evaluated the effect of 20 flavonoids on HP urease activity, observing IC₅₀ values between 11.2 μM and 4628 μM [69]. By means of structure-activity relationship analysis, they also highlighted 3-OH, 5-OH, and 3',4'-dihydroxyl groups as important for urease inhibitory activity. From our data, we expect IC₅₀ values of galangin and pinocembrin, which both possess the 5-OH group, to fit well in this range.

Table 4.4. Urease inhibition by DPE, galangin, and pinocembrin.

Sample	Concentration (mg/L)	Urease inhibition (%)	Vina binding energy (kcal/mol)
DPE	848.4	27.8 ± 1.3	
galangin	37.5	68.5 ± 7.1	-5.6
pinocembrin	18.8	57.9 ± 4.6	-5.6

Molecular docking simulation were performed to elucidate the possible binding mode of galangin and pinocembrin in the active site of HP urease.

The co-crystallized ligand, acetohydroxamic acid, binds the active site of urease by coordinating the dinuclear nickel metallocenter, which is involved in the decomposition of urea. Also, it makes hydrophobic contacts with Ala169 and Ala365, as well as a hydrogen bond with His221 (figure 4.2A).

Galangin and pinocembrin, in their top scored docking solutions, resulted in comparable binding energy (table 4.4) but assume different binding poses, which may explain the differences in the urease inhibitory activity: pinocembrin binds deep in the active site, close to the two nickel atoms, with the B-ring located outside the binding site, and assuming a flat conformation. Two main anchor points are represented by

the hydrogen bonds between the 4-OH group and the carboxyl moiety of Asp223 and between the 7-OH group and the backbone carbonyl of Ala365 (figure 4.2B). Galangin, on the contrary, binds farther from the nickel atoms, with the chromone group oriented in the opposite direction, compared to pinocembrin, and the B-ring perpendicular to it, assuming a binding pose similar to that reported by Xiao and colleagues for quercetin [69]. Due to the different binding mode, the hydrogen bond with Asp223 occurs through the 5-OH group, while the hydrogen bond with Ala365 is no more possible. Moreover, the B-ring is embedded between Cys321 and Met366 (figure 4.2C).

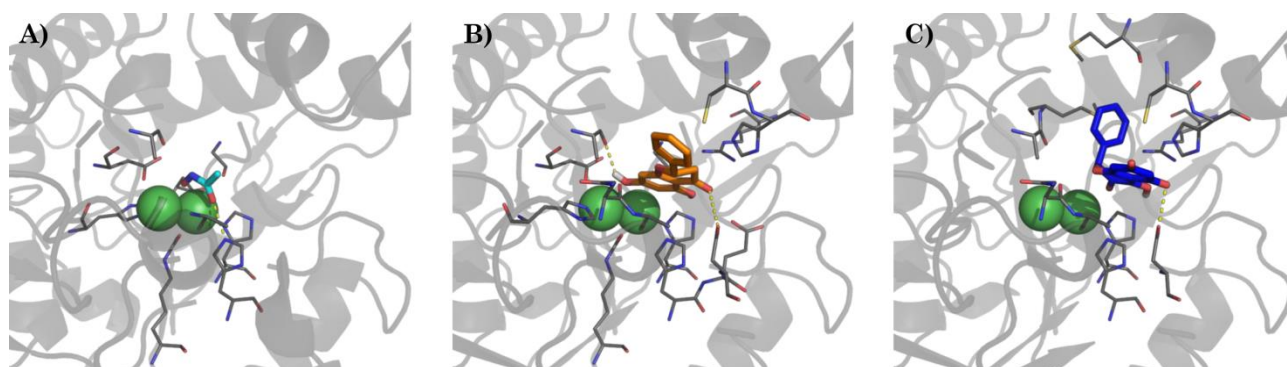


Figure 4.2. (A) Binding mode of acetohydroxamic acid (cyan) in the active site of HP urease (PDBID: 1e9y), and best docking pose of (B) pinocembrin and (C) galangin. Interacting residues are shown as gray line. Hydrogen bonds are represented by yellow dashed lines.

4.4. Conclusions

The current pharmacological management of HP infection is not ideal, as bacterial resistance phenomena are arising. Moreover, the side effects of the anti-HP therapy, such as nausea, vomiting, and gastrointestinal disorders, limit the patient's compliance. Thus, there is the need for the development of novel treatments, to be administered alone or in combination with other anti-HP drugs, which should be able to overcome this condition.

In this work we tested the ability of chemically characterized propolis extracts to act as anti-HP agents. We found that DPE may represent an interesting candidate, as it contains high amount of galangin and pinocembrin, which seem to be involved in

the anti-HP activity of propolis. Interestingly, both these flavonoids possess a rapid bactericidal activity, which is pivotal for counteracting the limited persistence in the stomach. Moreover, an additional therapeutic advantage is conferred by the inhibition of HP urease, a virulence factor involved in the colonization phase of the HP infection. While pinocembrin seems to be effective at lower concentration, compared to galangin, its stability in the gastric environment is scarce, which may suggest galangin as a better anti-HP candidate. Nevertheless, when using DPE, the gastric stability of pinocembrin significantly increases. Hence, the administration of an active dose of DPE is expected to maintain both galangin and pinocembrin levels above their effective anti-HP concentration.

In conclusion, we identified galangin and pinocembrin as interesting drug candidates for the management of HP infection. The antibiotic treatment is still essential for the eradication of HP, thus, we suggest these compounds to be administered in combination with the conventional antibiotic therapy, in order to reduce the risk of bacterial resistance development. Finally, as natural products stability to digestion is highly influenced by the co-administration of other constituents, such as in the case of herbal extracts, galangin and, particularly, pinocembrin should not be administered as isolated compounds. The use of a chemically characterized propolis extract may be favorable, as it helps maintaining the active concentration of these flavonoids for the whole gastric digestive process.

4.5. References

1. Kusters, J. G.; van Vliet, A. H. M.; Kuipers, E. J. Pathogenesis of *Helicobacter pylori* infection. *Clin. Microbiol. Rev.* **2006**, *19*, 449–490.
2. Suerbaum, S.; Josenhans, C. *Helicobacter pylori* evolution and phenotypic diversification in a changing host. *Nat. Rev. Microbiol.* **2007**, *5*, 441–452.
3. Logan, R. P.; Walker, M. M. ABC of the upper gastrointestinal tract: epidemiology and diagnosis of *Helicobacter pylori* infection. *BMJ* **2001**, *323*, 920–922.
4. Boreiri, M.; Samadi, F.; Etemadi, A.; Babaei, M.; Ahmadi, E.; Sharifi, A. H.;

Nikmanesh, A.; Houshiar, A.; Pourfarzai, F.; Yazdanbod, A.; Alimohammadian, M.; Sotoudeh, M. Gastric cancer mortality in a high incidence area: long-term follow-up of *Helicobacter pylori*-related precancerous lesions in the general population. *Arch. Iran. Med.* **2013**, *16*, 343–347.

5. Manente, L.; Perna, A.; Buommino, E.; Altucci, L.; Lucariello, A.; Citro, G.; Baldi, A.; Iaquinto, G.; Tufano, M. A.; De Luca, A. The *Helicobacter pylori*'s protein VacA has direct effects on the regulation of cell cycle and apoptosis in gastric epithelial cells. *J. Cell. Physiol.* **2008**, *214*, 582–587.

6. Perrais, M.; Rousseaux, C.; Ducourouble, M.-P.; Courcol, R.; Vincent, P.; Jonckheere, N.; Van Seuningem, I. *Helicobacter pylori* urease and flagellin alter mucin gene expression in human gastric cancer cells. *Gastric cancer* **2014**, *17*, 235–246.

7. Sycuro, L. K.; Wyckoff, T. J.; Biboy, J.; Born, P.; Pincus, Z.; Vollmer, W.; Salama, N. R. Multiple peptidoglycan modification networks modulate *Helicobacter pylori*'s cell shape, motility, and colonization potential. *PLoS Pathog.* **2012**, *8*, e1002603.

8. Eaton, K. A.; Suerbaum, S.; Josenhans, C.; Krakowka, S. Colonization of gnotobiotic piglets by *Helicobacter pylori* deficient in two flagellin genes. *Infect. Immun.* **1996**, *64*, 2445–2448.

9. Tomb, J.-F.; White, O.; Kerlavage, A. R.; Clayton, R. A.; Sutton, G. G.; Fleischmann, R. D.; Ketchum, K. A.; Klenk, H. P.; Gill, S.; Dougherty, B. A.; Nelson, K.; Quackenbush, J.; Zhou, L.; Kirkness, E. F.; Peterson, S.; Loftus, B.; Richardson, D.; Dodson, R.; Khalak, H. G.; Glodek, A.; McKenney, K.; Fitzgerald, L. M.; Lee, N.; Adams, M. D.; Hickey, E. K.; Berg, D. E.; Gocayne, J. D.; Utterback, T. R.; Peterson, J. D.; Kelley, J. M.; Cotton, M. D.; Weidman, J. M.; Fujii, C.; Bowman, C.; Watthey, L.; Wallin, E.; Hayes, W. S.; Borodovsky, M.; Karp, P. D.; Smith, H. O.; Fraser, C. M.; Venter, J. C. The complete genome sequence of the gastric pathogen *Helicobacter pylori*. *Nature* **1997**, *388*, 539–547.

10. Cover, T. L.; Blanke, S. R. *Helicobacter pylori* VacA, a paradigm for toxin multifunctionality. *Nat. Rev. Microbiol.* **2005**, *3*, 320–332.

11. Nešić, D.; Buti, L.; Lu, X.; Stebbins, C. E. Structure of the *Helicobacter pylori* CagA

oncoprotein bound to the human tumor suppressor ASPP2. *Proc. Natl. Acad. Sci.* **2014**, *111*, 1562–1567.

12. Kikuchi, K.; Murata-Kamiya, N.; Kondo, S.; Hatakeyama, M. *Helicobacter pylori* stimulates epithelial cell migration via CagA-mediated perturbation of host cell signaling. *Microbes Infect.* **2012**, *14*, 470–476.

13. Saleem, N.; Howden, C. W. Update on the management of *Helicobacter pylori* infection. *Curr. Treat. Options Gastroenterol.* **2020**, *18*, 476-487.

14. Megraud, F.; Coenen, S.; Versporten, A.; Kist, M.; Lopez-Brea, M.; Hirschl, A. M.; Andersen, L. P.; Goossens, H.; Glupczynski, Y. *Helicobacter pylori* resistance to antibiotics in Europe and its relationship to antibiotic consumption. *Gut* **2013**, *62*, 34–42.

15. Gisbert, J. P.; Calvet, X. Review article: rifabutin in the treatment of refractory *Helicobacter pylori* infection. *Aliment. Pharmacol. Ther.* **2012**, *35*, 209–221.

16. Kim, S. Y.; Choi, D. J.; Chung, J.-W. Antibiotic treatment for *Helicobacter pylori*: is the end coming? *World J. Gastrointest. Pharmacol. Ther.* **2015**, *6*, 183–198.

17. Yang, Z.-M.; Chen, W.-W.; Wang, Y.-F. Gene expression profiling in gastric mucosa from *Helicobacter pylori*-infected and uninfected patients undergoing chronic superficial gastritis. *PLoS One* **2012**, *7*, e33030.

18. McGee, D. J.; Mobley, H. L. Pathogenesis of *Helicobacter pylori* infection. *Curr. Opin. Gastroenterol.* **2000**, *16*, 24–31.

19. Ramarao, N.; Gray-Owen, S. D.; Meyer, T. F. *Helicobacter pylori* induces but survives the extracellular release of oxygen radicals from professional phagocytes using its catalase activity. *Mol. Microbiol.* **2000**, *38*, 103–113.

20. Montecucco, C.; de Bernard, M. Molecular and cellular mechanisms of action of the vacuolating cytotoxin (VacA) and neutrophil-activating protein (HP-NAP) virulence factors of *Helicobacter pylori*. *Microbes Infect.* **2003**, *5*, 715–721.

21. Bonifácio, B. V.; dos Santos Ramos, M. A.; da Silva, P. B.; Bauab, T. M. Antimicrobial activity of natural products against *Helicobacter pylori*: a review. *Ann.*

Clin. Microbiol. Antimicrob. **2014**, *13*, 54.

22. Sivam, G. P. Protection against *Helicobacter pylori* and other bacterial infections by garlic. *J. Nutr.* **2001**, *131*, 1106S–8S.

23. Yanaka, A.; Fahey, J. W.; Fukumoto, A.; Nakayama, M.; Inoue, S.; Zhang, S.; Tauchi, M.; Suzuki, H.; Hyodo, I.; Yamamoto, M. Dietary sulforaphane-rich broccoli sprouts reduce colonization and attenuate gastritis in *Helicobacter pylori*-infected mice and humans. *Cancer Prev. Res.* **2009**, *2*, 353–360.

24. Opekun, A. R.; Yeh, C. W.; Opekun, J. L.; Graham, D. Y. *In vivo* tests of natural therapy, Tibetan yogurt or fresh broccoli, for *Helicobacter pylori* infection. *Methods Find. Exp. Clin. Pharmacol.* **2005**, *27*, 327–329.

25. Asha, M. K.; Debraj, D.; Prashanth, D.; Edwin, J. R.; Srikanth, H. S.; Muruganantham, N.; Dethe, S. M.; Anirban, B.; Jaya, B.; Deepak, M.; Agarwal, A. *In vitro* anti-*Helicobacter pylori* activity of a flavonoid rich extract of *Glycyrrhiza glabra* and its probable mechanisms of action. *J. Ethnopharmacol.* **2013**, *145*, 581–586.

26. Fukai, T.; Marumo, A.; Kaitou, K.; Kanda, T.; Terada, S.; Nomura, T. Anti-*Helicobacter pylori* flavonoids from licorice extract. *Life Sci.* **2002**, *71*, 1449–1463.

27. Kim, J. M.; Zheng, H. M.; Lee, B. Y.; Lee, W. K.; Lee, D. H. Anti-*Helicobacter pylori* Properties of GutGard™. *Prev. Nutr. food Sci.* **2013**, *18*, 104–110.

28. Biagi, M.; Miraldi, E.; Figura, N.; Giachetti, D. Antiradical activity and *in vitro* inhibition of *Helicobacter pylori* by Italian red wines. *Nat. Prod. Commun.* **2009**, *4*, 255–260.

29. Ayala, G.; Escobedo-Hinojosa, W. I.; de la Cruz-Herrera, C. F.; Romero, I. Exploring alternative treatments for *Helicobacter pylori* infection. *World J. Gastroenterol.* **2014**, *20*, 1450–1469.

30. Ruggiero, P.; Tombola, F.; Rossi, G.; Pancotto, L.; Lauretti, L.; Del Giudice, G.; Zoratti, M. Polyphenols reduce gastritis induced by *Helicobacter pylori* infection or VacA toxin administration in mice. *Antimicrob. Agents Chemother.* **2006**, *50*, 2550–2552.

31. Shin, J.-E.; Kim, J.-M.; Bae, E.-A.; Hyun, Y.-J.; Kim, D.-H. *In vitro* inhibitory effect of flavonoids on growth, infection and vacuolation of *Helicobacter pylori*. *Planta Med.* **2005**, *71*, 197–201.
32. Kuropatnicki, A. K.; Szliszka, E.; Krol, W. Historical aspects of propolis research in modern times. *Evid. Based. Complement. Alternat. Med.* **2013**, *2013*, 964149.
33. de Groot, A. C. Propolis: a review of properties, applications, chemical composition, contact allergy, and other adverse effects. *Dermatitis* **2013**, *24*, 263–282.
34. Huang, S.; Zhang, C.-P.; Wang, K.; Li, G. Q.; Hu, F.-L. Recent advances in the chemical composition of propolis. *Molecules* **2014**, *19*, 19610–19632.
35. Omene, C.; Kalac, M.; Wu, J.; Marchi, E.; Frenkel, K.; O'Connor, O. A. Propolis and its active component, caffeic acid phenethyl ester (CAPE), modulate breast cancer therapeutic targets via an epigenetically mediated mechanism of action. *J. Cancer Sci. Ther.* **2013**, *5*, 334–342.
36. Toreti, V. C.; Sato, H. H.; Pastore, G. M.; Park, Y. K. Recent progress of propolis for its biological and chemical compositions and its botanical origin. *Evid. Based. Complement. Alternat. Med.* **2013**, *2013*, 697390.
37. Governa, P.; Cusi, M. G.; Borgonetti, V.; Sforcin, M.; Terrosi, C.; Baini, G.; Miraldi, E.; Biagi, M. Beyond the biological effect of a chemically characterized poplar propolis: antibacterial and antiviral activity and comparison with flurbiprofen in cytokines release by LPS-stimulated human mononuclear cells. *Biomedicines* **2019**, *7*, 73.
38. Tulsani, S. G.; Chikkanarasaiah, N.; Siddaiah, S. B.; Krishnamurthy, N. H. The effect of propolis and xylitol chewing gums on salivary *Streptococcus mutans* count: a clinical trial. *Indian J. Dent. Res.* **2014**, *25*, 737–741.
39. Boukraâ, L.; Sulaiman, S. A. Rediscovering the antibiotics of the hive. *Recent Pat. Antiinfect. Drug Discov.* **2009**, *4*, 206–213.
40. Haghdoost, N. S.; Salehi, T. Z.; Khosravi, A.; Sharifzadeh, A. Antifungal activity and influence of propolis against germ tube formation as a critical virulence attribute by clinical isolates of *Candida albicans*. *J. Mycol. Med.* **2016**, *26*, 298–305.

41. Freires, I. A.; Queiroz, V. C. P. P.; Furletti, V. F.; Ikegaki, M.; de Alencar, S. M.; Duarte, M. C. T.; Rosalen, P. L. Chemical composition and antifungal potential of Brazilian propolis against *Candida* spp. *J. Mycol. Med.* **2016**, *26*, 122–132.
42. Mirzoeva, O. K.; Grishanin, R. N.; Calder, P. C. Antimicrobial action of propolis and some of its components: the effects on growth, membrane potential and motility of bacteria. *Microbiol. Res.* **1997**, *152*, 239–246.
43. Speciale, A.; Costanzo, R.; Puglisi, S.; Musumeci, R.; Catania, M. R.; Caccamo, F.; Iauk, L. Antibacterial activity of propolis and its active principles alone and in combination with macrolides, beta-lactams and fluoroquinolones against microorganisms responsible for respiratory infections. *J. Chemother.* **2006**, *18*, 164–171.
44. Viuda-Martos, M.; Ruiz-Navajas, Y.; Fernández-López, J.; Pérez-Alvarez, J. A. Functional properties of honey, propolis, and royal jelly. *J. Food Sci.* **2008**, *73*, R117–24.
45. Medić-Sarić, M.; Rastija, V.; Bojić, M.; Males, Z. From functional food to medicinal product: systematic approach in analysis of polyphenolics from propolis and wine. *Nutr. J.* **2009**, *8*, 33.
46. Armutcu, F.; Akyol, S.; Ustunsoy, S.; Turan, F. F. Therapeutic potential of caffeic acid phenethyl ester and its anti-inflammatory and immunomodulatory effects (review). *Exp. Ther. Med.* **2015**, *9*, 1582–1588.
47. Fu, Q.; Gao, Y.; Zhao, H.; Wang, Z.; Wang, J. Galangin protects human rheumatoid arthritis fibroblast-like synoviocytes via suppression of the NF- κ B/NLRP3 pathway. *Mol. Med. Rep.* **2018**, *18*, 3619–3624.
48. Al-Abd, N. M.; Kassim, M.; Zajmi, A. The inhibitory effect of galangin on cytokines and nitric oxide in microglia BV2 cell line. *Malaysian J. Sci.* **2017**, *36*, 145–156.
49. Lee, H. N.; Shin, S. A.; Choo, G. S.; Kim, H. J.; Park, Y. S.; Kim, B. S.; Kim, S. K.; Cho, S. D.; Nam, J. S.; Choi, C. S.; Che, J. H.; Park, B. K.; Jung, J. Y. Anti-inflammatory effect of quercetin and galangin in LPS-stimulated RAW264.7

macrophages and DNCB-induced atopic dermatitis animal models. *Int. J. Mol. Med.* **2018**, *41*, 888–898.

50. Lu, H.; Yao, H.; Zou, R.; Chen, X.; Xu, H. Galangin suppresses renal inflammation via the inhibition of NF- κ B, PI3K/AKT and NLRP3 in uric acid treated NRK-52E tubular epithelial cells. *Biomed Res. Int.* **2019**, *2019*, 3018357.

51. Zhao, D.; Liu, Z.; Ding, J.; Li, W.; Sun, Y.; Yu, H.; Zhou, Y.; Zeng, J.; Chen, C.; Jia, J. *Helicobacter pylori* CagA upregulation of CIP2A is dependent on the Src and MEK/ERK pathways. *J. Med. Microbiol.* **2010**, *59*, 259–265.

52. Asim, M.; Chaturvedi, R.; Hoge, S.; Lewis, N. D.; Singh, K.; Barry, D. P.; Algood, H. S.; de Sablet, T.; Gobert, A. P.; Wilson, K. T. *Helicobacter pylori* induces ERK-dependent formation of a phospho-c-Fos c-Jun activator protein-1 complex that causes apoptosis in macrophages. *J. Biol. Chem.* **2010**, *285*, 20343–20357.

53. Sun, C.; Wu, Z.; Wang, Z.; Zhang, H. Effect of ethanol/water solvents on phenolic profiles and antioxidant properties of beijing propolis extracts. *Evid. Based Complement. Alternat. Med.* **2015**, *2015*, 595393.

54. Biagi, M.; Miraldi, E.; Figura, N.; Magnano, A. R.; Ierardi, G.; Manca, D.; Corsini, M.; Barlozzini, B.; Mannari, C.; Stiaccini, G.; Sodano, S.; Giachetti, D. Gastroprotective and anti *Helicobacter pylori* activities of propolis. *Planta Med* **2011**, *77*, PM75.

55. Coelho, L. G. V.; Bastos, E. M. A. F.; Resende, C. C.; Paula e Silva, C. M.; Sanches, B. S. F.; de Castro, F. J.; Moretzsohn, L. D.; Vieira, W. L. dos S.; Trindade, O. R. Brazilian green propolis on *Helicobacter pylori* infection. A pilot clinical study. *Helicobacter* **2007**, *12*, 572–574.

56. Collodel, G.; Moretti, E.; Del Vecchio, M. T.; Biagi, M.; Cardinali, R.; Mazzi, L.; Brecchia, G.; Maranesi, M.; Manca, D.; Castellini, C. Effect of chocolate and Propolfenol on rabbit spermatogenesis and sperm quality following bacterial lipopolysaccharide treatment. *Syst. Biol. Reprod. Med.* **2014**, *60*, 217–226.

57. Alminger, M.; Aura, A. M.; Bohn, T.; Dufour, C.; El, S. N.; Gomes, A.; Karakaya, S.; Martínez-Cuesta, M. C.; Mcdougall, G. J.; Requena, T.; Santos, C. N. *In vitro* models

for studying secondary plant metabolite digestion and bioaccessibility. *Compr. Rev. Food Sci. Food Saf.* **2014**, *13*, 413–436.

58. Governa, P.; Biagi, M. *Copaifera langsdorffii* Desf .: *in vitro* investigation on anti-*Helicobacter pylori* and anti-inflammatory activities of oleoresin and fruit methanolic extract. *Plant Biosyst.* **2020**, *154*, 117–124.

59. Berthelot, M. P. Berthelot's Reaction Mechanism. *Rep. Chim. Appl.* **1859**, *1*, 2884.

60. Berman, H. M.; Westbrook, J.; Feng, Z.; Gilliland, G.; Bhat, T. N.; Weissig, H.; Shindyalov, I. N.; Bourne, P. E. The Protein Data Bank. *Nucleic Acids Res.* **2000**, *28*, 235–242.

61. Morris, G. M.; Ruth, H.; Lindstrom, W.; Sanner, M. F.; Belew, R. K.; Goodsell, D. S.; Olson, A. J. AutoDock4 and AutoDockTools4: Automated docking with selective receptor flexibility. *J. Comput. Chem.* **2009**, *30*, 2785–2791.

62. Forli, S.; Huey, R.; Pique, M. E.; Sanner, M. F.; Goodsell, D. S.; Olson, A. J. Computational protein–ligand docking and virtual drug screening with the AutoDock suite. *Nat. Protoc.* **2016**, *11*, 905–919.

63. Gasteiger, J.; Marsili, M. Iterative partial equalization of orbital electronegativity—a rapid access to atomic charges. *Tetrahedron* **1980**, *36*, 3219–3228.

64. Sterling, T.; Irwin, J. J. ZINC 15 - ligand discovery for everyone. *J. Chem. Inf. Model.* **2015**, *55*, 2324–2337.

65. O'Boyle, N. M.; Banck, M.; James, C. A.; Morley, C.; Vandermeersch, T.; Hutchison, G. R. Open Babel: an open chemical toolbox. *J. Cheminform.* **2011**, *3*, 33.

66. Olegário, L. S.; Andrade, J. K. S.; Andrade, G. R. S.; Denadai, M.; Cavalcanti, R. L.; da Silva, M. A. A. P.; Narain, N. Chemical characterization of four Brazilian brown propolis: an insight in tracking of its geographical location of production and quality control. *Food Res. Int.* **2019**, *123*, 481–502.

67. He, M.; Wu, T.; Pan, S.; Xu, X. Antimicrobial mechanism of flavonoids against *Escherichia coli* ATCC 25922 by model membrane study. *Appl. Surf. Sci.* **2014**, *305*, 515–521.

68. Celli, J. P.; Turner, B. S.; Afdhal, N. H.; Keates, S.; Ghiran, I.; Kelly, C. P.; Ewoldt, R. H.; McKinley, G. H.; So, P.; Erramilli, S.; Bansil, R. *Helicobacter pylori* moves through mucus by reducing mucin viscoelasticity. *Proc. Natl. Acad. Sci. U. S. A.* **2009**, *106*, 14321–14326.
69. Xiao, Z.-P.; Wang, X.-D.; Peng, Z.-Y.; Huang, S.; Yang, P.; Li, Q.-S.; Zhou, L.-H.; Hu, X.-J.; Wu, L.-J.; Zhou, Y.; Zhu, H.-L. Molecular docking, kinetics study, and structure-activity relationship analysis of quercetin and its analogous as *Helicobacter pylori* urease inhibitors. *J. Agric. Food Chem.* **2012**, *60*, 10572–10577.

CHAPTER 5

Effect of *in vitro* simulated digestion on the antioxidant activity of different *Camellia sinensis* (L.) Kuntze leaves extracts

5.1. Introduction

Camellia sinensis (L.) Kuntze leaves have been used for centuries to produce tea. Once harvested, differences in the manufacturing process of *C. sinensis* leaves lead to different kind of tea, with green, black and Oolong tea being the most used worldwide [1]. In particular, green tea is produced by using freshly harvested leaves, which are immediately steamed or pan-fried to prevent polyphenols oxidation, thus, inhibiting fermentation. Differently, black and Oolong tea are typically produced using fully and semi-fermented withered rolled leaves, respectively [2]. Tea is one of the most popular antioxidants and its effectiveness, together with the effectiveness of its main constituents, has been observed in several *in vitro* and *in vivo* models [3–5].

The composition of *C. sinensis* leaves has been deeply investigated. Among the bioactive components of tea, flavan-3-ols (catechins), a group of phenolic compounds, are the most abundant [6]. They can be found as flavonol monomers (i.e. catechins, epicatechin) and as flavonol gallates (i.e. epigallocatechin gallate) and their content varies during the fermentation process, due to oxidation or condensation [7]. Epigallocatechin-3-gallate (EGCG) is the most abundant flavan-3-ol in the majority of tea variety. In addition, other polyphenols, such as gallic acid, chlorogenic acid, ellagic acid and flavonoids have been reported, with gallic acid being the most common. Theaflavins are present in smaller amount in fermented teas [8]. Caffeine is another characteristic component of tea and is present in considerable amount in tea, almost regardless of the variety [9].

The effect of gastrointestinal digestion on different tea polyphenols has been reported recently [10]. Moreover, the bioaccessibility and bioavailability of tea catechins have been demonstrated to be modulated by the co-administration of food

and common beverage additives such as citric acid, ascorbic acid, milk and citrus juice [11,12]. Also, tea and EGCG were found to modulate the stability of other food ingredients, such as soybean emulsion and starch, to digestion [13–15]. Simulated digestion has been observed to influence the antimicrobial activity of green tea [16]. The changes in the secretion of cholecystokinin and glucagon-like peptide induced by green tea *in vitro* was also found to be modulated by simulated digestion [17]. Nevertheless, information regarding the effect of digestion on biological properties of tea, such as the antioxidant activity, is lacking.

The complexity of tea composition may influence the stability of its constituents upon gastrointestinal digestion, thus, affecting the antioxidant activity, and this effect can differ based on the kind of tea used.

To verify this hypothesis, we performed *in vitro* simulated gastrointestinal digestion on different *C. sinensis* leaves infusions and we evaluated the influence of digestion on the antioxidant activity of tea using a validated cell free method and an *in vitro* model of intestinal epithelial cells.

5.2. Materials and methods

5.2.1. Sample preparation and chemical analysis

Green, black and Oolong tea leaves were purchased from Erbamea (San Giustino, Perugia, Italy). 3 g of leaves were extracted with 30 mL of ultrapure double-distilled water (DER 1:10) at 90 °C for 10 min. Green tea extract (GTE), black tea extract (BTE) and Oolong tea extract (OTE) were then filtered and their chemical characterization was performed by means of HPLC-DAD, using a Shimadzu Prominence LC 2030 3D instrument. A Bondpak® C18 column, 10 µm, 125 Å, 3.9 mm x 300 mm (Waters Corporation), was used as stationary phase. The mobile phase was composed of water with 0.1% V/V formic acid (A) and acetonitrile with 0.1% V/V formic acid (B), using the following gradient phases: B from 10% at 0 min to 25% at 15 min and then from 25% to 35% at 18 min and from 35% to 50% at 25 min. The flux was set to 0.8 mL/min and the injected volume was 10 µL. Absorbance was recorded at 280 nm

and calibration curves using gallic acid, (+)-catechin, caffeine, (-)-epicatechin and EGCG as reference standards (Sigma-Aldrich), ranging from 0.008 to 0.5 mg/mL ($R^2 > 0.99$), were used to quantify the amount of teas constituents.

The total phenolic content (TPC) was evaluated with the Folin-Ciocalteu method, as previously described [18].

5.2.2. *In vitro simulated digestion*

In vitro simulated digestion was carried out as previously described [19], with some modifications. Briefly, GTE, BTE and OTE (diluted 1:20) and reference standards (1 mg/mL) were suspended in 20 mL of simulated gastric juice, containing pepsin from porcine gastric mucosa (300 UI/mL, Sigma-Aldrich) and NaCl (10 mg/mL). The pH of the solution was adjusted to 1.7 using HCl. Samples were incubated for 2 h at 37 °C with shaking. Then, pancreatin from porcine pancreas (10 mg/mL, Sigma-Aldrich) and bile salts mixture (20 mg/mL, Sigma-Aldrich) were added and the pH was increased by adding Na₂CO₃ (15 mg/mL, Sodalco S.p.A.) to simulate the intestinal environment. Intestinal digestion was carried out for 2 h at 37 °C with shaking. Samples were then filtered and immediately used for further analysis.

5.2.3. *DPPH test*

The radical scavenging activity of the pre- and post-digestion samples was measured by means of the 2,2-diphenyl-1-picrylhydrazyl (DPPH) assay, as previously reported [20]. Briefly, 10 µL of different concentrations (10-0.16 mg/mL) of the samples were added to 190 µL of freshly prepared methanolic DPPH solution (0.1 mM) and incubated for 30 min at rt in the dark with shaking. Then, absorbance was recorded at 517 nm using a Victor® Nivo™ plate reader (PerkinElmer). ddH₂O was used as the blank control. The antiradical activity of the samples was calculated according to the following formula (Eq. 5.1):

$$\text{Antiradical activity \%} = \frac{(Abs_{blank} - Abs_{sample})}{Abs_{blank}} \times 100$$

Data were plotted using Microsoft Excel and the IC₅₀ (µg/mL) was determined for each sample.

5.2.4. Cell culture

Intestinal epithelial cells (Caco-2), a kind gift from Prof. Monica Montopoli (University of Padua, Italy) were cultured in 25 cm² flasks (Sarstedt, Verona, Italy) in high glucose Dulbecco's modified Eagle's medium (DMEM, Sigma-Aldrich), supplemented with 10% heat-inactivated fetal bovine serum (FBS, Sigma-Aldrich), 1% glutamine (Sigma-Aldrich) and 1% penicillin/streptomycin solution (Sigma-Aldrich). EDTA-trypsin (Sigma-Aldrich) solution was used for detaching cells from flasks, and cell counting was performed using a hemocytometer by Trypan Blue staining.

5.2.5. Evaluation of the antioxidant activity

Caco-2 cells (1×10^4) were seeded into 96-well plates and allowed to grow to confluence (70-80%). Cells were then pre-treated overnight with pre- and post-digestion GTE, BTE and OTE (diluted 1:1000, according to previously performed cell viability assays) and oxidative stress was induced by administering 5 mM hydrogen peroxide (H₂O₂) for 6 h. Medium were then removed, and cells were washed three times with phosphate buffered saline (PBS). Then, 100 μ L of Cell Counting Kit (CCK-8, Sigma-Aldrich) solution (1:100 in RPMI without phenol red) was added to each well and incubated for 1 h at 37 °C. Absorbance was recorded at 450 nm using a Victor® Nivo™ plate reader (PerkinElmer). Treatments were performed in sextuplicate in three independent experiments, and cell viability was calculated by normalizing the absorbance of the test wells to the untreated control.

5.2.6. Measurement of trans-epithelial electric resistance

The efficiency of the intestinal barrier functions was evaluated by measuring trans-epithelial electric resistance (TEER) using a voltmeter [21]. Caco-2 cells (8×10^5) were placed in transparent polyester membrane cell culture inserts with 0.4 μ m pore size (Sarstedt) as previously described [22]. Culture medium was replaced every other day. The integrity of the cell monolayers was monitored by measuring the TEER of the monolayer from day 14th to day 21st after seeding. When a stable value was reached, a 12 h pre-treatment was done by adding pre- and post-digested samples (diluted 1:1000) in the apical chamber in appropriate wells and TEER was measured after 0

and 12 h. Then, 0.5 mM H₂O₂ was added to the basal chamber and TEER was measured after 0, 4, 8, and 24 h. TEER measurements were performed in HBSS with 10 mM 4-(2-hydroxyethyl)-1-piperazineethanesulfonic acid (HEPES) and 10 mM D-glucose (pH = 7.4), after an equilibration period at rt, using a Millicell® ERS meter, (Millipore Corporation, Bedford, MA) connected to a pair of chopstick electrodes. Only cells with TEER value within 360 - 500 Ω x cm² were used for the experiments [23,24]. Treatments were performed in duplicate in three independent experiments and TEER was expressed as percentage of resistance, normalized to initial value.

5.2.7. DPPH-HPLC-DAD analysis

The DPPH-HPLC-DAD analysis was performed as described elsewhere [25]. Briefly, 100 μL of each sample were added to 300 μL of 10 mM DPPH solution and incubated for 30 min at rt in the dark, with shaking. Samples were then filtered and analyzed by means of HPLC-DAD, using the same chromatographic conditions described in the “*Sample preparation and chemical analysis*” paragraph.

5.2.8. Statistical analysis

The statistical differences between the biological results were determined by ANOVA. Pearson correlation test was used to analyze the correlation between TPC and DPPH. Values are expressed in the range of +/- standard deviation and $p < 0.05$ was considered statistically significant. Graphs and calculations were performed using GraphPad Prism.

5.3. Results and discussion

5.3.1. Chemical analysis

By comparison with reference standards retention time (RT) and UV spectra, we identified gallic acid (RT = 4.5 min), (+)-catechin (RT = 7.2 min), caffeine (RT = 8.3 min) and EGCG (RT = 10.4 min) in each sample. (-)-epicatechin (RT = 9.0 min) was quantifiable only in GTE.

The chemical characterization of the samples is reported in table 5.1. BTE and OTE contain comparable amount of gallic acid and (+)-catechin, whereas EGCG was significantly higher in BTE. The amount of gallic acid and (+)-catechin was lower in GTE, compared to the other two samples. On the contrary, a significantly higher presence of EGCG was found in GTE, compared to the other samples. (-)-epicatechin was quantifiable only in GTE, whereas caffeine content was comparable in each sample.

Table 5.1. Chemical characterization of the extracts. Values (mg/mL) are expressed as mean \pm standard deviation.

Sample	TPC	Gallic acid	(+)-catechin	Caffeine	(-)-epicatechin	EGCG
GTE	6.23 \pm 0.11	0.25 \pm 0.01	0.28 \pm 0.01	1.68 \pm 0.01	1.20 \pm 0.01	2.30 \pm 0.04
BTE	5.21 \pm 0.29	0.57 \pm 0.02	0.47 \pm 0.02	1.70 \pm 0.03	n.d.	1.56 \pm 0.04
OTE	3.84 \pm 0.53	0.51 \pm 0.02	0.37 \pm 0.01	1.58 \pm 0.20	n.d.	0.22 \pm 0.01

5.3.2. Stability of tea constituents under *in vitro* simulated digestion

Stability of tea constituents resulted to be highly influenced by *in vitro* simulated digestion (table 5.2). Indeed, the recovery of flavan-3-ols, tested as single reference standards, after the digestion process was very low, with EGCG being the most affected among the three flavan-3-ols tested. These data are consistent with that obtained by Krook & Hagerman (2012), who observed that, despite being stable at acidic pH similar to that of the stomach, 90% of EGCG was decomposed after intestinal digestion. Similarly, Yoshino and colleagues found that 80% of EGCG was already decomposed after 5 min in authentic intestinal juice [26]. In our work, we employed longer incubation time than the one used in these two studies (i.e., 4 h, compared to 2 h and 5 min, respectively), which explain why we observed a much more evident reduction of EGCG. Interestingly, (-)-epicatechin was reported to be more stable than EGCG at pH=7 [27], with a recovery of 90% after 17 h. We found that, although being higher than that of EGCG, the recovery of (+)-catechin and (-)-epicatechin after the whole gastrointestinal digestion process were 27.29% and 13.13%, respectively. Gallic acid recovery was also low and comparable to that of (-)-epicatechin. Caffeine was completely recovered, suggesting a very high stability to gastrointestinal digestion.

Table 5.2. Relative gastrointestinal stability of reference standards. Values (%) are expressed as mean \pm standard deviation.

Chemical classification	Sample	Gastrointestinal stability
Flavan-3-ols	(+)-catechin	27.29 \pm 0.49
	(-)-epicatechin	13.13 \pm 0.24
	EGCG	0.25 \pm 0.09
Phenolic acids	gallic acid	14.16 \pm 3.98
Xanthines	caffeine	98.77 \pm 4.87

The TPC recovery was also significantly reduced by the gastrointestinal digestion, with GTE showing the higher stability (figure 5.1A). Indeed, GTE, BTE and OTE relative gastrointestinal stability was 61.29% \pm 6.45%, 55.77% \pm 7.69% and 42.11% \pm 2.63%, with OTE recovery being significantly lower in comparison to GTE. Interestingly, teas phytocomplex protected flavan-3-ols and gallic acid from the degradation (figure 5.1B). Indeed, (+)-catechin recovery after simulated digestion was approximately 100 % in BTE and OTE and approximately 160% in GTE. (-)-epicatechin was not found in BTE and OTE, thus, its stability to digestion in BTE and OTE was not observable. However, in GTE, (-)-epicatechin completely disappeared after simulated digestion. A possible explanation of the increased recovery of (+)-catechin in digested GTE may be related to the partial degradation of flavan-3-ols oligomers and conversion of (-)-epicatechin to catechin, which may occur in aqueous solution as a consequence of temperature and pH changes [28]. The gastrointestinal stability of EGCG was found to depend on the tea sample, suggesting that different phytocomplex may specifically influence its recovery after digestion. Indeed, EGCG recovery was approximately 65%, 15% and 42% in GTE, BTE and OTE, respectively, with BTE being significantly lower compared to GTE and OTE. Interestingly, the relative recovery of EGCG contained in the test teas was always significantly higher compared to the reference standard alone. Similarly, gallic acid stability to digestion was different for each sample, with BTE resulting in the highest recovery and OTE in the lowest. The increased recovery of gallic acid in teas, compared to the reference standard alone, may result from the hydrolysis of the galloyl moiety from galloyl catechins such as catechin-gallate, gallocatechin-gallate, epicatechin-3-gallate and EGCG [29]. Consistently with this explanation, in fact, the recovery of gallic acid is increased in BTE, which had a lower recovery of EGCG. Similarly to its reference

standard, caffeine recovery was around 100% in each tea sample. Interestingly, caffeine has been demonstrated to modulate the oral bioavailability of EGCG in humans: beverages containing higher amount of EGCG than caffeine showed higher EGCG bioavailability compared to those containing higher amount of caffeine than EGCG [30]. These observations are consistent with our results in which GTE, which contained more EGCG than caffeine, showed a higher gastrointestinal stability of EGCG in comparison to BTE, which have similar amount of EGCG and caffeine, and to OTE, which contained more caffeine than EGCG.

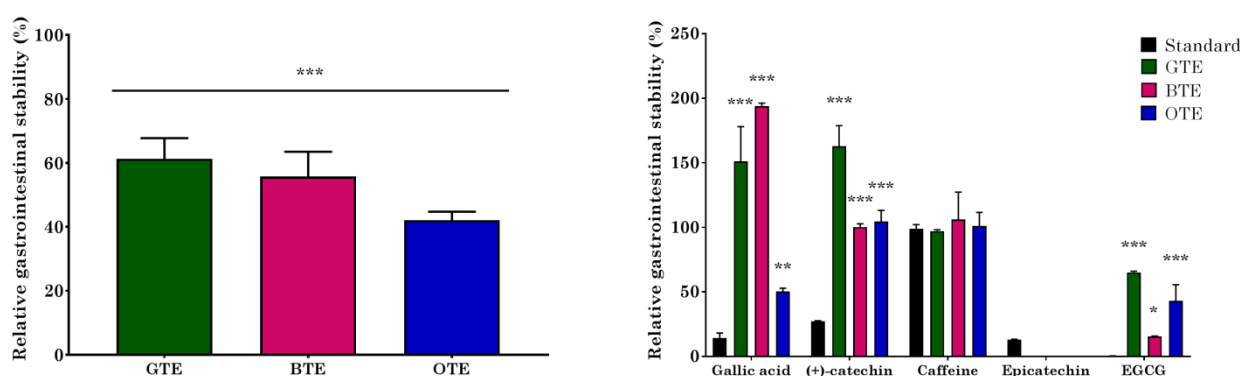


Figure 5.1. Relative gastrointestinal stability of GTE, BTE and OTE TPC (A) and main constituents (B). * $p < 0.05$ vs reference standard; ** $p < 0.01$ vs reference standard; * $p < 0.001$ vs reference standard; ° $p < 0.05$ vs GTE.**

5.3.3. The antioxidant activity of teas is reduced by digestion

The DPPH test was used as a fast and simple method to evaluate the effect of gastrointestinal digestion on the antioxidant activity of teas. The radical scavenging potential of pre-digestion samples (expressed as IC_{50} values in table 5.3) was less than 60 $\mu\text{g/mL}$, with GTE being the most active. Simulated digestion significantly increased the IC_{50} values of GTE, BTE and OTE by 2.3-, 9.6- and 5.5-fold, respectively, thus suggesting a negative effect of digestion on antioxidant potential.

The Pearson correlation test between the DPPH/TPC ratio of the samples before and after gastrointestinal digestion showed a good, though not statistically significant, correlation ($r = 0.99$, $p = 0.062$). Similarly, a strong correlation ($r = 0.99$, $p = 0.071$) was found between the DPPH/TPC ratio of the undigested and digested samples.

Table 5.3. IC₅₀ values (µg/mL) resulting from DPPH test performed before and after *in vitro* simulated digestion.

Sample	Pre-digestion	Post-digestion
GTE	74.5 ± 8.4	176.0 ± 14.1
BTE	122.8 ± 12.3	1176.2 ± 151.1
OTE	597.1 ± 56.3	3277.2 ± 19.7

By combining pre-column DPPH assay with HPLC-DAD analysis, it was possible to observe which of the identified teas constituent is predominantly involved in the radical scavenging activity of the samples. Indeed, upon reaction with DPPH, the peak of the anti-radical compounds should decrease or disappear in the HPLC-DAD chromatogram [25,31,32]. Figure 5.2 shows the complete disappearance of peaks area corresponding to gallic acid, (+)-catechin, (-)-epicatechin and EGCG, thus suggesting their pivotal role for the antioxidant activity of teas. Differently, caffeine peak was smaller but still present in the post-DPPH, compared to the pre-DPPH chromatogram (approximately -25% of the peak area).

In GTE, only EGCG recovery was significantly lower after simulated digestion, compared to the other tested constituents. This result, combined with the increased level of gallic acid and (+)-catechin, may account for the relatively small increase in DPPH IC₅₀. EGCG stability in BTE was the most affected by simulated digestion among the three different samples. This is consistent with the increase in DPPH IC₅₀, which is the highest, compared to the other teas. OTE can be distinguished from the other teas, because of the strong reduction of gallic acid levels after simulated digestion. EGCG, however, was more stable compared to BTE, thus explaining why the DPPH IC₅₀ was less affected, in terms of fold changes, compared to BTE, but more affected compared to GTE.

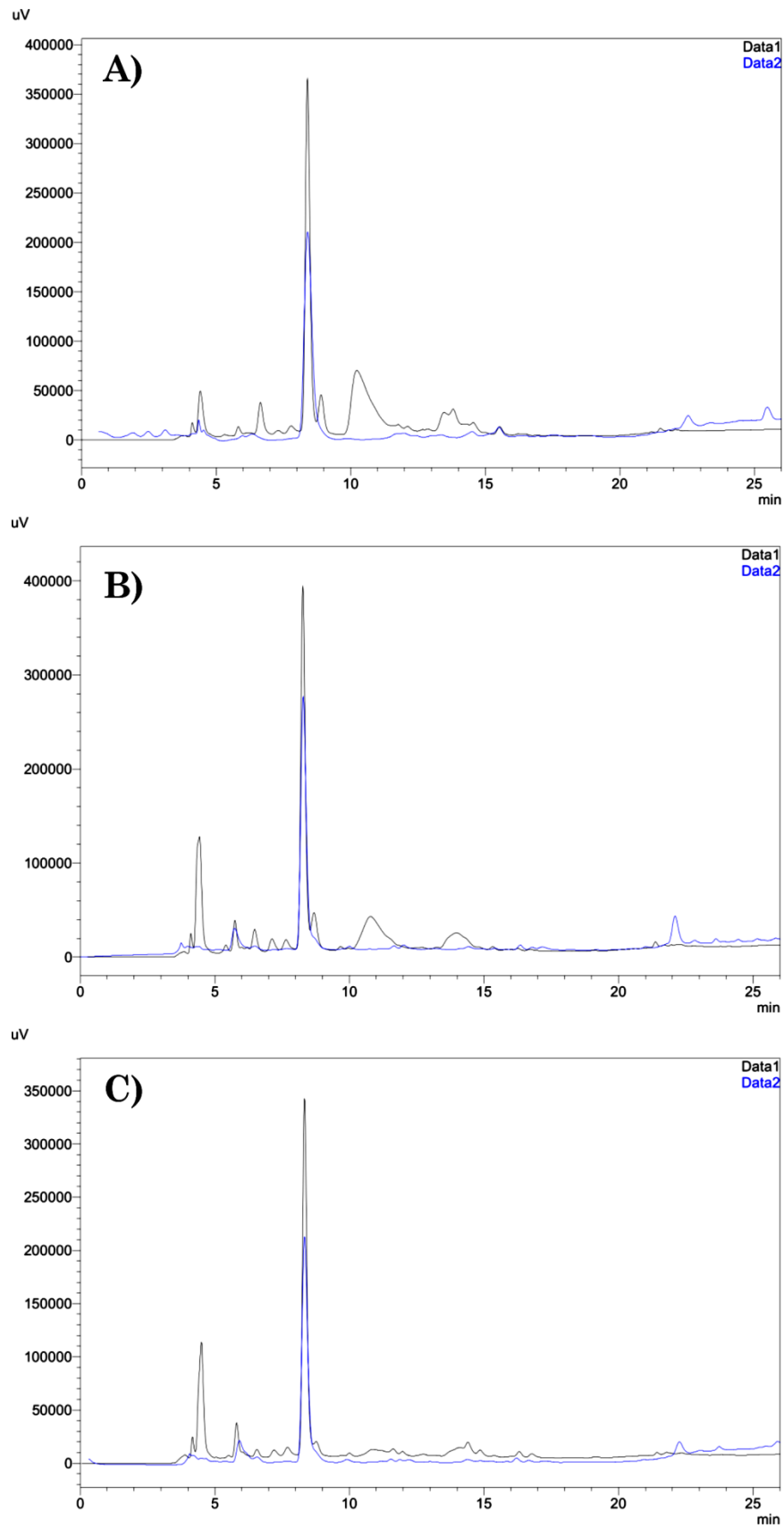


Figure 5.2. HPLC-DAD chromatograms of GTE (A), BTE (B) and OTE (C), before (black) and after (blue) DPPH addition, showing the almost complete oxidation of flavan-3-ols and gallic acid. Caffeine is still present in significant amount.

Caco-2 cells have been used as a stable and reliable model of intestinal epithelium [33,34]. 5 mM H₂O₂ induced a significant oxidative damage to Caco-2 cells, reducing cell viability by approximately 20% compared to the untreated control after 6 h. The pre-treatment with GTE, BTE and OTE significantly protected Caco-2 cells from the cytotoxic effect of H₂O₂, with GTE being the most active extract. The antioxidant activity, in terms of Caco-2 protection, of GTE after *in vitro* digestion was slightly reduced compared to the pre-digestion sample, although the difference was not statistically significant. On the contrary, BTE and OTE activity was significantly reduced after simulated digestion, with OTE completely losing its protective effect (figure 5.3A). Consistently, the prolonged stimulation with lower concentration of H₂O₂ (0.5 mM) caused a time-dependent alteration of the intestinal barrier integrity, with transepithelial electrical resistance values being reduced by approximately 45% after 24 h. GTE, BTE and OTE significantly reduced the oxidative damage provoked by H₂O₂, with similar effectiveness compared to the cell viability test. The protection from the H₂O₂-impaired intestinal barrier integrity of each sample was reduced after simulated digestion, even if statistical significance was obtained only for OTE (figure 5.3B).

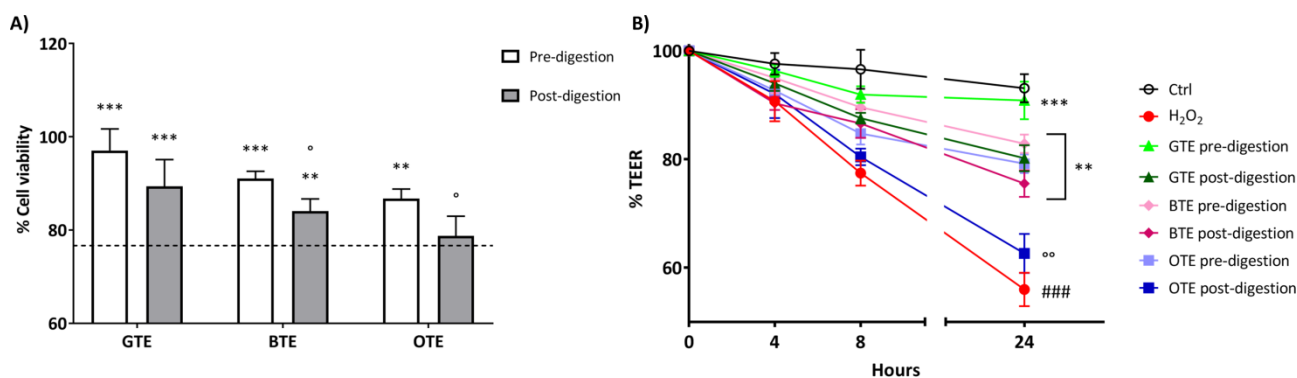


Figure 5.3. Effect of simulated digestion on the antioxidant activity of GTE, BTE and OTE in Caco-2 cells. (A): protection from H₂O₂-impaired cell viability. Data are expressed as percentage of cell viability compared to untreated cells. The effect of H₂O₂ is represented by the dashed line. (B): protection of the intestinal barrier function observed by transepithelial electrical resistance measurement. ### $p < 0.001$ vs untreated control; ** $p < 0.01$ vs stimulus; * $p < 0.001$ vs stimulus; ° $p < 0.05$ vs pre-digestion sample; °° $p < 0.01$ vs pre-digestion sample.**

Contrarily to the DPPH assay, the results obtained in the cell-based experiments suggest that the reduction of Caco-2 protection from the oxidative damage is not directly dependent on the degree of stability of teas main constituents alone, but rather depends on the original amount of antioxidant constituents (i.e. TPC) in the pre-digestion samples. Indeed, in the cell viability assay, the post-digestion antioxidant activity was reduced by 7%, 8% and 10% in GTE, BTE and OTE, respectively, compared to the pre-digestion samples. Moreover, in the TEER experiment, the post-digestion protection of the intestinal barrier integrity was reduced by 14%, 7% and 23% in GTE, BTE and OTE, respectively, compared to the pre-digestion samples.

5.4. Conclusion

Phenolic compounds are a major class of phytochemicals with known antioxidant properties. In this study, the effect of *in vitro* simulated gastrointestinal digestion on the antioxidant effect of three different *C. sinensis* extracts was evaluated.

The stability of teas main constituents was found to be influenced by the initial extract composition, with TPC being more stable in extract containing them in higher amount. EGCG degradation correlated well with changes in the DPPH inhibition assay, thus confirming its pivotal role in the antioxidant activity of tea. Differently, the antioxidant effect in the *in vitro* cell-based model was much more related to the initial TPC content of the extracts, with green tea being more effective than black tea and oolong tea.

Overall, gastrointestinal digestion was found to strongly affect the biological effectiveness of teas. Interestingly, the stability of teas antioxidant constituents was different when using teas extract, compared to the reference compound alone, thus, suggesting a protective role of the phytocomplex, which could lead to increased biological effectiveness.

In conclusion, the effect of gastrointestinal digestion should be taken into account when evaluating the biological properties of herbal extracts, as this may be different from one extract to another and information on the stability of active constituents during the digestion process cannot be extrapolated from data obtained using single compounds.

5.5. References

1. Zhang, L.; Ho, C.-T.; Zhou, J.; Santos, J. S.; Armstrong, L.; Granato, D. Chemistry and biological activities of processed *Camellia sinensis* Teas: a comprehensive review. *Compr. Rev. Food Sci. Food Saf.* **2019**, *18*, 1474–1495.
2. Hayat, K.; Iqbal, H.; Malik, U.; Bilal, U.; Mushtaq, S. Tea and its consumption: benefits and risks. *Crit. Rev. Food Sci. Nutr.* **2015**, *55*, 939–954.
3. Prasanth, M. I.; Sivamaruthi, B. S.; Chaiyasut, C.; Tencomnao, T. A review of the role of green tea (*Camellia sinensis*) in antiphotaging, stress resistance, neuroprotection, and autophagy. *Nutrients* **2019**, *11*, 474.
4. Song, J.-L.; Gao, Y. Effects of methanolic extract form Fuzhuan brick-tea on hydrogen peroxide-induced oxidative stress in human intestinal epithelial adenocarcinoma Caco-2 cells. *Mol. Med. Rep.* **2014**, *9*, 1061–1067.
5. Chen, T.; Yang, Y.; Zhu, S.; Lu, Y.; Zhu, L.; Wang, Y.; Wang, X. Inhibition of A β aggregates in Alzheimer's disease by epigallocatechin and epicatechin-3-gallate from green tea. *Bioorg. Chem.* **2020**, *105*, 104382.
6. de Mejia, E. G.; Ramirez-Mares, M. V.; Puangpraphant, S. Bioactive components of tea: cancer, inflammation and behavior. *Brain. Behav. Immun.* **2009**, *23*, 721–731.
7. Chaturvedula, V. S. P.; Prakash, I. The aroma, taste, color and bioactive constituents of tea. *J. Med. Plants Res.* **2011**, *5*, 2110–2124.
8. Tang, G.-Y.; Meng, X.; Gan, R.-Y.; Zhao, C.-N.; Liu, Q.; Feng, Y.-B.; Li, S.; Wei, X.-L.; Atanasov, A. G.; Corke, H.; Li, H.-B. Health functions and related molecular

mechanisms of tea components: an update review. *Int. J. Mol. Sci.* **2019**, *20*, 6196.

9. Gramza-Michalowska, A. Caffeine in tea *Camellia sinensis* - content, absorption, benefits and risks of consumption. *J. Nutr. Health Aging* **2014**, *18*, 143–149.

10. Annunziata, G.; Maisto, M.; Schisano, C.; Ciampaglia, R.; Daliu, P.; Narciso, V.; Tenore, G. C.; Novellino, E. Colon bioaccessibility and antioxidant activity of white, green and black tea polyphenols extract after *in vitro* simulated gastrointestinal digestion. *Nutrients* **2018**, *10*, 1711.

11. Green, R. J.; Murphy, A. S.; Schulz, B.; Watkins, B. A.; Ferruzzi, M. G. Common tea formulations modulate *in vitro* digestive recovery of green tea catechins. *Mol. Nutr. Food Res.* **2007**, *51*, 1152–1162.

12. Choi, E.-H.; Lee, D.-Y.; Kim, S.; Chung, J.-O.; Choi, J.-K.; Joo, K.-M.; Jeong, H. W.; Kim, J. K.; Kim, W. G.; Shim, S.-M. Influence of flavonol-rich excipient food (onion peel and *Dendropanax morbifera*) on the bioavailability of green tea epicatechins *in vitro* and *in vivo*. *Food Funct.* **2017**, *8*, 3664–3674.

13. Fu, T.; Niu, L.; Li, Y.; Li, D.; Xiao, J. Effects of tea products on *in vitro* starch digestibility and eating quality of cooked rice using domestic cooking method. *Food Funct.* **2020**.

14. Li, X.; Li, S.; Chen, M.; Wang, J.; Xie, B.; Sun, Z. (-)-Epigallocatechin-3-gallate (EGCG) inhibits starch digestion and improves glucose homeostasis through direct or indirect activation of PXR/CAR-mediated phase II metabolism in diabetic mice. *Food Funct.* **2018**, *9*, 4651–4663.

15. Ding, J.; Xu, Z.; Qi, B.; Jiang, L.; Sui, X. Physicochemical and oxidative stability of a soybean oleosome-based emulsion and its *in vitro* digestive fate as affected by (-)-epigallocatechin-3-gallate. *Food Funct.* **2018**, *9*, 6146–6154.

16. Marchese, A.; Coppo, E.; Sobolev, A. P.; Rossi, D.; Mannina, L.; Daglia, M. Influence of *in vitro* simulated gastroduodenal digestion on the antibacterial activity, metabolic profiling and polyphenols content of green tea (*Camellia sinensis*). *Food Res. Int.* **2014**, *63*, 182–191.

17. Planes-Muñoz, D.; López-Nicolás, R.; González-Bermúdez, C. A.; Ros-Berruezo, G.; Frontela-Saseta, C. *In vitro* effect of green tea and turmeric extracts on GLP-1 and CCK secretion: the effect of gastrointestinal digestion. *Food Funct.* **2018**, *9*, 5245–5250.
18. Governa, P.; Biagi, M. *Copaifera langsdorffii* Desf .: *in vitro* investigation on anti-*Helicobacter pylori* and anti-inflammatory activities of oleoresin and fruit methanolic extract. *Plant Biosyst. An Int. J. Deal. with all Asp. Plant Biol.* **2020**, *154*, 117–124.
19. Alminger, M.; Aura, A. M.; Bohn, T.; Dufour, C.; El, S. N.; Gomes, A.; Karakaya, S.; Martínez-Cuesta, M. C.; Mcdougall, G. J.; Requena, T.; Santos, C. N. *In vitro* models for studying secondary plant metabolite digestion and bioaccessibility. *Compr. Rev. Food Sci. Food Saf.* **2014**, *13*, 413–436.
20. Chiocchio, I.; Poli, F.; Governa, P.; Biagi, M.; Lianza, M. Wound healing and *in vitro* antiradical activity of five *Sedum* species grown within two sites of community importance in Emilia-Romagna (Italy). *Plant Biosyst. - An Int. J. Deal. with all Asp. Plant Biol.* **2019**, *153*, 610–615.
21. Catanzaro, D.; Rancan, S.; Orso, G.; Dall’Acqua, S.; Brun, P.; Giron, M. C.; Carrara, M.; Castagliuolo, I.; Ragazzi, E.; Caparrotta, L.; Montopoli, M. *Boswellia serrata* preserves intestinal epithelial barrier from oxidative and inflammatory damage. *PLoS One* **2015**, *10*, e0125375.
22. Governa, P.; Marchi, M.; Cocetta, V.; Leo, B. De; Saunders, P. T. K.; Catanzaro, D.; Miraldi, E.; Montopoli, M.; Biagi, M. Effects of *Boswellia serrata* Roxb . and *Curcuma longa* L . in an *in vitro* intestinal inflammation model using immune cells and Caco-2. *Pharmaceuticals* **2018**, *11*, 126.
23. Hubatsch, I.; Ragnarsson, E. G. E.; Artursson, P. Determination of drug permeability and prediction of drug absorption in Caco-2 monolayers. *Nat. Protoc.* **2007**, *2*, 2111.
24. Natoli, M.; Leoni, B. D.; D’Agnano, I.; Zucco, F.; Felsani, A. Good Caco-2 cell culture practices. *Toxicol. In Vitro* **2012**, *26*, 1243–1246.
25. Meda, N. R.; Fraisse, D.; Gnoula, C.; Vivier, M.; Felgines, C.; Senejoux, F.

Characterization of antioxidants from *Detarium microcarpum* Guill. et Perr. leaves using HPLC-DAD coupled with pre-column DPPH assay. *Eur. Food Res. Technol.* **2017**, *243*, 1659–1666.

26. Yoshino, K.; Suzuki, M.; Sasaki, K.; Miyase, T.; Sano, M. Formation of antioxidants from (-)-epigallocatechin gallate in mild alkaline fluids, such as authentic intestinal juice and mouse plasma. *J. Nutr. Biochem.* **1999**, *10*, 223–229.

27. Henning, S. M.; Choo, J. J.; Heber, D. Nongallated compared with gallated flavan-3-ols in green and black tea are more bioavailable. *J. Nutr.* **2008**, *138*, 1529S-1534S.

28. Komatsu, Y.; Suematsu, S.; Hisanobu, Y.; Saigo, H.; Matsuda, R.; Hara, K. Effects of pH and temperature on reaction kinetics of catechins in green tea infusion. *Biosci. Biotechnol. Biochem.* **1993**, *57*, 907–910.

29. Krook, M. A.; Hagerman, A. E. Stability of polyphenols epigallocatechin gallate and pentagalloyl glucose in a simulated digestive system. *Food Res. Int.* **2012**, *49*, 112–116.

30. Nakagawa, K.; Nakayama, K.; Nakamura, M.; Sookwong, P.; Tsuduki, T.; Niino, H.; Kimura, F.; Miyazawa, T. Effects of co-administration of tea epigallocatechin-3-gallate (EGCG) and caffeine on absorption and metabolism of EGCG in humans. *Biosci. Biotechnol. Biochem.* **2009**, *73*, 2014–2017.

31. Qiu, J.; Chen, L.; Zhu, Q.; Wang, D.; Wang, W.; Sun, X.; Liu, X.; Du, F. Screening natural antioxidants in peanut shell using DPPH-HPLC-DAD-TOF/MS methods. *Food Chem.* **2012**, *135*, 2366–2371.

32. Wang, G.; Huang, X.; Pei, D.; Duan, W.; Quan, K.; Li, X.; Di, D. DPPH-HPLC-DAD analysis combined HSCCC for screening and identification of radical scavengers in *Cynomorium songaricum* Rupr. *New J. Chem.* **2016**, *40*, 3885–3891.

33. Cocetta, V.; Catanzaro, D.; Borgonetti, V.; Ragazzi, E.; Giron, M. C.; Governa, P.; Carnevali, I.; Monica, M.; Biagi, M. A fixed combination of probiotics and herbal extracts attenuates intestinal barrier dysfunction from inflammatory stress in an *in vitro* model using Caco-2 cells. *Recent Pat. Food. Nutr. Agric.* **2019**, *10*, 62–69.

34. Dall'Acqua, S.; Catanzaro, D.; Cocetta, V.; Igl, N.; Ragazzi, E.; Giron, M. C.; Ceconello, L.; Montopoli, M. Protective effects of psi taraxasterol 3-O-myristate and arnidiol 3-O-myristate isolated from *Calendula officinalis* on epithelial intestinal barrier. *Fitoterapia* **2016**, *109*, 230–235.

PART 2

CHAPTER 6

Exploiting the Caco-2 permeability model to study the bioavailability of complex mixtures of compounds

6.1. Introduction

The bioavailability of natural products is one of the major factors limiting their clinical use. Indeed, natural products have low water solubility, can be instable to digestive processes, can undergo metabolism by the intestinal bacterial flora, are scarcely absorbed by the intestinal epithelium, can be substrate of efflux protein, and are usually extensively metabolized by the first pass effect [1].

In the part 1 of this thesis, we evaluated the effect of simulated gastrointestinal digestion on the stability of some herbal extracts, together with their main constituents. The following step for evaluating the bioavailability of natural products should be the analysis of their intestinal absorption. This can be achieved experimentally using different models [2].

In vivo studies are the most accurate and can provide detailed information on the overall pharmacokinetics of the studied natural products. However, these studies are time-consuming, are expensive, and limited by ethical issues [3].

To overcome the limitation of *in vivo* studies, several *in vitro* models have been developed. Two major experimental models can be used for the evaluation of compounds permeability through a membrane barrier: the parallel artificial membrane permeability assay (PAMPA), and the Caco-2 permeability assay [4].

The PAMPA is a fast and high-throughput cell-free model, which use a lipid-infused artificial membrane to separate a donor and a receiving compartment. The compound is added into the donor compartment and after an incubation time, the amount of compound is measured in both the donor and the receiving compartment. This allows to calculate the permeability coefficient of the test compound through a

variety of membranes, which can mimic a variety of biological barriers, including the gastrointestinal barrier, the blood-brain barrier and the skin barrier. Although its easiness of use and high degree of customization, this model can only simulate the passive transport and is not suitable for studying the effect of active transport proteins on the permeability of test compounds [5,6].

The Caco-2 model is a well-established and validated cell-based model of intestinal epithelium. Indeed, it is accepted by the FDA as a surrogate for human intestinal permeability measurement to support new drug applications [7]. This model is similar to PAMPA, but it uses a monolayer of differentiated human colon carcinoma cells (Caco-2) in place of the artificial membrane, with the main advantage of being able to simulate active transport. When grown on particular filters, in fact, Caco-2 cells differentiate, assuming a polarized enterocyte-like phenotype, which resemble the small intestinal epithelium. The main features of this model are represented by the formation of tight junctions and the expression of transport proteins, which allow it to be used for the measurement of passive transcellular permeation, paracellular diffusion, and active transport [8]. Together with active transport proteins, such as solute carriers and ATP-binding cassette transporters, more than 300 ADME-related proteins were found to be expressed by Caco-2 [9]. Moreover, even if a low level of cytochrome P450 isoforms has been found in Caco-2, their expression can be enhanced, thus allowing to include the effect of intestinal metabolism when evaluating the permeability of a compound [10]. The main limitations of the Caco-2 model are due to their heterogeneity and their complex and time-consuming culture technique, which requires expert operators [11].

The presence of more than one molecule in the test samples, such as in the case of herbal extracts, can modify the expected permeability of a compound, by inhibiting or inducing the active transport and metabolic proteins, as well as by partitioning into the cell membrane and altering their fluidity [12].

In 2003, Laitinen and co-workers evaluated the suitability of Caco-2 model for studying the permeability of several n-in-one cocktails of heterogeneous compounds in a single assay [13,14]. Their method improved the throughput of permeability studies, also reducing the normal variation caused by the different passage number and age of

the cell culture. The same research group also evaluated the possible interaction of food supplements and herbal extracts with the permeability of drugs across the Caco-2 cell monolayer, finding that, depending on the composition of the co-administered extract, changes in the permeability of drugs can occur, mainly due to pH modification, extract concentration, reversible alterations of monolayer integrity, and alteration of transport protein function [15–17].

Caco-2 have been used to develop computational models able to predict the intestinal permeability of drug candidates [18]. However, these methods predict the pharmacokinetic properties of single compounds only and they cannot be applied to more complex mixtures of molecules, such as herbal products.

The aim of this work is to exploit the suitability of the Caco-2 model to predict the intestinal permeability of multiple compounds at the same time, to obtain experimental data that will then be used to build a computational model able to predict the pharmacokinetic properties of mixture of compounds.

6.2. Materials and methods

6.2.1. Computational details

The structures of an in-house library of 24 natural compounds (dataset A) and of a second larger library of 424 natural and synthetic compounds (dataset B) were imported in VolSurf+ [19] to calculate molecular descriptors from 3D molecular interaction fields, as previously described [20]. The 24 natural compounds in dataset A were used as reference compounds and a principal component analysis (PCA) was performed to identify similar compounds, based on principal component 1, 2 and 3. The resulting compounds were then combined with compounds from dataset A and analyzed again, based on the same PCA analysis, to generate couples of diverse compounds.

6.2.2. Chemicals

All solvents used in this work were purchased from Sigma-Aldrich. 3,4-dihydroxyhydrocinnamic acid, 3,5-dihydroxybenzoic acid, amoxicillin, anthraquinone, apigenin, apigenin-7-glucoside, astilbin, β -sitosterol, caffeic acid, carbadox, (+)-catechin, chlorogenic acid, chrysin, curcumin, (-)-epicatechin, famciclovir, folic acid, furosemide, galangin, gallic acid, ginkgolide A, isoquercetin, kaempferol, lanosterol, luteolin, olaquinox, pinocembrin, polydatin, quercetin, resveratrol, rutin, sulfamonomethoxine, and voriconazole were purchased from Sigma-Aldrich. Hyperoside, isoliquiritin and luteolin-7-O-glucoside were purchased from Extrasynthese. Cannabidiol was purchased from Linnea SA. Berberine chloride was kindly provided by Biodue (Tavarnelle val di Pesa, Florence, Italy). Acyclovir was purchased from Generon (Slough, United Kingdom). Ketoprofen was purchased from MP Biomedicals (Eschwege, Germany). N²-butylpteridine-2,4-diamine, 2-phenylquinoxalin-6-amine, 5-phenyl-7-(trifluoromethyl)pyrazolo[1,5-*a*]pyrimidine-3-carboxylic acid, and N,N'-(ethane-1,2-diyl)bis(quinoline-8-carboxamide were purchased from Specs (Zoetermeer, The Netherlands). 5-(4-((1*H*-pyrrol-2-yl)methyl)piperazin-1-yl)-8-nitroisoquinoline was purchased from Enamine (Riga, Latvia). 8-bromo-N-cyclohexyl-7*H*-purin-6-amine and N-(2-(pyrrolidin-1yl)phenyl)-1*H*-indole-2-carboxamide were synthesized by the laboratory of Prof. Gabriele Cruciani (University of Perugia, Italy). DMSO (Sigma-Aldrich) was used for preparing 10 mM stock solutions of the samples.

6.2.3. Cell culture

Caco-2 cells were used as a stable *in vitro* model for the intestinal epithelium [21]. Cells were a kind gift by Prof. Monica Montopoli (University of Padua, Italy) and were cultured in 75 cm² cell culture flask (Sarstedt) in DMEM supplemented with 10% fetal bovine serum (FBS), 1% glutamine and 1% penicillin/streptomycin antibiotic (Sigma-Aldrich) [22,23]. EDTA-trypsin (Sigma-Aldrich) solution was used for detaching cells from flasks, and cell counting was performed using a hemocytometer, by Trypan Blue staining.

6.2.4. Caco-2 permeability assay

The Caco-2 permeability assay was performed following the protocol by Hubatsch [24], with slight modification. Briefly, Caco-2 cells (8×10^5) were seeded into transparent polyester membrane cell culture inserts with 0.4 μm pore size (Sarstedt) and grown for 21 days, in a 24-well plate, with 600 μL and 200 μL of medium in the basolateral and apical chamber, respectively. Media were changed every second day, and 12 h before the permeability experiments.

The integrity of the cell monolayers was monitored by measuring the trans-epithelial electric resistance (TEER) of the monolayer from day 14th to day 21st after seeding. TEER measurements were performed in phenol red-free HBSS (Sigma-Aldrich) with 10 mM Glucose (Sigma-Aldrich) and 10 mM HEPES (pH = 7.4), after an equilibration period at rt [25,26], using a Millicell[®] ERS meter, (Millipore Corporation) connected to a pair of chopstick electrodes. Only cells with TEER value within 360 - 500 $\Omega \times \text{cm}^2$ were used for the experiments [24,27,28].

The day of the experiment, the filter supports were washed three times, TEER was measured, and media were replaced with pre-warmed (37 °C) buffered HBSS. To improve the recovery of highly lipophilic compounds, bovine serum albumin at a 2% m/v final concentration was added to the receiving chamber. Samples were added at the final concentration of 10 μM in donor chamber and incubated at 37 °C with an orbital shaker (300 rpm). Sampling was performed after 0 and 120 min, from the donor chamber, and after 10, 30 and 60 min, from the receiving chamber. The sampling volume was 100 μL for the apical side and 300 μL from the basolateral side. Buffered HBSS was used to replace the withdrawn volume. Experiments were performed in the apical to basolateral (a>b) and basolateral to apical (b>a) directions.

To verify that the tested compounds did not affect the integrity of the cell monolayers, TEER was measured immediately after the permeability experiment, followed by a paracellular permeability assay. Phenol red flux across Caco-2 cell monolayers was used as a measure of paracellular permeability. The apical media were replaced with a 500 mM phenol red solution (Sigma-Aldrich) in buffered HBSS and the basolateral media were replaced with fresh buffered HBSS. After 60 min of incubation at 37 °C, 100 μL was collected from the basolateral chamber and added to

10 μL of 1N NaOH in 96-well plates. Phenol red leakage was measured using a Victor® Nivo™ plate reader (PerkinElmer) by recording the absorbance at 540 nm and quantified according to a calibration curve set up using serial dilutions (500 - 0.5 mM) of phenol red solution in HBSS [29–31].

The apparent permeability coefficient (P_{app}) was determined using the following formula (Eq. 6.1):

$$P_{\text{app}} = \left(\frac{dQ}{dt}\right) \left(\frac{1}{A \times C_0}\right)$$

where $\left(\frac{dQ}{dt}\right)$ represents the steady-state flux expressed as $\mu\text{mol s}^{-1}$, A is the surface area of the filter expressed as cm^2 and C_0 is the initial concentration (μM) of the sample in the donor chamber.

6.2.5. Chromatographic conditions

The analysis of the samples from the Caco-2 permeability assay was performed by LC-MS, using an Agilent 1290 infinity LC system, equipped with a Luna Omega C18 Polar (1.6 μm , 2.1 \times 100 mm) column (Phenomenex, Castel Maggiore, Bologna, Italy), and composed of an autosampler, an isocratic pump, a binary pump, a column compartment and a diode array detector (all Agilent Technology, Santa Clara, CA). The LC was performed by injecting 1 μL of the sample in the column, maintained at 40 $^{\circ}\text{C}$ for a 10 min run. The mobile phase consisted of double distilled water with 0.1 v/v formic acid (A) and acetonitrile with 0.1 v/v formic acid (B), and the following gradient was applied: B from 5% at 0 min to 95% at 8 min and then back to 5% at 10 min. The flux was set to 0.65 mL/min. The LC was interfaced to an Agilent 6540 quantitative time-of-flight (Q-TOF) system by an Agilent Dual JetStream ESI source that operated both positive and negative ionization with N_2 as desolvation gas (gas temperature 350 $^{\circ}\text{C}$, sheath gas temperature 400 $^{\circ}\text{C}$, flow 9 L/min, nebulizer 35 psi, capillary 4000 V, fragmentor 120 V). The Q-TOF operated in an AutoMS/MS mode in a range of 100-1200 m/z for the positive ionization and 100-1500 m/z for the negative ionization.

6.2.6. Statistical analysis

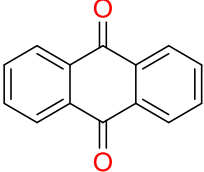
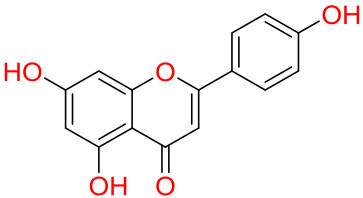
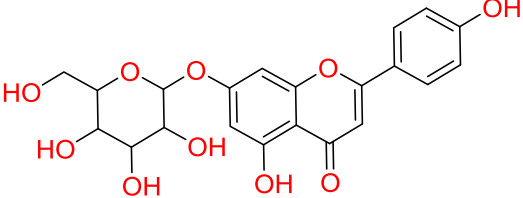
Experiments were performed in duplicate. The statistical differences between the results were determined by using the Student's t-test. Values are expressed in the range of +/- standard deviation and $p < 0.05$ was considered statistically significant. Graphs and calculations were performed using GraphPad Prism.

6.3. Results and discussion

6.3.1. In silico selection and coupling of compounds

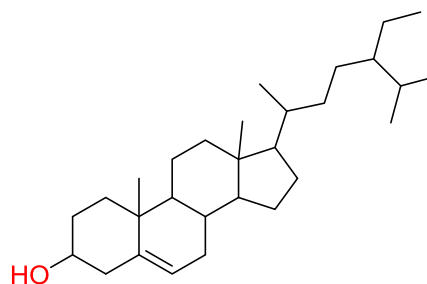
A total of 23 compounds from dataset B, including both natural and synthetic molecules, were identified by the PCA. Together with Dataset A, we obtained a total of 47 compounds (table 6.1), which were then used for the Caco-2 permeability assay.

Table 6.1. 2D structures of selected compounds.

ID	Compound	Structure
A	Antraquinone	
B	Apigenin	
C	Apigenin_7_Glucoside	

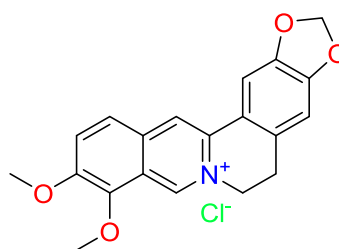
D

β -Sitosterol



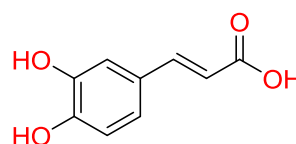
E

Berberine Chloride



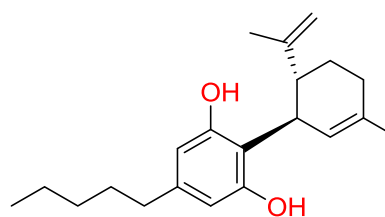
F

Caffeic Acid



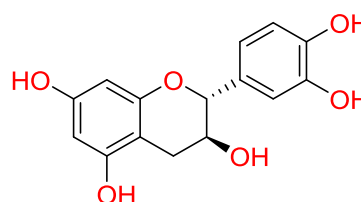
G

Cannabidiol



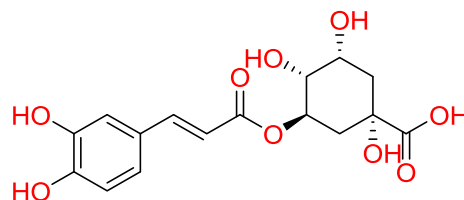
H

(+)-catechin



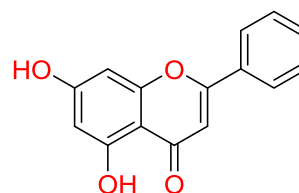
I

Chlorogenic Acid



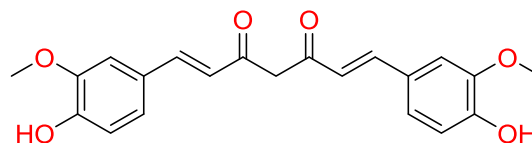
J

Chrysin



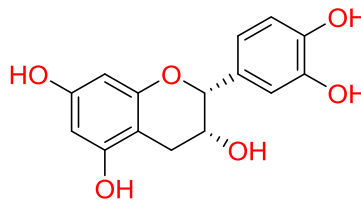
K

Curcumin



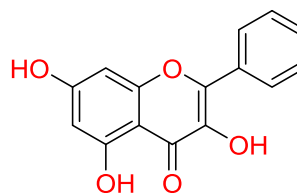
L

(-)-epicatechin



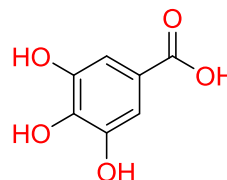
M

Galangin



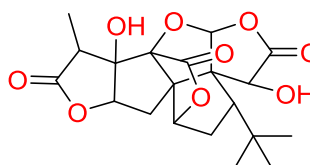
N

Gallic Acid



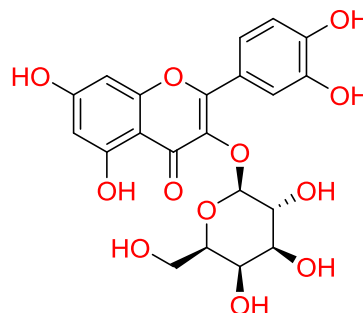
O

Ginkgolide_A



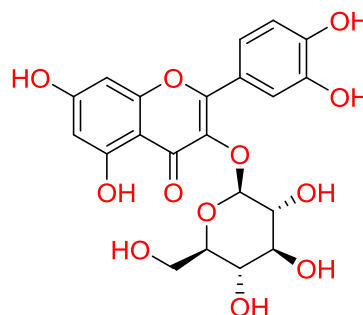
P

Hyperoside



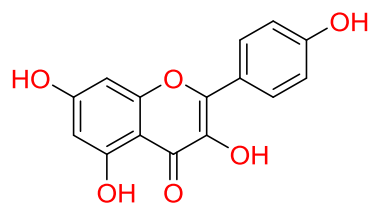
Q

Isoquercetin



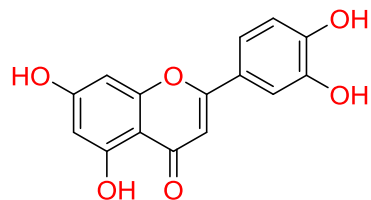
R

Kaempferol



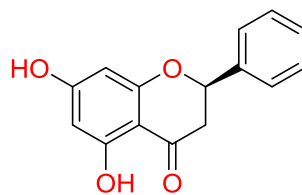
S

Luteolin



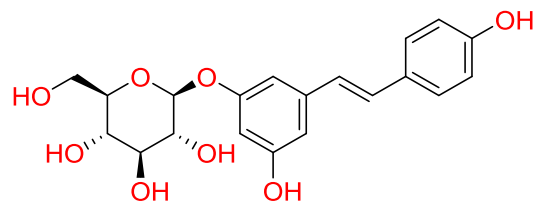
T

Pinocembrin



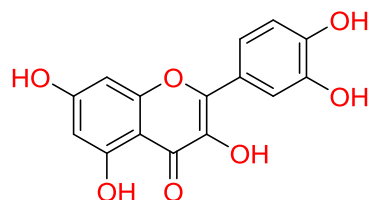
U

Polydatin



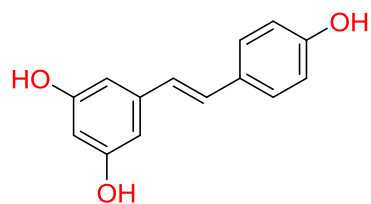
V

Quercetin



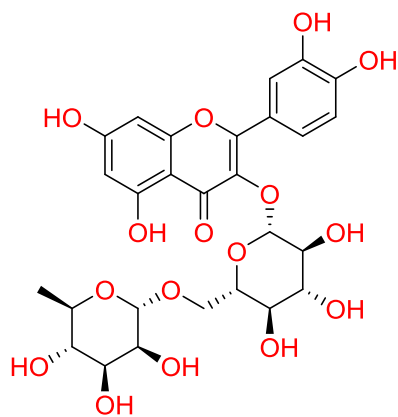
W

Resveratrol



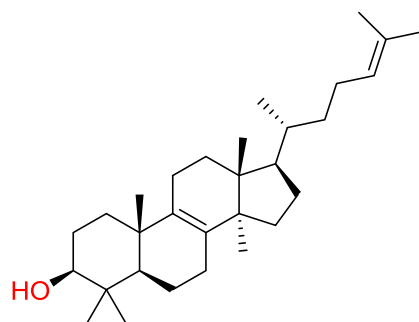
X

Rutin



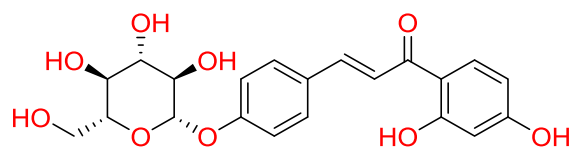
1

Lanosterol



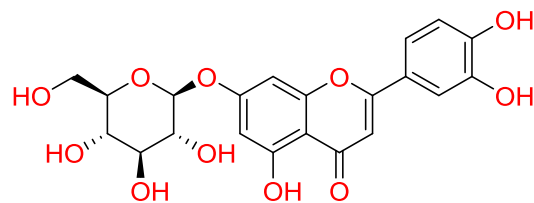
2

Isoliquiritin



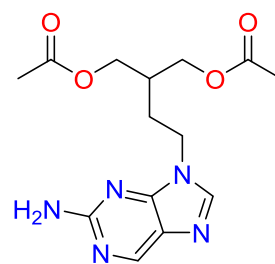
3

Luteolin 7-O-glucoside



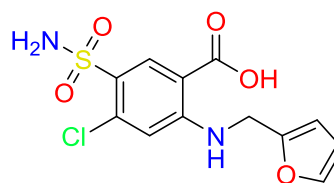
4

Famciclovir

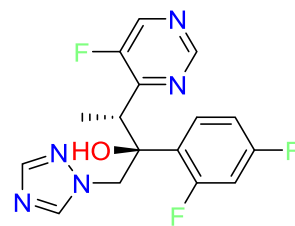


5

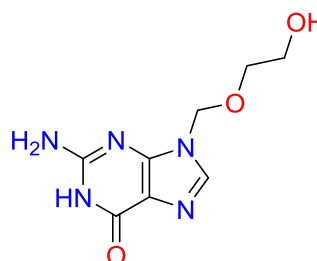
Furoseimide



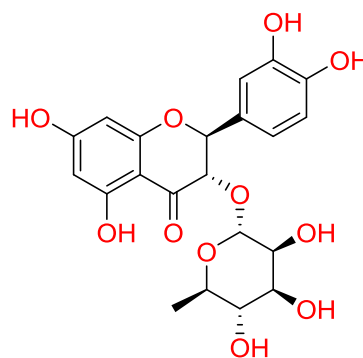
6 Voriconazole



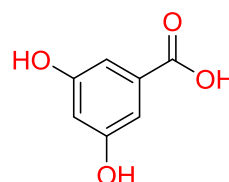
7 Acyclovir



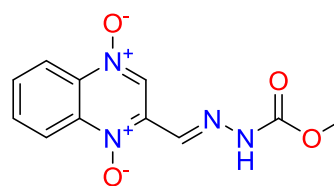
8 Astilbin



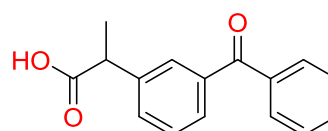
9 3,5-Dihydroxybenzoic acid



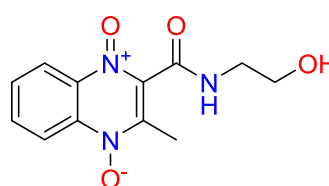
10 Carbadox



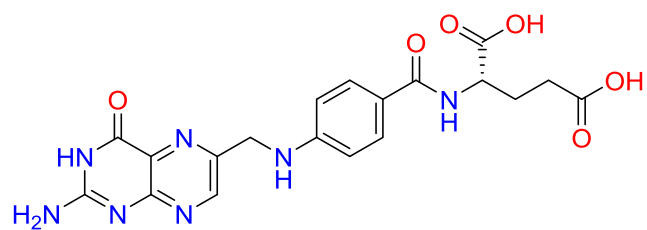
11 Ketoprofen



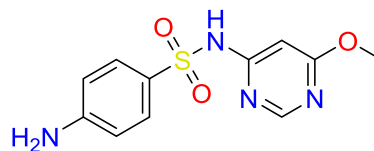
12 Olaquinox



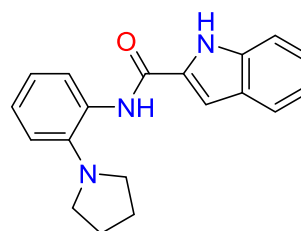
13 Folic Acid



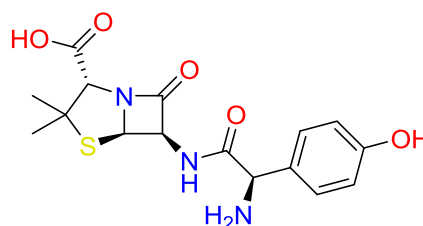
14 Sulfamonomethoxine



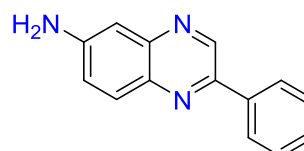
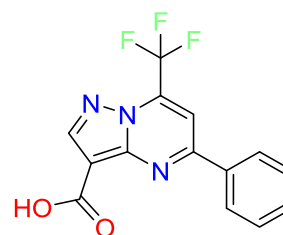
15 N-(2-(pyrrolidin-1-yl)phenyl)-1H-indole-2-carboxamide



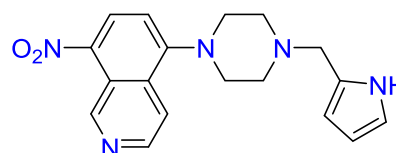
16 Amoxicillin

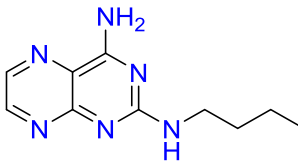
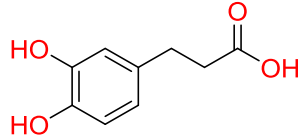
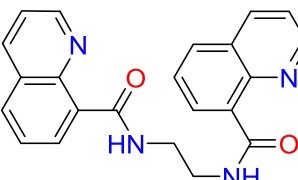
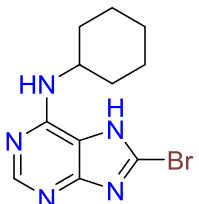


17 2-phenylquinoxalin-6-amine

18 5-phenyl-7-(trifluoromethyl)pyrazolo[1,5-*a*]pyrimidine-3-carboxylic acid

19 5-(4-((1H-pyrrol-2-yl)methyl)piperazin-1-yl)-8-nitroisoquinoline



20	N ² -butylpteridine-2,4-diamine	
21	3,4-Dihydroxyhydrocynamic acid	
22	N,N'-(ethane-1,2-diy)bis(quinoline-8-carboxamide)	
23	8-bromo-N-cyclohexyl-7H-purin-6-amine	

To assess if the presence of another molecule could affect the Caco-2 permeability, the compounds were then coupled based on similarity and dissimilarity characteristic (Table 6.2).

Table 6.2. Couples of similar and diverse compounds used for the Caco-2 permeability assay.

Similar compounds	Diverse compounds
A-17	X-1
B-14	D-S
C-3	G-Q
D-1	15-13
E-19	P-17
F-21	A-16
G-15	E-3
H-4	19-8

I-16	22-9
J-11	K-N
K-22	C-23
L-6	I-20
M-18	T-2
N-9	F-U
O-12	J-O
P-8	21-4
Q-13	W-12
R-5	11-7
S-10	H-M
T-20	L-5
U-2	6-18
V-7	V-14
W-23	B-R
X-3	S-10

6.3.2. Caco-2 permeability assay

Using the LC-MS method, we were able to analyze the Caco-2 permeability of 38 out of 47 single compounds (Table 6.3). Detectable P_{app} were obtained for 27 compounds in the a>b direction, while the permeability of the remaining 11 compounds was lower than the detection limit, suggesting a scarce bioavailability. Differently, when analyzing the b>a direction, only three compounds were not transported. This could mean that the bioavailability of 8 out of the 11 compounds which were not transported in the a>b direction could be limited by efflux phenomena induced by active transport proteins. Indeed, 11 out of 38 compounds had an efflux ratio higher than 1.

Table 6.3. P_{app} (cm s⁻¹) and efflux ratio of each single tested compounds. Data are expressed as mean \pm standard deviation. n.d. = not determined.

Compound ID	$P_{app} a>b \times 10^{-6}$	$P_{app} b>a \times 10^{-6}$	Efflux ratio
A	n.d.	n.d.	n.d.
B	40.01 \pm 7.24	13.00 \pm 2.31	0.32
C	16.62 \pm 1.39	18.84 \pm 1.26	1.13
D	28.46 \pm 1.69	47.00 \pm 35.31	1.65
E	0.41 \pm 0.04	18.82 \pm 1.25	45.67
F	<0.01	0.60	>100
G	<0.01	<0.01	n.d.
H	<0.01	<0.01	n.d.
I	<0.01	0.48 \pm 0.01	>100
J	7.70 \pm 4.47	6.39 \pm 2.55	0.83
K	1.82	1.45 \pm 1.04	0.79
L	<0.01	0.55	>100
M	n.d.	n.d.	n.d.
N	n.d.	n.d.	n.d.
O	1.04 \pm 0.72	1.84 \pm 0.37	1.78
P	1.23	5.44	0.44
Q	19.12 \pm 5.47	0.52 \pm 0.42	0.03
R	n.d.	n.d.	n.d.
S	<0.01	<0.01	n.d.
T	7.05 \pm 0.72	0.91 \pm 0.09	1.29
U	1.41	0.86 \pm 0.09	0.60
V	n.d.	n.d.	n.d.
W	3.37 \pm 2.95	1.13 \pm 0.05	0.34
X	17.89 \pm 7.23	0.23 \pm 0.07	0.01
1	n.d.	n.d.	n.d.

2	1.07 ± 0.02	0.91 ± 0.20	0.86
3	18.07 ± 2.38	9.31	0.52
4	7.34 ± 1.84	21.56 ± 19.41	2.94
5	<0.01	0.62 ± 0.40	>100
6	$0.25 \times \pm 0.04$	0.37 ± 0.01	1.45
7	<0.01	0.90 ± 0.38	>100
8	<0.01	0.55 ± 0.07	>100
9	n.d.	n.d.	n.d.
10	0.76 ± 0.10	0.84 ± 0.06	1.11
11	<0.01	2.35 ± 1.69	>100
12	0.38 ± 0.01	0.62 ± 0.32	1.64
13	<0.01	<0.01	n.d.
14	0.81 ± 0.18	0.72 ± 0.06	0.89
15	2.58 ± 2.11	0.52 ± 0.06	0.20
16	<0.01	0.65 ± 0.12	>100
17	0.04 ± 0.01	2.69 ± 1.5	72.61
18	0.23 ± 0.03	0.32 ± 0.06	1.43
19	0.50 ± 0.20	0.37 ± 0.13	0.74
20	2.62 ± 0.01	4.16 ± 0.02	1.59
21	n.d.	n.d.	n.d.
22	0.04 ± 0.01	0.02 ± 0.01	0.66
23	0.53 ± 0.05	0.69 ± 0.07	1.30

The P_{app} in the a>b direction ranged from 40.01×10^{-6} to $<0.01 \times 10^{-6}$ cm s⁻¹, while in the b>a direction ranged from 47.00×10^{-6} to $<0.01 \times 10^{-6}$ cm s⁻¹. These values are consistent with the available literature on polyphenols transport across the Caco-2 monolayer [32–34].

The coupling with a similar molecule lead to the increase of P_{app} in the a>b direction of 9 compounds, namely **G, H, 6, 11, 12, 14, 16, 18, and 22**, while the P_{app} in the b>a direction increased for 6 compounds, namely **G, H, I, J, 12, and 18**. The P_{app} was reduced for 15 compounds, namely **B, C, D, E, O, P, Q, T, U, W, X, 2, 3, 4, and 15** in the a>b. A reduction of the P_{app} in the b>a direction was also observed for 15 compounds, namely **C, D, E, K, L, O, P, W, X, 3, 4, 6, 8, 17, and 20** (table 6.4). Interestingly, the P_{app} of **3** was reduced when coupled with both compound **C** and **X** in the a>b and b<a directions.

The efflux ratio is a measure of the involvement of active transport: compounds with efflux ratio higher than 2 are usually considered actively transported [11]. Overall, the efflux ratio was increased for 8 compounds, namely **B, C, D, P, Q, U, 3** (when coupled with **C**, not with **X**), and **15**, and decreased for 14 compounds, namely **E, J, 4, 6, 10, 11, 12, 14, 16, 17, 18, 20, 22, and 23**. Interestingly, the efflux ratio of compounds **K, P, Q, U, and 14** changed from lower than 2 to higher than 2, suggesting that the coupled molecule may have acted as inducer of active transport protein. On the contrary, the efflux ratio of compounds **16** and **17** changed from higher than 2 to lower than 2, meaning that the co-administered compounds may have acted as an active transport protein inhibitor.

Table 6.4. P_{app} (cm s⁻¹) and efflux ratio of couples of similar compounds. Data are expressed as mean \pm standard deviation. n.d. = not determined.

Couple ID	P_{app} a>b $\times 10^{-6}$		P_{app} b>a $\times 10^{-6}$		Efflux ratio	
	A	17	A	17	A	17
A-17	n.d.	0.03 \pm 0.01	n.d.	0.02 \pm 0.01	n.d.	0.88
	B	14	B	14	B	14
B-14	17.07	0.02 \pm 0.01	8.54 \pm 2.48	1.26 \pm 0.94	0.50	57.28
	C	3	C	3	C	3
C-3	0.64 \pm 0.34	0.62 \pm 0.31	0.99 \pm 0.03	1.15 \pm 0.17	1.53	1.83
	D	1	D	1	D	1
D-1	1.88 \pm 0.01	n.d.	0.91 \pm 0.08	n.d.	0.48	n.d.

E-19	E	19	E	19	E	19
	0.10 ± 0.01	0.64 ± 0.04	0.25 ± 0.17	0.57 ± 0.37	2.52	0.89
F-21	F	21	F	21	F	21
	n.d.	n.d.	n.d.	n.d.	n.d.	n.d.
G-15	G	15	G	15	G	15
	14.70 ± 2.94	0.32 ± 0.14	4.29	0.62 ± 0.15	0.29	1.90
H-4	H	4	H	4	H	4
	6.91	1.04 ± 0.14	17.15	1.04 ± 0.14	2.48	1.00
I-16	I	16	I	16	I	16
	<0.01	1.92 ± 1.67	25.05 ± 1.49	0.59 ± 0.46	>100	0.31
J-11	J	11	J	11	J	11
	4.90 ± 2.46	0.93 ± 0.44	1.67 ± 0.50	0.93 ± 0.44	0.34	1.00
K-22	K	22	K	22	K	22
	n.d.	0.45 ± 0.34	5.14	0.05 ± 0.04	>100	0.12
L-6	L	6	L	6	L	6
	<0.01	1.20 ± 1.13	<0.01	0.09 ± 0.03	n.d.	0.08
M-18	M	18	M	18	M	18
	n.d.	1.76 ± 0.32	n.d.	1.71 ± 0.29	n.d.	1.00
N-9	N	9	N	9	N	9
	n.d.	n.d.	n.d.	n.d.	n.d.	0.97
O-12	O	12	O	12	O	12
	<0.01	1.75 ± 0.23	<0.01	1.78 ± 0.27	n.d.	1.02
P-8	P	8	P	8	P	8
	<0.01	<0.01	1.57 ± 0.01	<0.01	>100	n.d.
Q-13	Q	13	Q	13	Q	13
	<0.01	<0.01	0.64 ± 0.15	<0.01	>100	n.d.
R-5	R	15	R	15	R	15

Exploiting the Caco-2 permeability model to study the bioavailability of complex mixtures of compounds

	<0.01	<0.01	<0.01	0.62 ± 0.15	n.d.	>100
S-10	S	10	S	10	S	10
	<0.01	1.52 ± 1.00	<0.01	1.09 ± 0.05	n.d.	0.71
T-20	T	20	T	20	T	20
	1.16 ± 0.66	2.80 ± 1.08	1.32 ± 0.15	0.92 ± 0.01	1.14	0.33
U-2	U	2	U	2	U	2
	<0.01	0.65 ± 0.04	1.15 ± 0.31	0.51 ± 0.17	>100	0.78
V-7	V	7	V	7	V	7
	n.d.	<0.01	n.d.	0.96 ± 0.30	n.d.	>100
W-23	W	23	W	23	W	23
	<0.01	0.96 ± 0.30	<0.01	0.58 ± 0.08	n.d.	0.61
X-3	X	3	X	3	X	3
	<0.01	0.56 ± 0.10	<0.01	0.25 ± 0.11	n.d.	0.45

The coupling with diverse compounds, instead, lead to the increase of P_{app} in the a>b direction of compound **17** and **23**, only, while the P_{app} in the b>a direction increased for 5 compounds, namely **Q**, **T**, **12**, **15**, and **22**. The P_{app} was reduced for 19 compounds, namely **B**, **C**, **E**, **J**, **O**, **P**, **Q**, **T**, **U**, **X**, **2**, **3**, **4**, **6**, **12**, **15**, **18**, **19**, and **20**, and for 20 compounds, namely **B**, **C**, **E**, **F**, **I**, **L**, **O**, **P**, **X**, **3**, **4**, **6**, **7**, **8**, **11**, **16**, **17**, **18**, **19**, and **20**, in the a>b and b>a direction, respectively (table 6.5). The efflux ratio increased for 8 compounds, namely **P**, **Q**, **6**, **8**, **10**, **14**, **15**, **22**, and decreased for 5 compounds, namely **C**, **T**, **4**, **17**, and **23**. Among these, the efflux ratio of compounds **P**, **Q**, **15**, and **22** changed from lower than 2 to higher than 2, suggesting that the coupled molecule may have acted as an inducer of active transport protein. On the contrary, the efflux ratio of compounds **4**, **17**, and **23** changed from higher than 2 to lower than 2, meaning that the co-administered compounds may have acted as an active transport protein inhibitor.

Table 6.5. P_{app} (cm s⁻¹) and efflux ratio of couples of diverse compounds. Data are expressed as mean \pm standard deviation. n.d. = not determined.

Couple ID	$P_{\text{app}} \text{ a>b} \times 10^{-6}$		$P_{\text{app}} \text{ b>a} \times 10^{-6}$		Efflux ratio	
	X	1	X	1	X	1
X-1	<0.01	n.d.	<0.01	n.d.	n.d.	n.d.
	D	S	D	S	D	S
D-S	n.d.	<0.01	n.d.	<0.01	n.d.	n.d.
G-Q	G	Q	G	Q	G	Q
	n.d.	<0.01	n.d.	1.05 ± 0.16	n.d.	>100
15-13	15	13	15	13	15	13
	<0.01	<0.01	1.26 ± 0.14	<0.01	>100	n.d.
P-17	P	17	P	17	P	17
	<0.01	0.71	1.98 ± 0.48	0.36 ± 0.05	>100	0.50
A-16	A	16	A	16	A	16
	n.d.	<0.01	n.d.	<0.01	n.d.	n.d.
E-3	E	3	E	3	E	3
	<0.01	1.13 ± 0.05	<0.01	0.29 ± 0.01	n.d.	0.26
19-8	19	8	19	8	19	8
	<0.01	<0.01	<0.01	<0.01	n.d.	n.d.
22-9	22	9	22	9	22	9
	<0.01	n.d.	0.16 ± 0.03	n.d.	>100	n.d.
K-N	K	N	K	N	K	N
	n.d.	n.d.	n.d.	n.d.	n.d.	n.d.
C-23	C	23	C	23	C	23
	0.41 ± 0.09	1.18 ± 0.05	0.61	0.63 ± 0.06	1.50	0.54
I-20	I	20	I	20	I	20
	<0.01	0.62 ± 0.05	<0.01	0.99 ± 0.28	n.d.	1.61

Exploiting the Caco-2 permeability model to study the bioavailability
of complex mixtures of compounds

T-2	T	2	T	2	T	2
	1.01 ± 0.22	0.70 ± 0.16	1.86 ± 0.33	0.46 ± 0.39	1.85	0.66
F-U	F	U	F	U	F	U
	<0.01	0.70 ± 0.11	<0.01	0.48 ± 0.31	n.d.	0.69
J-O	J	O	J	O	J	O
	<0.01	<0.01	n.d.	<0.01	n.d.	n.d.
21-4	21	4	21	4	21	4
	n.d.	1.20 ± 0.27	n.d.	0.37 ± 0.10	n.d.	0.31
W-12	W	12	W	12	W	12
	n.d.	>0.01	n.d.	1.56 ± 0.05	n.d.	>100
11-7	11	7	11	7	11	7
	<0.01	<0.01	<0.01	<0.01	n.d.	n.d.
H-M	H	M	H	M	H	M
	<0.01	<0.01	<0.01	8.09 ± 3.87	n.d.	>100
L-5	L	5	L	5	L	5
	<0.01	<0.01	<0.01	0.20	n.d.	>100
6-18	6	18	6	18	6	18
	<0.01	<0.01	0.26 ± 0.02	1.40 ± 0.35	>100	>100
V-14	V	14	V	14	V	14
	<0.01	0.82 ± 0.01	<0.01	0.98 ± 0.16	n.d.	1.19
B-R	B	R	B	R	B	R
	<0.01	<0.01	<0.01	<0.01	n.d.	n.d.
S-10	S	10	S	10	S	10
	<0.01	0.65 ± 0.22	<0.01	0.87 ± 0.11	n.d.	1.34

6.4. Conclusions

Caco-2 are a suitable model for testing the bioavailability of drugs. Evaluating the effect of multiple co-administered compounds at a single time is complex and has to take into account the influence of factors, such as active transport and modification of the membrane permeability. Natural products are often administered as herbal extracts, which lead to the co-administration of a wide number of constituents at the same time.

The aim of this work was to combine similar and diverse compounds, to obtain experimental data on their Caco-2 permeability. We started by combining two compounds. In the future, we aim at increasing the complexity of the experiments, by co-administering more than two compounds at the same time. The experimental data will then be used to create a computational model, able to predict the eCaco-2 permeability of mixtures of compounds. This will be useful for the *in silico* prediction of the bioavailability of herbal extracts, thus reducing the number of *in vivo* experiments needed for this purpose.

Although the data presented in this work are not complete, and there is the need to fill the gap left by compounds which we were not able to analyze yet, it is evident that combining molecules can lead to different Caco-2 permeability, compared to the single compounds, often negatively influencing the results, and that molecular similarity could potentially represent a predictor for the changes in Caco-2 permeability of mixtures of compounds. Once the experimental data will be complete, structure-properties relationship analysis will be performed, in the attempt to identify structural properties which may be involved in the permeability changes.

6.5. References

1. Bhattaram, V. A.; Graefe, U.; Kohlert, C.; Veit, M.; Derendorf, H. Pharmacokinetics and bioavailability of herbal medicinal products. *Phytomedicine* **2002**, *9*, 1–33.
2. Kirchmair, J.; Göller, A. H.; Lang, D.; Kunze, J.; Testa, B.; Wilson, I. D.; Glen, R. C.; Schneider, G. Predicting drug metabolism: experiment and/or computation? *Nat. Rev.*

Drug Discov. **2015**, *14*, 387–404.

3. Galetin, J. B. H. and A. Methods for predicting *in vivo* pharmacokinetics using data from *in vitro* assays. *Curr. Drug Metab.* **2008**, *9*, 940–951.

4. Teksin, Z. S.; Seo, P. R.; Polli, J. E. Comparison of drug permeabilities and BCS classification: three lipid-component PAMPA system method versus Caco-2 monolayers. *AAPS J.* **2010**, *12*, 238–241.

5. Faller, B. Artificial membrane assays to assess permeability. *Curr. Drug Metab.* **2008**, *9*, 886–892.

6. Avdeef, A. The rise of PAMPA. *Expert Opin. Drug Metab. Toxicol.* **2005**, *1*, 325–342.

7. Larregieu, C. A.; Benet, L. Z. Drug discovery and regulatory considerations for improving *in silico* and *in vitro* predictions that use Caco-2 as a surrogate for human intestinal permeability measurements. *AAPS J.* **2013**, *15*, 483–497.

8. Flanagan, S. D.; Takahashi, L. H.; Liu, X.; Benet, L. Z. Contributions of saturable active secretion, passive transcellular, and paracellular diffusion to the overall transport of furosemide across adenocarcinoma (Caco-2) cells. *J. Pharm. Sci.* **2002**, *91*, 1169–1177.

9. Ölander, M.; Wiśniewski, J. R.; Matsson, P.; Lundquist, P.; Artursson, P. The proteome of filter-grown Caco-2 cells with a focus on proteins involved in drug disposition. *J. Pharm. Sci.* **2016**, *105*, 817–827.

10. Küblbeck, J.; Hakkarainen, J. J.; Petsalo, A.; Vellonen, K. S.; Tolonen, A.; Reponen, P.; Forsberg, M. M.; Honkakoski, P. Genetically modified Caco-2 cells with improved cytochrome P450 metabolic capacity. *J. Pharm. Sci.* **2016**, *105*, 941–949.

11. Hubatsch, I.; Ragnarsson, E. G. E.; Artursson, P. Determination of drug permeability and prediction of drug absorption in Caco-2 monolayers. *Nat. Protoc.* **2007**, *2*, 2111.

12. Walle, T. Absorption and metabolism of flavonoids. *Free Radic. Biol. Med.* **2004**, *36*, 829–837.

13. Laitinen, L.; Kangas, H.; Kaukonen, A. M.; Hakala, K.; Kotiaho, T.; Kostianen, R.; Hirvonen, J. N-in-one permeability studies of heterogeneous sets of compounds across Caco-2 cell monolayers. *Pharm. Res.* **2003**, *20*, 187–197.
14. Hakala, K. S.; Laitinen, L.; Kaukonen, A. M.; Hirvonen, J.; Kostianen, R.; Kotiaho, T. Development of LC/MS/MS Methods for cocktail dosed Caco-2 samples using atmospheric pressure photoionization and electrospray ionization. *Anal. Chem.* **2003**, *75*, 5969–5977.
15. Laitinen, L. A.; Tammela, P. S. M.; Galkin, A.; Vuorela, H. J.; Marvola, M. L. A.; Vuorela, P. M. Effects of extracts of commonly consumed food supplements and food fractions on the permeability of drugs across Caco-2 cell monolayers. *Pharm. Res.* **2004**, *21*, 1904–1916.
16. Kreander, K.; Galkin, A.; Vuorela, S.; Tammela, P.; Laitinen, L.; Heinonen, M.; Vuorela, P. In-vitro mutagenic potential and effect on permeability of co-administered drugs across Caco-2 cell monolayers of *Rubus idaeus* and its fortified fractions. *J. Pharm. Pharmacol.* **2006**, *58*, 1545–1552.
17. Laitinen, L.; Takala, E.; Vuorela, H.; Vuorela, P.; Kaukonen, A. M.; Marvola, M. Anthranoid laxatives influence the absorption of poorly permeable drugs in human intestinal cell culture model (Caco-2). *Eur. J. Pharm. Biopharm.* **2007**, *66*, 135–145.
18. Cabrera-Pérez, M. Á.; Pham-The, H. Computational modeling of human oral bioavailability: what will be next? *Expert Opin. Drug Discov.* **2018**, *13*, 509–521.
19. Cruciani, G.; Crivori, P.; Carrupt, P.-A.; Testa, B. Molecular fields in quantitative structure–permeation relationships: the VolSurf approach. *J. Mol. Struct. THEOCHEM* **2000**, *503*, 17–30.
20. Cruciani, G.; Pastor, M.; Guba, W. VolSurf: a new tool for the pharmacokinetic optimization of lead compounds. *Eur. J. Pharm. Sci.* **2000**, *11*, S29–S39.
21. Sambuy, Y.; De Angelis, I.; Ranaldi, G.; Scarino, M. L.; Stamatii, A.; Zucco, F. The Caco-2 cell line as a model of the intestinal barrier: influence of cell and culture-related factors on Caco-2 cell functional characteristics. *Cell Biol. Toxicol.* **2005**, *21*, 1–26.

22. Dall'Acqua, S.; Catanzaro, D.; Cocetta, V.; Igl, N.; Ragazzi, E.; Giron, M. C.; Ceconello, L.; Montopoli, M. Protective effects of psi taraxasterol 3-O-myristate and arnidiol 3-O-myristate isolated from *Calendula officinalis* on epithelial intestinal barrier. *Fitoterapia* **2016**, *109*, 230–235.
23. Carullo, G.; Governa, P.; Spizzirri, U. G.; Biagi, M.; Sciubba, F.; Giorgi, G.; Loizzo, M. R.; Di Cocco, M. E.; Aiello, F.; Restuccia, D. Sangiovese cv pomace seeds extract-fortified kefir exerts anti-inflammatory activity in an *in vitro* model of intestinal epithelium using Caco-2 cells. *Antioxidants (Basel, Switzerland)* **2020**, *9*.
24. Hubatsch, I.; Ragnarsson, E. G. E.; Artursson, P. Determination of drug permeability and prediction of drug absorption in Caco-2 monolayers. *Nat. Protoc.* **2007**, *2*, 2111–2119.
25. Liu, T.; Chang, L.-J.; Uss, A.; Chu, I.; Morrison, R. A.; Wang, L.; Prelusky, D.; Cheng, K.-C.; Li, C. The impact of protein on Caco-2 permeability of low mass balance compounds for absorption projection and efflux substrate identification. *J. Pharm. Biomed. Anal.* **2010**, *51*, 1069–1077.
26. Vidau, C.; Brunet, J.-L.; Badiou, A.; Belzunces, L. P. Phenylpyrazole insecticides induce cytotoxicity by altering mechanisms involved in cellular energy supply in the human epithelial cell model Caco-2. *Toxicol. In Vitro* **2009**, *23*, 589–597.
27. Natoli, M.; Leoni, B. D.; D'Agnano, I.; Zucco, F.; Felsani, A. Good Caco-2 cell culture practices. *Toxicol. In Vitro* **2012**, *26*, 1243–1246.
28. Srinivasan, B.; Kolli, A. R.; Esch, M. B.; Abaci, H. E.; Shuler, M. L.; Hickman, J. J. TEER measurement techniques for *in vitro* barrier model systems. *J. Lab. Autom.* **2015**, *20*, 107–126.
29. Smetanová, L.; Štětínová, V.; Svoboda, Z.; Květina, J. Caco-2 cells , biopharmaceutics classification system (BCS) and biowaiver. *Acta Medica.* **2011**, *54*, 3–8.
30. Gujral, N.; Suh, J. W.; Sunwoo, H. H. Effect of anti-gliadin IgY antibody on epithelial intestinal integrity and inflammatory response induced by gliadin. *BMC Immunol.* **2015**, *16*, 41.

31. Fleet, J. C.; Wood, R. J.; James, C.; Specific, R. J. W. Specific 1,25(OH)₂D₃-mediated regulation of transcellular calcium transport in Caco-2 cells. *Am. J. Physiol.* **1999**, *276*, G958-964.
32. Teng, Z.; Yuan, C.; Zhang, F.; Huan, M.; Cao, W.; Li, K.; Yang, J.; Cao, D.; Zhou, S.; Mei, Q. Intestinal absorption and first-pass metabolism of polyphenol compounds in rat and their transport dynamics in Caco-2 cells. *PLoS One* **2012**, *7*, 1–9.
33. Yang, Y.; Bai, L.; Li, X.; Xiong, J.; Xu, P.; Guo, C.; Xue, M. Transport of active flavonoids, based on cytotoxicity and lipophilicity: an evaluation using the blood-brain barrier cell and Caco-2 cell models. *Toxicol. In Vitro* **2014**, *28*, 388–396.
34. Fang, Y.; Cao, W.; Xia, M.; Pan, S.; Xu, X. Study of structure and permeability relationship of flavonoids in Caco-2 cells. *Nutrients* **2017**, *9*, 1301.

CHAPTER 7

Structure-based identification of P-glycoprotein inhibitors from natural sources

7.1. Introduction

Efflux phenomena, caused by transport proteins, are often responsible for the poor oral bioavailability of natural products, which lead to difficulties in their clinical application [1].

Adenosine triphosphate binding cassette (ABC) transporters are a large family of proteins involved in membrane transport of a wide variety of substrates [2]. Among the 48 human ABC-transporters identified, ABCB1, also called MDR-1 or P-glycoprotein (P-gp), is the best characterized for its involvement in the drug discovery process [3]. P-gp has been found to mediate multidrug resistance in cancer cells; in fact, its physiological role is to protect sensitive tissues from the accumulation of toxic xenobiotics [4]. In particular, as P-gp is expressed in membrane barrier such as the intestine, it can affect the bioavailability of orally administered drugs [5], including natural products [6].

Thus, the discovery of effective P-gp inhibitors/modulators has been the focus of many researches, to the extent that the European Medicines Agency and the USA Food and Drug Administration have proposed their own guidelines on how to conduct this kind of research [2].

Three generations of P-gp inhibitors have been developed so far, but, unfortunately, none of them has been able to prove their effectiveness in clinical trials [7]. Hence, further investigations are needed to develop more effective drugs, which would be useful in overcoming multidrug resistance, but also in increasing the oral bioavailability of natural compounds acting as P-gp substrates.

Together with *in vivo* experiments, which are limited by the cost, complexity, and ethics issues, several *in vitro* and *in silico* tests have been developed to predict the behavior of drug candidates towards P-gp. Among the most widespread *in vitro* tests, the membrane-based ATPase assay and the cell-based cytotoxicity, accumulation, and efflux assays, using Caco-2 cells, are characterized by high-throughput, being cost-effective and easy to perform. On the other hand, computational models provide rapid and inexpensive screening platforms, which have been successfully applied for the design of P-gp ligand candidates [8].

Until recently, ligand- and pharmacophore-based approaches have been preferred, due to the small amount of structural information available [9]. However, a number of three-dimensional structures have been reported: the crystallographic structures of the apo and ligand-bound murine P-gp [10–12], the apo P-gp from *Caenorhabditis elegans* [13], and the apo and ligand-bound P-gp homolog from *Cyanidioschyzon merolae* [14] (figure 7.1). Therefore, structure-based techniques, such as homology modelling, molecular dynamics, and molecular docking, have been applied to evaluate the possible binding mode of drug candidates, thus, providing structural information on the ligand binding sites and the residues involved in ligand binding.

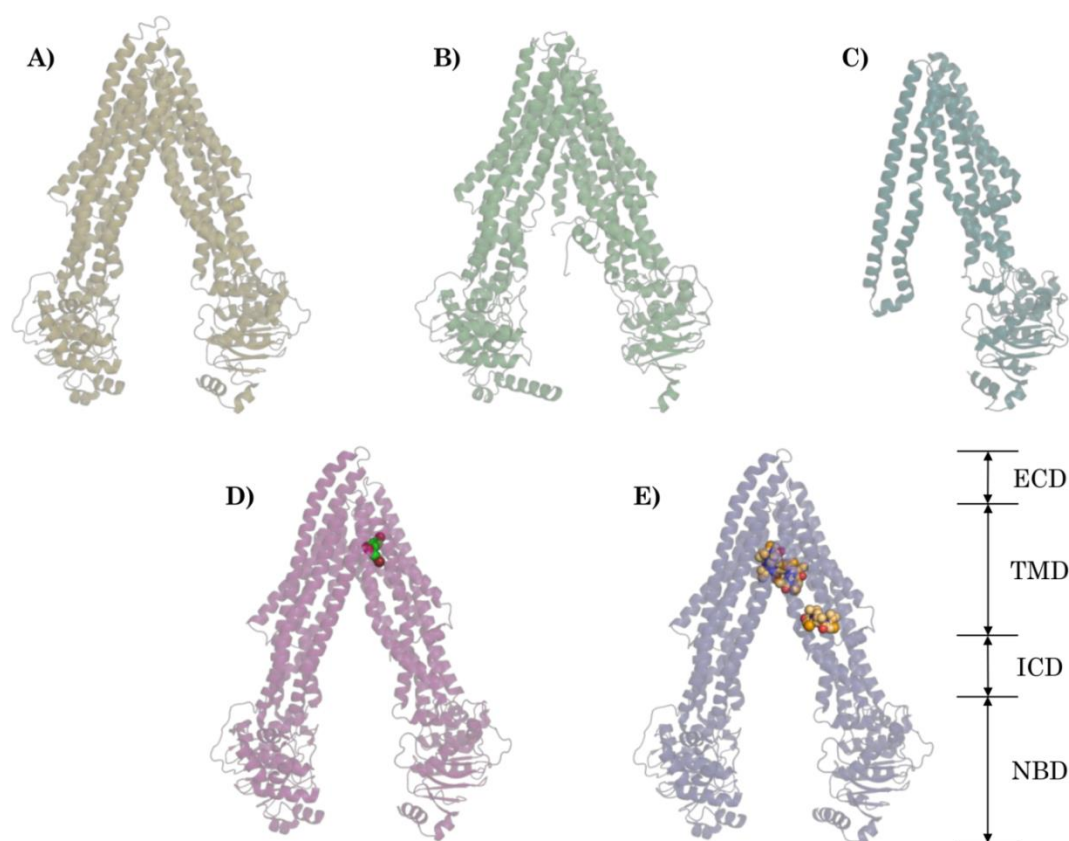


Figure 7.1. Representative 3D structures of (A) murine (PDBID: 4q9h), (B) *C. elegans* (PDBID: 4f4c) and (C) *C. merolae* (PDBID: 3wme) P-gp in the apo conformation. (D-E) Putative ligand binding sites observed in murine structures (PDBID: 4xwk; 4qvj) are shown. ECD: extracellular domain; TMD: transmembrane domain; ICD: intracellular domain; NBD: nucleotide-binding domain.

The murine P-gp shares 87% sequence identity and 94% similarity with human P-gp, with even higher conservation in the binding site [15], and can be suitably used for predicting interactions between ligands and human P-gp [16]. Indeed, several molecular docking and virtual screening studies have been performed on the murine

P-gp, using different docking suites [17], including AutoDock Vina [18]. The murine crystal structure also proved to be an excellent template for the generation of homology models, which gave a better understanding of the possible binding mode of ligands within the human protein [19,20].

Nevertheless, these structures have been captured at limited resolution (higher than 3.3 Å) and, despite the presence of ligands, they all reveal the inward-facing conformation, with varying degrees of nucleotide-binding domain (NBD) separation and small differences in transmembrane domain (TMD) and substrate translocation pathway. As a consequence, there is the need to solve high resolution structures, particularly regarding drug-bound complexes [17,21].

The promiscuity of P-gp binding site, which allows the binding of a broad range of structurally and functionally diverse compounds, is strictly related to its structural flexibility, and is highlighted by the prominent presence of hydrophobic residues, which are involved in van der Waals interactions with lipophilic ligands. Additional complexity is added by the fact that P-gp ligands can act as substrates or inhibitors. When a substrate binds the TMD cavity, it induces TM4 kinking [11], decreasing the transition energy for ATP-dependent NBD dimerization [22]. ATP binding facilitates NBD dimerization which causes the transition to the outward-facing conformation [23]. This causes the repositioning of substrate-interacting side chains, thus, reducing substrate affinity for the binding site. With the outward opening, the substrate equilibrates with the extracellular space and is consequentially released [4]. ATP hydrolysis, releasing phosphate and ADP, leads to NBD dimer destabilization and separation, bringing the protein back to the inward-facing configuration [24]. On the contrary, inhibitors binding prevents P-gp structure to switch from the inward-facing to the outward-facing conformation [22]. Thus, the discovery of selective P-gp inhibitors is a multifaceted process, in which structural information should be carefully taken into consideration. A structure-based protocol, able to efficiently discriminate between possible substrates and inhibitors could potentially be of great help for medicinal chemists involved in this field of research.

To date, X-ray structures of the human P-gp are not available. However, different conformations of the human P-gp have been recently resolved using cryo-electron microscopy (cryoEM) techniques. Compared to the murine and microbial X-ray structures, all of which represent the inward-facing conformation, the cryoEM structures have the advantages of being from a human source and of representing different conformations of the P-gp (i.e. inward-facing, intermediate ligand-bound and outward-facing). Moreover, they have been resolved in the presence of compounds of clinical use (such as taxol and zosuquidar), providing useful insights for structure-based drug discovery. Indeed, in 2018, Kim and Chen reported the molecular structure of human P-gp in the ATP-bound, outward-facing conformation [4]. ATP binding causes the reorientation of the drug-binding cavity, leading to the release of the

substrate into the extracellular space. Right after this publication, Alam and co-workers described the UIC2-bound structure of human P-gp with the ligand-free or inhibitor-bound binding cavity [25]. Remarkably, this is the first paper reporting the tridimensional structure of P-gp bound to a drug of current clinical use, zosuquidar, a third generation P-gp inhibitor, which reveals an intermediate conformation in which the gap between the two NBD is partially closed. In 2019, the same research group used lipidic nanodiscs to reconstitute a substrate-bound (with the chemotherapeutic agent taxol) and an inhibitor-bound (with zosuquidar) P-gp intermediate conformations [26]. This work suggested that only minor structural differences occurred in the binding of substrate and inhibitor to the same P-gp site, while structural differences were amplified along the structure, leading to altered conformations of the NBD, which are responsible for ATP hydrolysis and substrate release. Moreover, it confirmed the ability of P-gp to bind two molecules of zosuquidar in the same drug-binding pocket, as reported in their previous publication. Additionally, the analysis of the ligand binding pocket of the taxol- and zosuquidar-bound structures confirms that most of the ligand-interacting residues are aromatic and hydrophobic, with only one hydrogen bond found between the quinoline moiety of zosuquidar and Y953, and four hydrogen bonds between taxol and Y307, Y310, Q725 and Q991.

Figure 7.2 shows the different conformations of human P-gp, together with a view of the cavity with two molecules of zosuquidar bound.

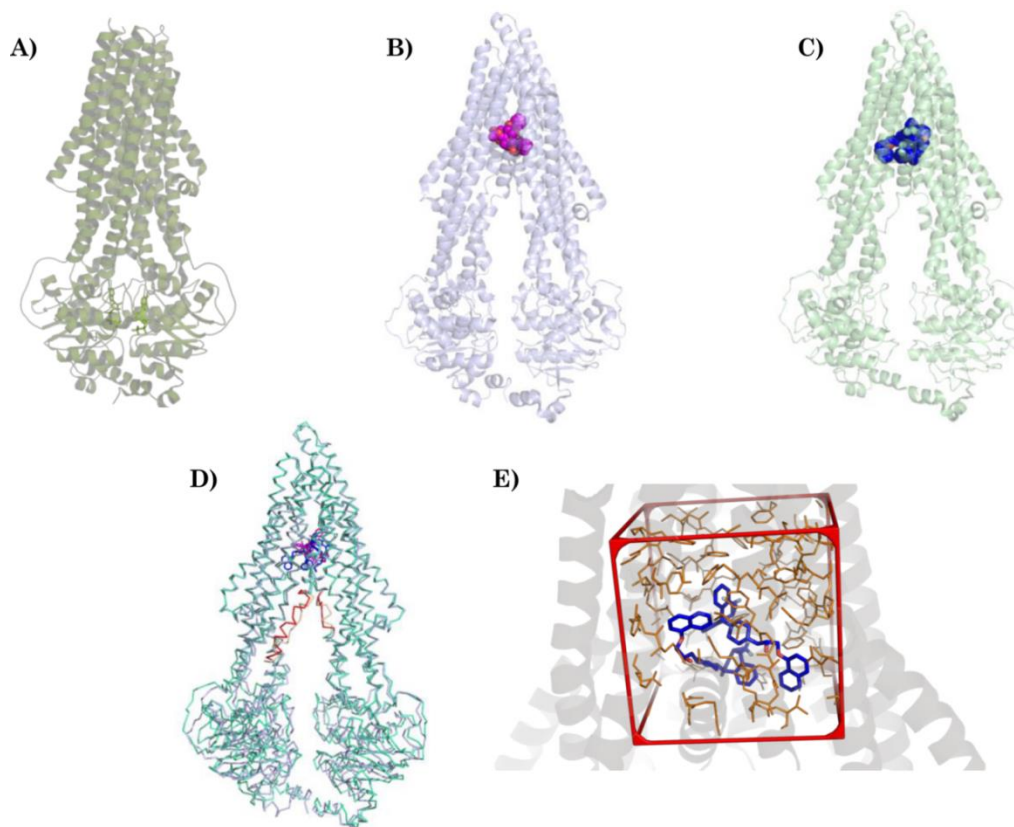


Figure 7.2. 3D structure of the human P-gp in the (A) closed outward-facing ligand-free (PDBID: 6c0v), (B) substrate-bound (PDBID: 6qex) and (C) inhibitor-bound (PDBID: 6qee) intermediate conformations as obtained by cryoEM. (D) Superimposition of the substrate- (light blue) and inhibitor-bound (pale green) structures with backbone differences highlighted. (E) Focus on the binding site of the inhibitor-bound intermediate conformation, showing two copies of zosuquidar that bind to the same cavity.

The aim of this work was to set up an *in silico* model for the virtual screening of curated natural compounds libraries from the ZINC database, to identify hit compounds with potential P-gp inhibitory activity. *In vitro* assays on selected compounds will provide full validation of the virtual screening approach.

7.2. Materials and methods

7.2.1. Computational details

7.2.1.1. Protein and ligands preparation

The human cryoEM 3D structure of the P-gp in the inhibitor-bound intermediate form (PDBID: 6qee) was obtained from the Protein Data Bank (PDB) [27].

The protein was prepared using AutoDock Tools [28], following the standard preparation protocol [29]: adding polar hydrogens, assigning Gasteiger-Marsili atomic charges [30], then merging non-polar hydrogens.

To test the ability of the docking protocol in discerning between binders (i.e. known substrate or inhibitors of P-gp,) and non-binders (molecules which do not interact with P-gp) compounds, a small dataset of 186 compounds, comprised of 77 binders and 109 non-binders, was retrieved from the work of Broccatelli and colleagues [31], and used for docking simulations. This dataset was defined as “Validation set 1”. This dataset was used as a quick test for evaluating the plausibility of using compounds with known activity to validate the docking reliability.

As encouraging results were obtained using Validation set 1, a second larger dataset of 3250 compounds with known activity, including 1243 P-gp inhibitors and 487 substrates, as well as 1520 non-binders, retrieved from the work of Lagares and colleagues [32], was used to build a more robust model able to discriminate between substrate and inhibitors, to be used eventually to filter virtual screening results. This dataset was defined as “Validation set 2”.

The tridimensional coordinates of 197374 commercially available natural compounds were downloaded from the ZINC database [33] in Mol2 format and used for the virtual screening. This library was defined as “Screening set”.

All ligands were converted to PDBQT format using OpenBabel [34]. An overview of the chemical properties of the used libraries is reported in table 7.1.

Table 7.1. Properties of the libraries used for the virtual screening.

Library	N° Ligands	Heavy atoms	Hba	Hbd	Molecular weight	Torsion	AutoDock atom types
Validation set 1	186	10 - 90	0 - 17	0 - 5	131 - 1175	0 - 19	A, Br, C, Cl, F, HD, N, NA, OA, S
Validation set 2	3250	2 - 99	0 - 25	0 - 10	29 - 1285	0 - 37	A, Br, C, Cl, F, HD, I, N, NA, OA, P, S
Screening set	197374	4 - 59	0 - 24	0 - 14	51 - 895	0 - 35	A, Br, C, Cl, F, HD, I, N, NA, OA, P, S

Hba: Hydrogen bond acceptor; Hbd: Hydrogen bond donor.

7.2.1.2. Molecular docking

Raccoon2 and AutoDock Vina (v1.1.2) [29] were used for performing the molecular docking simulations on the Garibaldi High Performance Computing (HPC) cluster, available at The Scripps Research Institute, La Jolla, CA, USA, consisting of:

- 62 Dell Poweredge R420 servers with two intel quad core E5-2450 processors, 48GB RDIMM memory;
- 8 Dell Poweredge R720 servers with two intel quad core E5-2650 processors, 126GB RDIMM memory;
- 64 Dell Poweredge M610 blades with two 2.40 GHz Intel quad core E5530 XEON-EMT processors, 48GB of ECC DDR3 memory;
- 96 Dell Poweredge M610 blades with two 2.27 GHz Intel quad core E5520 XEON-EMT processors, 48GB of ECC DDR3 memory;
- 96 Dell Poweredge M600 blades with two 2.66 GHz Intel quad core E5430 XEON-EMT processors, 32GB of ECC DDR2 memory.

The theoretical peak performance of Garibaldi HPC is 46 TFlops for a total of 17 TBytes of memory. All the computing nodes are interconnected by a series of 8 Gigabit Ethernet Summit X450a switches which are linked to each other by two 10 Gigabit Ethernet Summit X650 switches. For the tightly-coupled parallel applications that

require low latency and high bandwidth connections, Infiniband DDR interconnects are available on a large subset of the nodes. Garibaldi HPC also includes a high performance SFA10K unit from Data Direct Networks (DDN) which delivers 750 TBytes of distributed and persistent storage via the IBM GPFS file system.

The protein was treated as rigid, and the grid box was centered on the co-crystallized ligands (box center: x:173.911, y:168.536, z:162,747) and sized to be 22×24×24 Å. Exhaustiveness was set to 40.

7.2.1.3. 3D common pharmacophore generation

The software DataWarrior [35] was used for independently clustering the P-gp substrates and inhibitors from Validation set 2. Six molecular descriptors, namely *FragFp*, *PathFp*, *SphereFp*, *SkelSpheres*, *OrgFunctions* and *Flexophore*, were used to perform structural similarity clustering, based on Tanimoto similarity. A description of the used molecular descriptors, together with the number of clusters obtained for both substrates and inhibitors are included in table 7.2.

For each clustering method, the most representative molecule of each generated cluster (i.e., the closest molecule to the cluster centroid) was selected, thus, producing 6 groups of inhibitors and 6 groups of substrates. For each of these groups, the best docking pose of each selected molecule was used for generating 3D common pharmacophore hypotheses [36], based on the AutoDock force field/atom type set. The 3D common pharmacophore includes a representation of the most representative chemical features (such as hydrogen bond acceptors and donors, aromatic rings and aliphatic carbons), together with special sets representing recurrent atom type clusters present in the ligand set (i.e., sulfur or halogen). A total of 6 pharmacophore hypotheses for the inhibitors and 6 for the substrates (i.e., one for each initial clustering method) were generated.

Table 7.2. Descriptors used for structural similarity clustering of the known-activity dataset

ID	Descriptor	Type	N° inhibitor clusters	N° substrate clusters
1	<i>FragFp</i>	Substructure fragment dictionary based binary fingerprint.	230	126
2	<i>PathFp</i>	Encodes any linear strand of up to 7 atoms into a hashed binary fingerprint of 512 bits.	226	134
3	<i>SphereFp</i>	Encodes circular spheres of atoms and bonds into a hashed binary fingerprint of 512 bits.	299	185
4	<i>SkelSpheres</i>	Byte vector with a resolution of 1024 bits. It is related to the <i>SphereFp</i> descriptor, but also considers stereochemistry, counts duplicate fragments, in addition encodes hetero-atom depleted skeletons, and has twice the resolution leading to less hash collisions.	289	172
5	<i>OrgFunctions</i>	Neither a fingerprint nor an integer vector. It focuses on available functional groups from a synthetic chemist's point of view. It also recognizes the steric or electronic features of the neighborhood of the functional groups.	175	128
6	<i>Flexophore</i>	Allows predicting 3D-pharmacophore similarities, matching entire conformer sets, rather than comparing individual conformers.	193	144

The pharmacophores were then used to re-score virtual screening results. Molecules with high pharmacophore score as inhibitors and low pharmacophore score as substrates were chosen for visual inspection.

A consensus scoring, with a value between 0 and 1, was then generated by combining the AutoDock Vina binding energy with the pharmacophore rescoring, using the following equation (Eq. 7.1):

$$\textit{Consensus scoring} = \left(\frac{S_{\textit{docking}} - S_{\textit{docking min}}}{(S_{\textit{docking max}} - S_{\textit{docking min}}) \times 2} \right) + \left(\frac{S_{\textit{pharma}} - S_{\textit{pharma min}}}{(S_{\textit{pharma max}} - S_{\textit{pharma min}}) \times 2} \right)$$

where $S_{\textit{docking}}$ is the AutoDock Vina binding energy and $S_{\textit{pharma}}$ is the pharmacophore score.

7.2.2. Statistical analysis

Unpaired t test with Welch's correction was used to analyze the differences in the Vina binding energies and ligand efficiency of Validation set 1 and Validation set 2.

7.3. Results and discussion

7.3.1. Validation of the docking protocol

7.3.1.1. Redocking of zosuquidar

The first step for evaluating the reliability of a docking algorithm is commonly known as "redocking" or "self-docking" simulation. This consists of extracting the coordinates of the co-crystallized conformation of a ligand, randomizing and re-docking it to verify if the experimental binding mode can be reproduced [37]. In the case of the P-gp/zosuquidar complex, this process is complicated by the ability of P-gp to bind two molecules of zosuquidar in the same pocket. Hence, we performed the redocking experiment in two different ways: first by removing both copies of the ligand and redocking them in the ligand-free binding site, and then by removing only one of the two copies and redocking it in the respective ligand-occupied binding site.

Figure 7.3A shows the results of the redocking simulations. When using the ligand-free binding site, AutoDock Vina scoring function showed a preference to dock zosuquidar in position 2, with a root-mean-squared deviation (RMSD) of 5.287 Å, compared to the original conformation in the same position. While a high overall RMSD was obtained, the difluoro-tetracyclo-piperazine (DTP) moiety was well positioned by the docking algorithm (RMSD of this group alone: 0.823 Å), restoring the key interactions found in the bound conformation, whereas docking the oxypropanol-quinoline moiety resulted to be more difficult, because of the large binding site dimension and the lack of constraints induced by the absence of the second copy of the inhibitor. Indeed, when using the two ligand-occupied binding sites, the accuracy of the redocking increased dramatically, with RMSD values of 1.103 Å and 1.791 Å, compared to the original positions 1 and 2, respectively.

To investigate the interactions that involve the two copies of zosuquidar within the site, we performed additional redocking simulations, using the recently developed version of AutoDock Vina (v1.2.0 beta), which features the possibility to dock multiple ligands simultaneously. As reported in figure 7.3B, by docking two molecules of zosuquidar we obtained a significant improvement of the molecule pose in position 2, reducing its RMSD value from 5.287 Å to 2.255 Å. Noticeably, the pose in position 1 showed an RMSD value of 3.796 Å, compared to the original conformation. While for this pose the software still was not able to reproduce the orientation of the quinolone moiety, the RMSD of the DTP moiety alone was 1.514, confirming the ability of Vina to correctly dock this portion of the ligand.

These results further support the assumption that both the docking protocol and the Vina force fields can be considered sufficiently reliable for this target, and therefore Vina was chosen for performing the virtual screening.

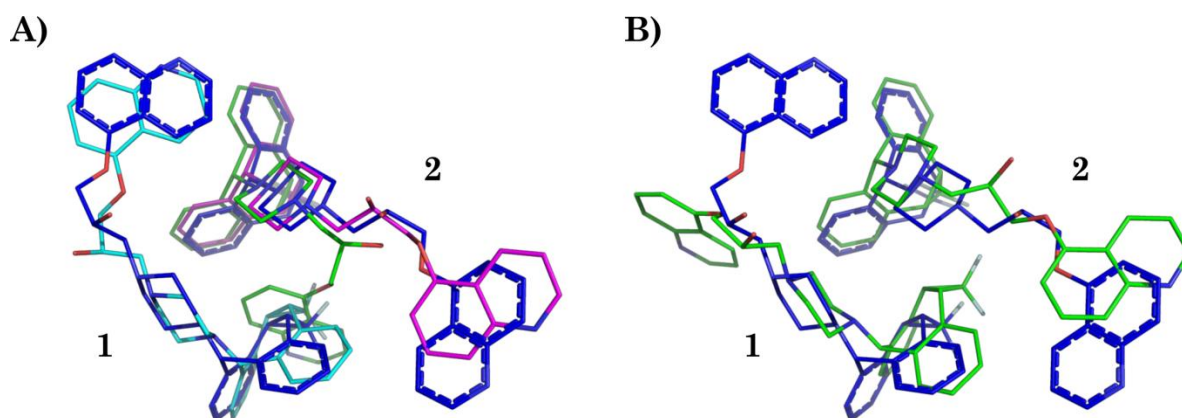


Figure 7.3. (A) Single ligand redocking of zosuquidar in the apo (green), zosuquidar 1- (magenta) and zosuquidar 2-occupied (cyan) P-gp binding site. (B) Multiple ligand redocking of zosuquidar (green) using the beta version of AutoDock Vina 1.2.0. The experimental 3D coordinates of zosuquidar from PDBID 6qee are showed in blue.

7.3.1.2. Docking of Validation Set 1

The docking protocol used performed well in distinguishing binders from non-binders, using Validation Set 1. Indeed, the average binding energy of the binders was -8.4 kcal/mol, which was lower than that obtained with non-binders (-7.3 kcal/mol) (figure 7.4A). While the statistical analysis showed that the difference is significant ($p < 0.001$), it is smaller than the standard error of the AutoDock Vina scoring function (estimated to be around 2.8 kcal/mol [38]). Hence, even if the discrimination power can be considered sufficiently reliable, care must be taken when using it for virtual screening purposes.

When analyzing the ranking of compounds based on AutoDock Vina binding energy, it is evident that most of the binders are predicted to have a better binding energy compared to the non-binders (figure 7.4C). Indeed, in the first quartile of the ranking, 36 out of total 47 ligands (77%) are binders. The enrichment of results decreases when proceeding toward lower quartiles, with 60% of the binders scoring better than the average ranking of the 186 total ligands.

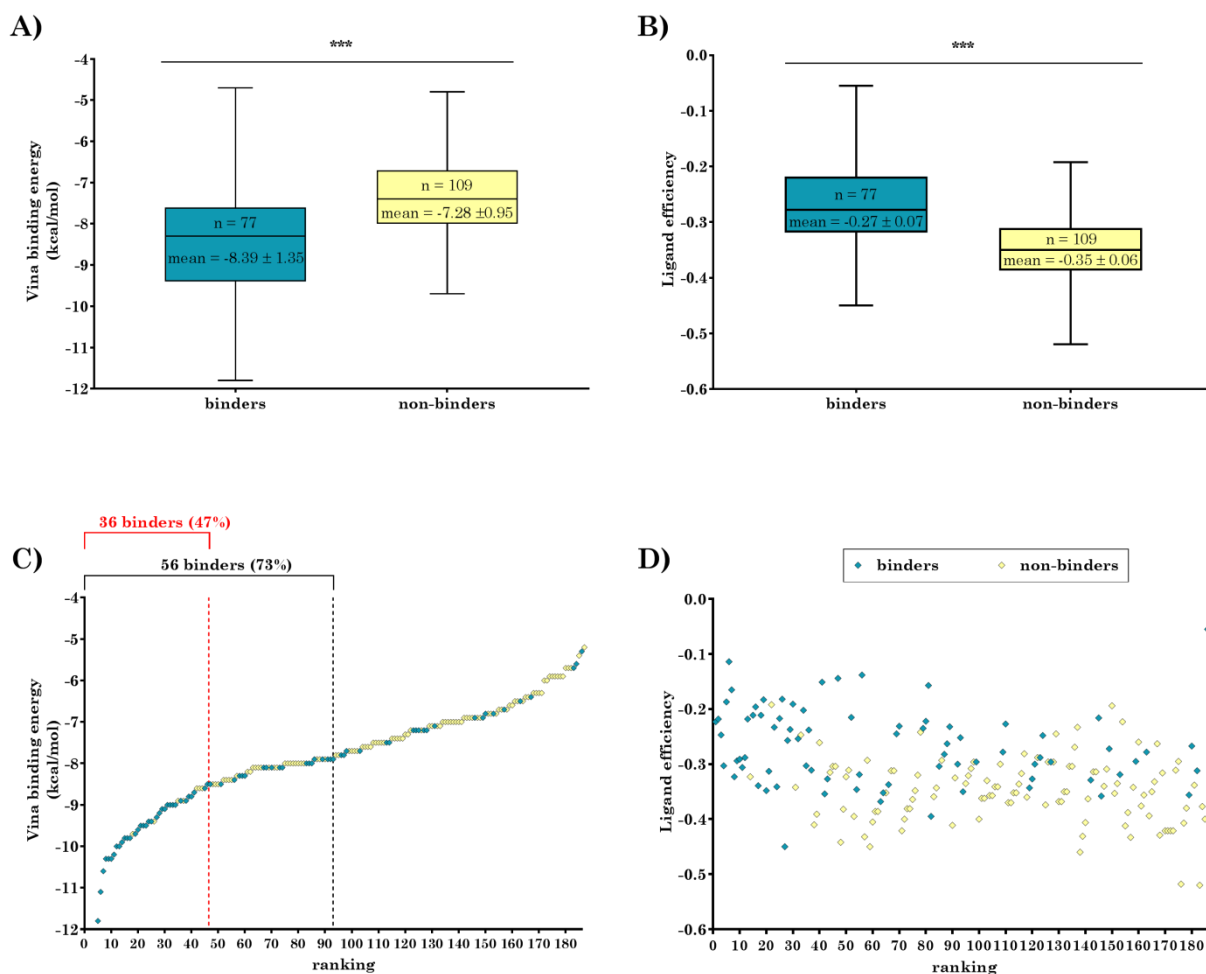


Figure 7.4. AutoDock Vina performance in discerning between known binders and non-binders using (A, C) Vina binding energy and (B, D) ligand efficiency. * $p < 0.001$, unpaired t test with Welch's correction.**

A similar trend was observed when considering ligand efficiency as a parameter to discern between different classes of ligands. Figure 7.4B shows that ligand efficiency of binders is higher on average compared to that of non-binders (-0.27 vs -0.35, $p < 0.001$). Potentially, this could be related to differences in molecular weight, which is higher for binders than for non-binders (482.9 ± 187.8 vs 341.9 ± 152.8 , respectively; $p < 0.001$). However, no evident correlation was found with the binding energy ranking of this set (figure 7.4D), making it difficult to find the determinant factors of the predictive power.

These results encouraged us to perform a second set of docking simulations, using Validation set 2, which classifies ligands as inhibitor binders, substrate binders, and non-binders.

7.3.1.3. Docking of Validation set 2 and 3D common pharmacophore generation

The results obtained for this dataset are extremely consistent with those obtained using Validation set 1, both in terms of binding energies (figure 7.5A) and ligand efficiency (figure 7.5B), with very similar trends for the average binding energy and ligand efficiency of binders, which are respectively lower and higher, compared to the non-binders. Interestingly, no differences can be found when comparing the average binding energy and ligand efficiency of inhibitors and substrates.

High correlation between ranking and docking score is found. The quartile ranking of compounds, based on the binding energy (figure 7.5C), shows that there is increasing probability to find a binder moving from the last to the first quartile. An inverse trend can be observed for non-binders, which are much more represented in the last quartile. Focusing on the first quartile, although binders are homogeneously distributed, the probability to find non-binder continues to decrease while moving to the very first section of the ranking (figure 7.5D).

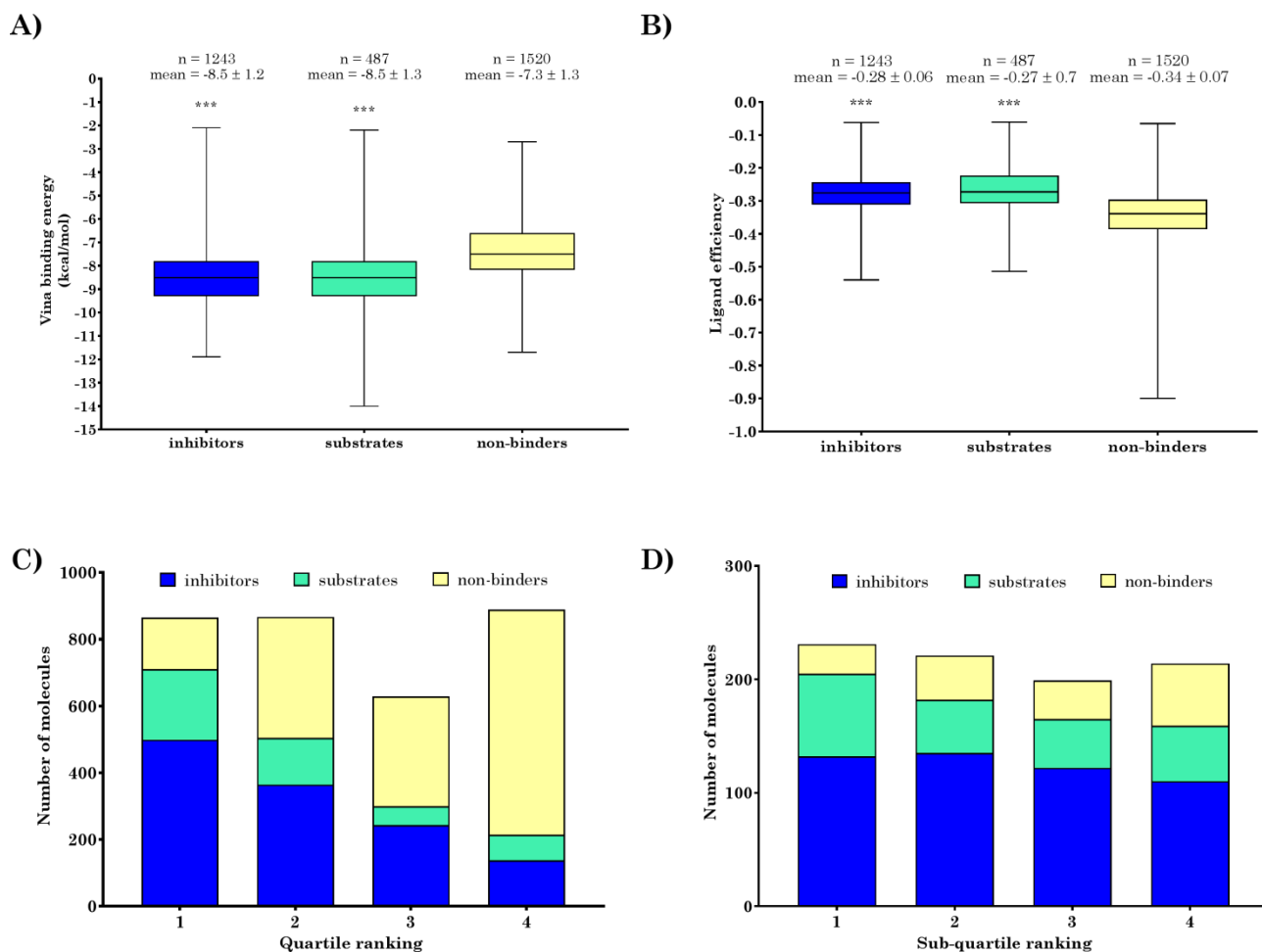


Figure 7.5. AutoDock Vina performance in discerning between known inhibitors, substrates and non-binders using (A) Vina binding energy and (B) ligand efficiency. (C) Quartile ranking of compounds in terms of binding energy and (D) top quartile sub-ranking. * $p < 0.001$, unpaired t test with Welch's correction.**

Based on these results, we argued that this docking protocol can be successfully used to enrich the top ranked results of a virtual screening for the identification of P-gp binders. In absence of evidence of binding of multiple copies of known P-gp binders other than zosuquidar and considering the good enrichment of binders/non-binders found with the single ligand docking, we choose to use this protocol over the multiple ligand docking one, available in the beta version of AutoDock Vina 1.2.0, for the virtual screening of the Screening set. Moreover, filtering the virtual screening results by selecting only those with a binding energy lower than the average obtained with active compounds (-8.5 kcal/mol) could represent a strategy for reducing the number of results to be evaluated in the subsequent steps of the analysis. However, the results show also that more accurate analyses are needed for discerning between inhibitors

and substrates candidates. Thus, we generated 3D common pharmacophores hypotheses, using the best docking poses of selected inhibitors and substrates, independently.

Table 7.3 reports the main features of the generated pharmacophores. On average, a higher number of hydrogen bond acceptor, aliphatic carbon and halogen features, is present in the 3D common pharmacophore hypotheses of substrates. On the contrary, a higher number of aromatic and sulfur features were found in the 3D common pharmacophore hypotheses of inhibitors. Finally, no difference was found in the number of hydrogen bond donor features.

Table 7.3. 3D common pharmacophore features for P-gp inhibitors and substrates.

3D common pharmacophore hypothesis	N° ligands	Features					
		Hba	Hbd	Aromatic	Aliphatic carbon	Sulfur	Halogen
Inhibitor 1	230	51	26	42	18	9	20
Inhibitor 2	226	50	26	34	19	13	22
Inhibitor 3	299	54	26	39	22	9	25
Inhibitor 4	289	56	24	37	20	9	26
Inhibitor 5	175	49	21	31	18	8	16
Inhibitor 6	193	51	24	44	19	10	17
Substrate 1	126	53	23	38	20	7	21
Substrate 2	134	55	26	38	21	8	25
Substrate 3	185	63	28	37	23	9	26
Substrate 4	172	59	26	37	22	7	26
Substrate 5	128	54	22	31	23	5	22
Substrate 6	144	56	27	32	23	6	21

Hba: Hydrogen bond acceptor; Hbd: Hydrogen bond donor.

7.3.2. Virtual screening results

The ranking of the natural products library used for the virtual screening is reported in figure 7.6. A nearly ideal Gaussian distribution of compounds can be observed when evaluating the ranking based on binding energy. Interestingly, the mean value of the curve is -8.4 kcal/mol, which corresponds to the average value obtained with the binders of the Validation set 1 and 2. Hence, based on the results of this dataset, 50% of the screened compounds could qualify as possible P-gp binders, according to Vina binding energies alone.

On the other hand, the distribution of the screened compounds according to ligand efficiency is also bell-shaped, with the mean value being -0.33 kcal/mol, and 38% of the compounds having a ligand efficiency higher than -0.28 kcal/mol, which is the average ligand efficiency obtained with the binders of the Validation set 1 and 2.

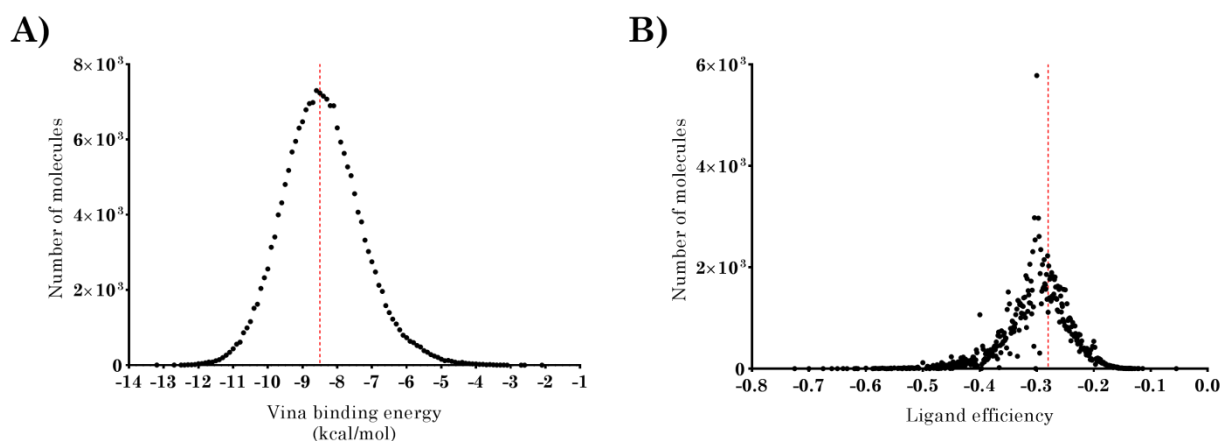


Figure 7.6. (A) AutoDock Vina binding energy and (B) ligand efficiency of the natural products library. The dashed red lines represent the average values obtained from the active molecules of Validation set 1 and 2.

The best docked poses of the screened compounds were then re-scored with the 6 inhibitor pharmacophore hypotheses and the 6 substrate pharmacophore hypotheses, in the attempt to enrich results with inhibitors. Results were then compared to select only molecules matching all the inhibitor pharmacophore hypotheses and none of the substrate pharmacophore hypotheses. These filtering methods, combined with the predicted binding energy cutoff of -8.5 kcal/mol led to the selection of 33 candidates,

reported in table 7.4, which were then clustered using the *FragFp* method of DataWarrior, to reduce the number of compounds to be tested, maximizing chemical diversity.

Table 7.4. Virtual screening candidates selected for clustering.

Compound	ZINCID	Vina binding energy	Pharmacophore re-scoring	Consensus scoring
1	ZINC000824596131	-9.9	11.54	0.69
2	ZINC000824751051	-10.5	10.71	0.69
3	ZINC000824595887	-9.7	11.59	0.68
4	ZINC000828534103	-10.2	10.60	0.67
5	ZINC000524730654	-10.3	10.34	0.67
6	ZINC000824596481	-9.8	10.98	0.66
7	ZINC000049841246	-9.9	10.66	0.66
8	ZINC000079221590	-10.3	10.03	0.66
9	ZINC000263585922	-9.9	10.55	0.66
10	ZINC000102986418	-9.8	10.37	0.65
11	ZINC001547138921	-9	11.47	0.65
12	ZINC000263586282	-9.6	10.52	0.64
13	ZINC001547138595	-9.9	9.88	0.63
14	ZINC000824595807	-8.8	11.38	0.63
15	ZINC000085893681	-9.6	10.19	0.63
16	ZINC000824596563	-8.9	11.15	0.63
17	ZINC000021992916	-9.4	10.45	0.63
18	ZINC000253402083	-9.8	9.89	0.63
19	ZINC000824595813	-9.1	10.67	0.63
20	ZINC000079216638	-9.2	10.50	0.62

21	ZINC000824596273	-9.2	10.40	0.62
22	ZINC000008964837	-9.4	10.10	0.62
23	ZINC000085866958	-8.9	10.62	0.62
24	ZINC000824664756	-9.4	9.92	0.61
25	ZINC000824595877	-9.1	10.27	0.61
26	ZINC000034499029	-9.3	9.86	0.61
27	ZINC000004235462	-8.5	10.84	0.60
28	ZINC000003943903	-9.3	9.68	0.60
29	ZINC000150484449	-8.9	10.14	0.60
30	ZINC000004235535	-8.7	10.34	0.60
31	ZINC000002156967	-8.6	10.25	0.59
32	ZINC000005412089	-8.5	10.11	0.58
33	ZINC000263586757	-8.5	9.51	0.56

14 different clusters were obtained and the most representative molecule of each cluster was selected for *in vitro* validation. The structures of the 14 selected compounds, namely compounds 2, 4, 5, 6, 8, 10, 13, 14, 17, 18, 20, 23, 27 and 29, are reported in figure 7.7.

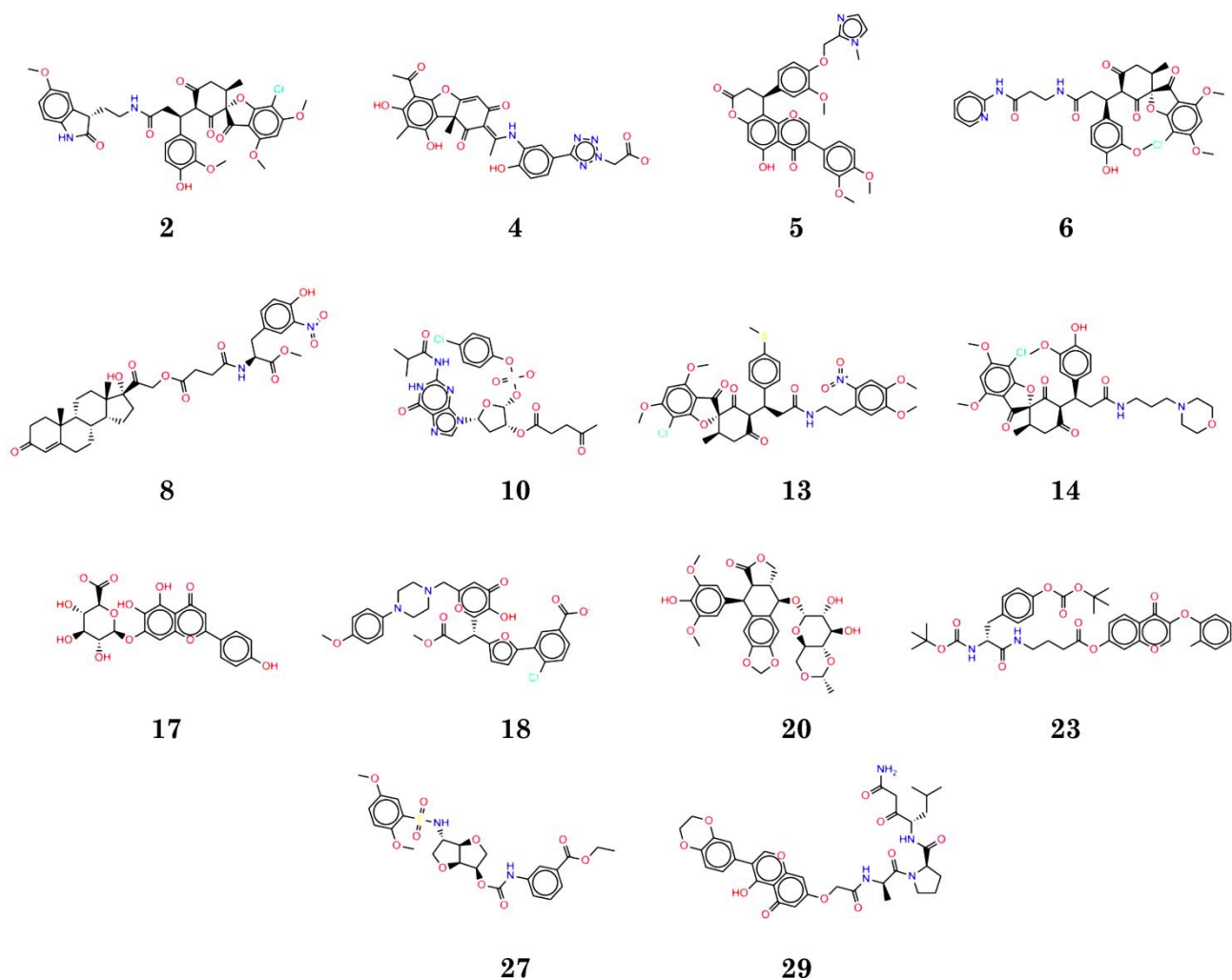


Figure 7.7. 2D structures of the 14 compounds selected for *in vitro* validation.

Compound 2, a griseofulvin derivative, was the most representative molecule of the most populated cluster and, among the 14 selected compounds, is the one with the lowest Vina binding energy and the higher consensus score. As shown in figure 7.8, the best docked pose of compound 2 occupies the position 2 of the zosuquidar binding site, with the exception of the 4-hydroxy-3-methoxyphenyl moiety, which interact with residues involved in the binding of the DTP moiety of zosuquidar in position 1. Consistently with the lipophilic nature of the P-gp binding site, the majority of the interactions are represented by van der Waals contacts with hydrophobic residues such as Met68, Trp231, Met298, Phe302, Ile305, Tyr306, Tyr309, Phe335, Ile339, Asn720, Gly721, Gln724, Phe727, Phe769, Gln837, Asn841, Met875, Phe982, Met985, Ala986 and Gln989. Four important anchor points are represented by the hydrogen bonds between the methoxyl group in position 4 of the benzofurane moiety and the

hydroxyl group of Tyr309, the carbonyl group on the propanamide moiety and the hydroxyl group of Tyr306, the carbonyl group on the oxindole moiety and the backbone NH moiety of Asn841, and the hydroxyl group and the indole nitrogen of Trp231.

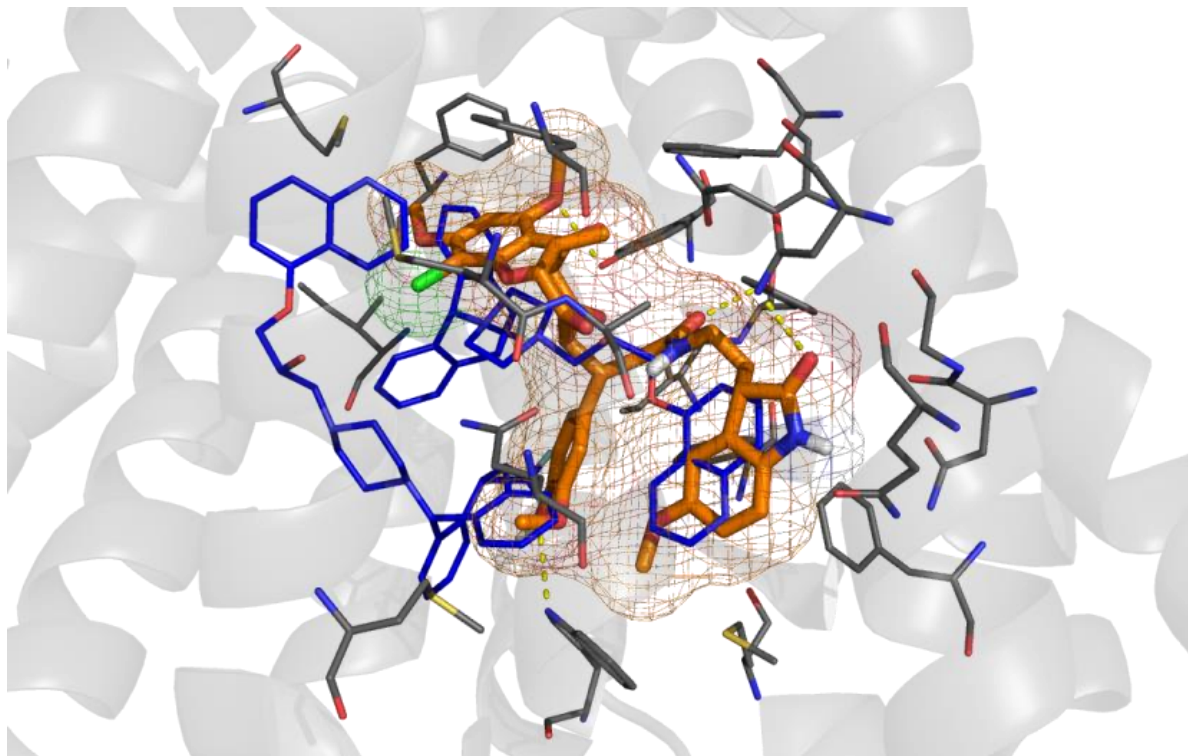


Figure 7.8. Best docked pose of compound 2 (orange stick with mesh surface) in the binding site of P-gp. Interacting residues are shown as gray line. For comparison, the experimental binding pose of zosuquidar is also shown as blue line. Hydrogen bonds are represented by yellow dashed lines.

Currently, no literature data is available to support the P-gp binding activity of compound 2. However, the possible P-gp binding activity of griseofulvin has been speculated, even if more experimental support is required to delineate this hypothesis more concisely [39].

7.4. Conclusions

P-gp affects the bioavailability of drugs and is involved in multidrug resistance by transporting xenobiotics from the cell membrane to the extracellular space, thus limiting their absorption and intracellular accumulation. Clinical effective inhibitors are still lacking as most of the currently available drugs failed in reducing multidrug resistance or caused severe side effects.

The *in silico* structure-based virtual screening approach used in this work was able to efficiently differentiate between P-gp binders and non-binders, based on the inhibitors enrichment factor obtained using Validation set 1 and Validation set 2.

However, more accurate analyses are needed for discerning between inhibitors and substrates candidates. Pharmacophore modeling has been successfully used in the past for the identification of P-gp substrates or inhibitors. Thus, we used 3D common pharmacophores hypotheses, generated using the best docking poses of selected inhibitors and substrates, independently, to filter the virtual screening results.

By combining molecular docking and pharmacophore modeling, we identified 14 potential P-gp inhibitors, out of a total of 197374 commercially available natural compounds.

In vitro assays of the selected compounds are ongoing and will provide validation of the computational protocol described.

7.5. References

1. He, S.; Chan, E.; Zhou, S. ADME properties of herbal medicines in humans: evidence, challenges and strategies. *Curr. Pharm. Des.* **2011**, *17*, 357–407.
2. Robey, R. W.; Pluchino, K. M.; Hall, M. D.; Fojo, A. T.; Bates, S. E.; Gottesman, M. M. Revisiting the role of ABC transporters in multidrug-resistant cancer. *Nat. Rev. Cancer* **2018**, *18*, 452–464.
3. Arana, M. R.; Altenberg, G. A. ATP-binding cassette exporters: structure and mechanism with a focus on P-glycoprotein and MRP1. *Curr. Med. Chem.* **2019**, *26*, 1062–1078.
4. Kim, Y.; Chen, J. Molecular structure of human P-glycoprotein in the ATP-bound, outward-facing conformation. *Science* **2018**, *359*, 915–919.
5. Yano, K.; Tomono, T.; Ogihara, T. Advances in studies of P-Glycoprotein and its expression regulators. *Biol. Pharm. Bull.* **2018**, *41*, 11–19.

6. Porat, D.; Dahan, A. Active intestinal drug absorption and the solubility-permeability interplay. *Int. J. Pharm.* **2018**, *537*, 84–93.
7. Callaghan, R.; Luk, F.; Bebawy, M. Inhibition of the multidrug resistance P-glycoprotein: time for a change of strategy? *Drug Metab. Dispos.* **2014**, *42*, 623–631.
8. Gameiro, M.; Silva, R.; Rocha-Pereira, C.; Carmo, H.; Carvalho, F.; de Lourdes Bastos, M.; Remiao, F. Cellular models and *in vitro* assays for the screening of modulators of P-gp, MRP1 and BCRP. *Molecules* **2017**, *22*.
9. Castagnolo, D.; Contemori, L.; Maccari, G.; Avramova, S. I.; Neri, A.; Sgaragli, G.; Botta, M. From taxuspine X to structurally simplified taxanes with remarkable P-Glycoprotein inhibitory activity. *ACS Med. Chem. Lett.* **2010**, *1*, 416–421.
10. Aller, S. G.; Yu, J.; Ward, A.; Weng, Y.; Chittaboina, S.; Zhuo, R.; Harrell, P. M.; Trinh, Y. T.; Zhang, Q.; Urbatsch, I. L.; Chang, G. Structure of P-glycoprotein reveals a molecular basis for poly-specific drug binding. *Science* **2009**, *323*, 1718–1722.
11. Szewczyk, P.; Tao, H.; McGrath, A. P.; Villaluz, M.; Rees, S. D.; Lee, S. C.; Doshi, R.; Urbatsch, I. L.; Zhang, Q.; Chang, G. Snapshots of ligand entry, malleable binding and induced helical movement in P-glycoprotein. *Acta Crystallogr. D. Biol. Crystallogr.* **2015**, *71*, 732–741.
12. Nicklisch, S. C. T.; Rees, S. D.; McGrath, A. P.; Gokirmak, T.; Bonito, L. T.; Vermeer, L. M.; Cregger, C.; Loewen, G.; Sandin, S.; Chang, G.; Hamdoun, A. Global marine pollutants inhibit P-glycoprotein: environmental levels, inhibitory effects, and cocrystal structure. *Sci. Adv.* **2016**, *2*, e1600001.
13. Jin, M. S.; Oldham, M. L.; Zhang, Q.; Chen, J. Crystal structure of the multidrug transporter P-glycoprotein from *Caenorhabditis elegans*. *Nature* **2012**, *490*, 566–569.
14. Kodan, A.; Yamaguchi, T.; Nakatsu, T.; Sakiyama, K.; Hipolito, C. J.; Fujioka, A.; Hirokane, R.; Ikeguchi, K.; Watanabe, B.; Hiratake, J.; Kimura, Y.; Suga, H.; Ueda, K.; Kato, H. Structural basis for gating mechanisms of a eukaryotic P-glycoprotein homolog. *Proc. Natl. Acad. Sci.* **2014**, *111*, 4049–4054.
15. Chufan, E. E.; Kapoor, K.; Sim, H. M.; Singh, S.; Talele, T. T.; Durell, S. R.;

Ambudkar, S. A. Multiple transport-active binding sites are available for a single substrate on human P-glycoprotein (ABCB1). *PLoS One* **2013**, *8*, 1–16.

16. Mollazadeh, S.; Sahebkar, A.; Hadizadeh, F.; Behravan, J.; Arabzadeh, S. Structural and functional aspects of P-glycoprotein and its inhibitors. *Life Sci.* **2018**, *214*, 118–123.

17. Vilar, S.; Sobarzo-Sanchez, E.; Uriarte, E. *In silico* prediction of P-glycoprotein binding: insights from molecular docking studies. *Curr. Med. Chem.* **2019**, *26*, 1746–1760.

18. Ferreira, R. J.; Ferreira, M.-J. U.; dos Santos, D. J. V. A. Molecular docking characterizes substrate-binding sites and efflux modulation mechanisms within P-glycoprotein. *J. Chem. Inf. Model.* **2013**, *53*, 1747–1760.

19. Klepsch, F.; Vasanthanathan, P.; Ecker, G. F. Ligand and structure-based classification models for prediction of P-glycoprotein inhibitors. *J. Chem. Inf. Model.* **2014**, *54*, 218–229.

20. Pajeva, I. K.; Globisch, C.; Wiese, M. Combined pharmacophore modeling, docking, and 3D QSAR studies of ABCB1 and ABCC1 transporter inhibitors. *ChemMedChem* **2009**, *4*, 1883–1896.

21. Waghray, D.; Zhang, Q. Inhibit or evade multidrug resistance P-Glycoprotein in cancer treatment. *J. Med. Chem.* **2018**, *61*, 5108–5121.

22. Dastvan, R.; Mishra, S.; Peskova, Y. B.; Nakamoto, R. K.; Mchaourab, H. S. Mechanism of allosteric modulation of P-glycoprotein by transport substrates and inhibitors. *Science (80-.)*. **2019**, *364*, 689–692.

23. Dawson, R. J. P.; Locher, K. P. Structure of the multidrug ABC transporter Sav1866 from *Staphylococcus aureus* in complex with AMP-PNP. *FEBS Lett.* **2007**, *581*, 935–938.

24. Srikant, S.; Gaudet, R. Mechanics and pharmacology of substrate selection and transport by eukaryotic ABC exporters. *Nat. Struct. Mol. Biol.* **2019**, *26*, 792–801.

25. Alam, A.; Küng, R.; Kowal, J.; McLeod, R. A.; Tremp, N.; Broude, E. V.; Roninson, I.

- B.; Stahlberg, H.; Locher, K. P. Structure of a zosuquidar and UIC2-bound human-mouse chimeric ABCB1. *Proc. Natl. Acad. Sci.* **2018**, *115*, E1973--E1982.
26. Alam, A.; Kowal, J.; Broude, E.; Roninson, I.; Locher, K. P. Structural insight into substrate and inhibitor discrimination by human P-glycoprotein. *Science* **2019**, *363*, 753–756.
27. Berman, H. M.; Westbrook, J.; Feng, Z.; Gilliland, G.; Bhat, T. N.; Weissig, H.; Shindyalov, I. N.; Bourne, P. E. The Protein Data Bank. *Nucleic Acids Res.* **2000**, *28*, 235–242.
28. Morris, G. M.; Ruth, H.; Lindstrom, W.; Sanner, M. F.; Belew, R. K.; Goodsell, D. S.; Olson, A. J. AutoDock4 and AutoDockTools4: Automated docking with selective receptor flexibility. *J. Comput. Chem.* **2009**, *30*, 2785–2791.
29. Forli, S.; Huey, R.; Pique, M. E.; Sanner, M. F.; Goodsell, D. S.; Olson, A. J. Computational protein–ligand docking and virtual drug screening with the AutoDock suite. *Nat. Protoc.* **2016**, *11*, 905–919.
30. Gasteiger, J.; Marsili, M. Iterative partial equalization of orbital electronegativity - a rapid access to atomic charges. *Tetrahedron* **1980**, *36*, 3219–3228.
31. Broccatelli, F. QSAR models for P-glycoprotein transport based on a highly consistent data set. *J. Chem. Inf. Model.* **2012**, *52*, 2462–2470.
32. Mora Lagares, L.; Minovski, N.; Novič, M. Multiclass classifier for P-Glycoprotein substrates, i, and non-active compounds. *Molecules* **2019**, *24*, 2006.
33. Sterling, T.; Irwin, J. J. ZINC 15 - ligand discovery for everyone. *J. Chem. Inf. Model.* **2015**, *55*, 2324–2337.
34. O’Boyle, N. M.; Banck, M.; James, C. A.; Morley, C.; Vandermeersch, T.; Hutchison, G. R. Open Babel: an open chemical toolbox. *J. Cheminform.* **2011**, *3*, 33.
35. Sander, T.; Freyss, J.; von Korff, M.; Rufener, C. DataWarrior: an open-source program for chemistry aware data visualization and analysis. *J. Chem. Inf. Model.* **2015**, *55*, 460–473.

36. Perryman, A. L.; Santiago, D. N.; Forli, S.; Martins, D. S.; Olson, A. J. Virtual screening with AutoDock Vina and the common pharmacophore engine of a low diversity library of fragments and hits against the three allosteric sites of HIV integrase: participation in the SAMPL4 protein-ligand binding challenge. *J. Comput. Aided. Mol. Des.* **2014**, *28*, 429–441.
37. Cosconati, S.; Forli, S.; Perryman, A. L.; Harris, R.; Goodsell, D. S.; Olson, A. J. Virtual Screening with AutoDock: Theory and Practice. *Expert Opin. Drug Discov.* **2010**, *5*, 597–607.
38. Trott, O.; Olson, A. J. AutoDock Vina: improving the speed and accuracy of docking with a new scoring function, efficient optimization, and multithreading. *J. Comput. Chem.* **2010**, *31*, 455–461.
39. Coyne, C. P.; Jones, T.; Bear, R. Anti-Neoplastic Cytotoxicity of Gemcitabine-(C₄-amide)-[anti-HER2/neu] in Combination with Griseofulvin against Chemotherapeutic-Resistant Mammary Adenocarcinoma (SKBr-3). *Med. Chem.* **2013**, *3*, 210-223.

CHAPTER 8

Conclusions

Different natural compounds, belonging to the widely distributed molecular class of polyphenols, and herbal extracts containing them were compared for their stability to *in vitro* simulated gastrointestinal digestion. Specific examples were evaluated for investigating the effect of the digestive processes on the bioaccessibility and biological activity of selected samples. The effect of co-administration of two compounds on the Caco-2 permeability of the single compound was also examined as a simplification of the complex mixture of constituents present in a phytocomplex. Finally, an *in silico* virtual screening was performed to identify possible P-glycoprotein inhibitors from natural sources.

Several conclusions can be drawn from the results of this study:

- The complex mixture of constituents that are present in an herbal extract can positively or negatively modulate the stability to gastrointestinal digestion of the single compounds. Using *Matricaria recutita* L, *Cynara scolymus* L., and *Curcuma longa* L. extracts, we found an increase of gastrointestinal stability of the single constituents when using the whole phytocomplex. On the contrary, the gastrointestinal stability of cannabidiol alone was higher, compared to different *Cannabis sativa* L. extracts.
- The bioaccessibility of herbal extract constituents is also affected by the extraction methods used. Using *C. sativa* as an example, we observed that the gastrointestinal stability and bioaccessibility are strongly influenced by the extraction solvent used. This suggests the need to standardize herbal extracts and their derived preparations, not only to obtain the maximum yield of constituents, but also taking into account the effect of the extraction method on the overall gastrointestinal stability, bioaccessibility and bioavailability.
- Gastrointestinal digestion can strongly affect the biological activity of

- natural products. Depending on the original herbal material used, the phytocomplex of herbal extracts can protect their constituents from losing their biological activity after being digested. Dark propolis was found to be the best candidate for maintaining the anti-*Helicobacter pylori* activity of galangin and pinocembrin, compared to green propolis and a commercial propolis-based product. Similarly, green tea was more effective than black and Oolong tea in maintaining the antioxidant activity *in vitro*.
- Using couples of compounds, we found that the Caco-2 permeability of single compounds can be modified. We still need to perform additional experiments to confirm these results. However, we believe that this simple experimental model could be useful to understand the mechanism underlying the differences in the intestinal absorption between single natural products and herbal extract. If we will succeed in confirming our preliminary data, we aim at setting up a computational model able to predict the Caco-2 permeability of complex mixtures of compounds, which will be of great advantage, compared to the current *in silico* models that can only deal with one molecule at a time.
- Finally, *in silico* virtual screening can be successfully exploited for discerning between P-glycoprotein binders and non-binders, and can also guide the identification of novel inhibitors from natural sources.

Lot of work and experimental validation still remain to be done for being able to fully understand the mechanisms involved in the biological activity of herbal phytocomplexes. This work contributed to the field by providing useful experimental data on some important pharmacokinetic parameters, such as stability to gastrointestinal digestion, bioaccessibility, intestinal permeability, and active transport mechanisms of selected natural compounds.

Only 10% of the world biodiversity has been evaluated for its possible therapeutic application, thus, it is expected that, together with pharmacodynamics investigation, data on the pharmacokinetics of natural products, as well as simple methods for obtaining them, such as those used in this work, will be increasingly needed in the future.

ACKNOWLEDGEMENTS

I have been listening to so many colleagues complaining about their PhD during the last three years, that I was beginning to believe this was not the right choice for me. Now that the end of this journey is approaching, I cannot but look back with a proud smile on my face. Not that this was an easy task, at all! It was a long, tiresome, stressful, and consuming journey, indeed. For sure, it was one of the most complex experiences I have ever done. But it was also full of satisfactions and funny moments, and I did learn a lot, that is for sure. I grew as a researcher, and as a person, as well. And I am glad I had the chance to prove myself that I was able to overcome all the obstacles and, most importantly, to learn a lesson from each of them.

There are so many people that took a part in this journey and to whom I wish to express my gratitude.

I wish to thank my supervisor, Professor Fabrizio Manetti, for giving me the opportunity to work under his supervision and for teaching me the importance of being a rigorous and meticulous researcher.

I also wish to thank Professor Stefano Forli and his research group (Christina, Giulia, Martina, Andreas, Batuu, Diogo, Jerome and Matt), but also Adam, Andrew, Anna, Ludovic, Tim, Michelle, Professor Michel Sanner, Professor David Goodsell, and Professor Arthur Olson, for the wonderful experience at The Scripps Research Institute. It was an honour to meet all of you! Being more than 10000 km away from home, during a pandemic, was certainly not easy, but your support changed what could have been an horrible period to a fantastic and unforgettable one. I miss all those weekly lab meeting on Zoom a lot!

My thanks also goes to Dr. Marco Biagi, who introduced me to the world of scientific research and played a key role in my decision to keep doing research after my master thesis internship, also leading me to choose the topic of my PhD project.

I cannot forget to thank Professor Daniela Giachetti, who has always been a source of inspiration, since the first day of my master thesis internship, transferring to me her deep love for natural products and medicinal plants.

During the course of my PhD, I have been lucky enough to collaborate and get to know so many extraordinary scientist. My thanks goes to Professor Gabriele Cruciani and his research group in Perugia, Professor Monica Montopoli and her research group in Padova, Professor Nicoletta Galeotti in Firenze, Professor Francesca Aiello and her research group in Cosenza, Professor Federica Pessina and Professor

ACKNOWLEDGEMENTS

Antonella Brizzi in Siena, and Professor Lorenzo Corsi in Modena. I also wish to thank Dr. Veronica Cocetta and Dr. Gabriele Carullo.

I also wish to thank the Italian Society of Phytotherapy (S.I.Fit.), SIFITLab and S.I.Fit. Giovani.

I feel that even if he was not directly involved in my PhD journey, Professor Luca De Vico played an immense role in inspiring me as a researcher, during my visit at the University of Copenhagen, and I wish to thank him.

It may seem weird, but three years of PhD are not only based on scientific collaborations and meetings. You cannot complete a PhD without the support of family, friends and people from outside the academic world. At least not without losing your mind!

Talking, chatting, joking and laughing with friends was of tremendous help to make me relieve stress during the short breaks between one experiment and another, or while I was overwhelmed by papers to read/write. My special thanks goes to Corradino&Sere, Ciampa&Sere, Boni&Gaia, Panno&Bene, Leo&Effie, and Grassi&tuaveviapresentarcelasevolevichescrivevoilsuonome. It is so frustrating that we have not been able to see each other since we left for San Diego, but I hope we will be together soon.

I wish to thank Mister Francesco Martire and all the guys in the CUS team for the time spent playing football, even during storms and cold nights.

Visiting San Diego was one of the most exciting and beautiful experiences I have ever had. Ok, there was a pandemic, the beaches have been closed most of the time and I did not have the chance to surf in the ocean. But I am not going to forget the amazing landscapes, the bioluminescent waves, the seals and sea lions, the dolphins, the deserts, the canyons, the giant sequoias, the mountains, the bears, the Grand Canyon, and all the incredible things that I get to see in California and nearby. Not even the marine layer, the “sandwich-stealing” seagulls or the Macaroni&cheese (who would have guessed?). It sounds weird to thank a city, but I really wish to thank San Diego for all these memories! And of course Patricia and Mary, they were so kind and cute, always worrying to find ways to fix our “pandemic-influenced” visit.

Family keeps you going. Nothing I have been able to achieve so far would have been possible without the immeasurable support of my wonderful family.

Mamma e Papà where would I be without your education, help, and sacrifices? For sure, I would not be the man I am today if it were not for you. I am thankful for the shine in your eyes every time you look at me. Thank you so much!

Alberto, Gianluca and Rosa, no one could understand what great brothers and sister you are. No matter what happens, I always know that I can rely on you and I

am extremely grateful for this. Thank you so much! I also wish to thank Giada, whose “several-years membership” in our family is going to be “legally” certified soon.

Andrea, Rosaria and Maria, thank you for being part of my family too. Not many people are lucky enough to find someone like you. You always believed in, encouraged and supported me while taking every single decision of my life. Thank you so much!

And of course I cannot forget to thank... Neve (better known as “Cane”) and Giotto. Neve, you were actually at my side while I was writing every single word of this thesis. And you still are now, while I am working from home (of course you are in love with me, not with the sofa next to my desk...). Giotto, you are exactly what I see when I think of a dog: excited, noisy, rowdy, frantic, and extremely cute. Thank you both!

This was a very long list and I am sure I forgot to mention someone. So I also wish to thank all the people that directly or indirectly participated to my PhD journey, but were not mentioned in this list.

With that said, there is still a person I feel I have to thank and to whom I wish to dedicate this thesis. You have been on my side for the whole PhD, both while I was working and while I was at home. You even followed me to San Diego! You helped me in taking hard decisions, always understanding and supporting me, with unconditional love. You shared with me the good and bad of this PhD. You became part of my life from the very first moment we met each other and I would not be the same without you. *Vittoria sei la mia vita e questo risultato è per te!*

Paolo

APPENDIX I

List of publications

1. **Governa P.**, Caroleo M.C., Carullo G., Aiello F., Cione E., Manetti F. “FFAR1/GPR40: one target, different binding sites, many agonists, no drugs, but a continuous and unprofitable tug-of-war between ligand lipophilicity, activity, and toxicity”. *Bioorganic & Medicinal Chemistry Letters* (2021), *submitted*.
2. Borgonetti V., **Governa P.**, Manetti F., Miraldi E., Biagi M., Galeotti N. “A honokiol-enriched *Magnolia officinalis* Rehder & E.H. Wilson. bark extract possesses anxiolytic-like activity with neuroprotective effect through the modulation of CB1 receptor”. *Journal of Pharmacy and Pharmacology* (2021), *submitted*.
3. **Governa P.**, Manetti F., Miraldi E., Biagi M. “Effect of *in vitro* simulated digestion on the antioxidant activity of different *Camellia sinensis* (L.) Kuntze leaves extracts”. *Food & Function* (2021), *submitted*.
4. Mazzotta S.°, **Governa P.**°, Borgonetti V., Marcolongo P., Nanni C., Gamberucci A., Manetti F., Pessina F., Carullo G., Brizzi A., Aiello F. “Pinocembrin and its Linolenoyl Ester Derivative induce Wound Healing Activity in HaCaT cell line potentially involving a GPR120/FFAR4 mediated pathway”. *Bioorganic Chemistry* (2021): 104657. Ahead of print. DOI: 10.1016/j.bioorg.2021.104657.
5. Borgonetti V., **Governa P.**, Biagi M., Pellati F., Galeotti N. “*Zingiber officinale* Roscoe rhizome extract alleviates neuropathic pain by inhibiting neuroinflammation in mice”. *Phytomedicine* (2020), 78: 153307.
6. Borgonetti V.°, **Governa P.**°, Biagi M., Galeotti N. “Novel Therapeutic Approach for the Management of Mood Disorders: *In Vivo* and *In Vitro* Effect of a Combination of L-Theanine, *Melissa officinalis* L. and *Magnolia officinalis* Rehder & E.H. Wilson”. *Nutrients* (2020), 12(6): 1803.
7. Borgonetti V., Cocetta V., Biagi M., Carnevali I., **Governa P.***, Montopoli M. “Anti-inflammatory activity of a fixed combination of probiotics and herbal extract in an *in vitro* model of intestinal inflammation by stimulating Caco-2 cells with LPS- conditioned THP-1 cells medium”. *Minerva Pediatrica* (2020), Ahead of print, DOI: 10.23736/S0026-4946.20.05765-5.
8. Carullo G., Sciubba F., **Governa P.**, Mazzotta S., Frattaruolo L., Grillo G., Cappello A.R., Cravotto G., Di Cocco M.E., Aiello F. “Mantonico and Pecorello Grape Seed Extracts: Chemical Characterization and Evaluation of *In Vitro*

- Wound-Healing and Anti-Inflammatory Activities”. *Pharmaceuticals* (2020), 13(5): 97.
9. Borgonetti V.°, **Governa P.**°, Biagi M., Dalia P., Corsi L. “*Rhodiola rosea* L. modulates inflammatory processes in a CRH-activated bv2 cell model”. *Phytomedicine* (2020), 68: 153143.
 10. Carullo G.°, **Governa P.**°, Spizzirri U.G., Biagi M., Sciubba F., Giorgi G., Loizzo M., Di Cocco M.E., Aiello F., Restuccia D. “Sangiovese cv pomace seeds extract-fortified kefir exerts anti-inflammatory activity in an *in vitro* model of intestinal epithelium using caco-2 cells”. *Antioxidants* (2020), 9(1): 54.
 11. **Governa P.**, Biagi M. “*Copaifera langsdorffii* Desf.: *in vitro* investigation on anti-*Helicobacter pylori* and anti-inflammatory activities of oleoresin and fruit methanolic extract”. *Plant Biosystems* (2020), 154(1): 117-124.
 12. **Governa P.**, Cusi M.G., Borgonetti V., Sforcin J.M., Terrosi C., Bains G., Miraldi E., Biagi M. “Beyond the Biological Effect of a Chemically Characterized Poplar Propolis: Antibacterial and Antiviral Activity and Comparison with Flurbiprofen in Cytokines Release by LPS-Stimulated Human Mononuclear Cells”. *Biomedicines* (2019), 7(4): 73.
 13. Petricci E., **Governa P.**, Manetti F. “Chemical Hybridization Approaches Applied to Natural and Synthetic Compounds for the Discovery of Drugs Active Against Neglected Tropical Diseases”, in “Medicinal Chemistry of Neglected and Tropical Diseases: Advances in the Design and Synthesis of Antimicrobial Agents” Publisher: CRC Press (2019).
 14. Carullo G.°, **Governa P.**°, Leo A., Gallelli L., Citraro R., Cione E., Caroleo M.C., Biagi M., Aiello F., Manetti F. “Quercetin-3-Oleate Contributes to Skin Wound Healing Targeting FFA1/GPR40”. *ChemistrySelect* (2019), 4(29): 8429-8433.
 15. Borgonetti V., **Governa P.***, Montopoli M., Biagi M. “Cannabis sativa L. constituents and their role in neuroinflammation”. *Current Bioactive Compounds* , 15(2)147-158.
 16. **Governa P.**°, Carullo G.°, Biagi M., Rago V., Aiello F. 2019. “Evaluation of the *In Vitro* Wound-Healing Activity of Calabrian Honeys”. *Antioxidants* (2019), 8:36.
 17. Cocetta V., Catanzaro D., Borgonetti V., Ragazzi E., Giron M.C., **Governa P.**, Carnevali I., Biagi M., Montopoli M. “A Fixed Combination of Probiotics and Herbal Extracts Attenuates Intestinal Barrier Dysfunction from Inflammatory Stress in an *In vitro* Model Using Caco-2 Cells”. *Recent Patents on Food, Nutrition & Agriculture* (2019), 10(1): 62-69.

18. Chiocchio I., Poli F., **Governa P.***, Biagi M., Lianza M. 2018. "Wound healing and *in vitro* antiradical activity of five Sedum species grown within two sites of community importance in Emilia-Romagna (Italy)". *Plant Biosystems* (2019), 153(4): 610-615.
19. **Governa P.***, Marchi M., Cocetta V., De Leo B., Saunders P.T.K., Catanzaro D., Miraldi E., Montopoli M., Biagi M. "Effects of *Boswellia Serrata* Roxb. and *Curcuma longa* L. in an *In Vitro* Intestinal Inflammation Model Using Immune Cells and Caco-2". *Pharmaceuticals* (2018), 11(4): 126.
20. **Governa P.***, Baini G., Borgonetti V., Cettolin G., Giachetti D., Magnano AR., Miraldi E., Biagi M. "Phytotherapy in the Management of Diabetes: a Review". *Molecules* (2018), 23(1): 105.
21. Tsiuotsiou EE., Miraldi E., **Governa P.**, Biagi M., Giordani P., Cornara L. "Skin Wound Healing: From Mediterranean Ethnobotany to Evidence based Phytotherapy". *Athens Journal of Sciences* (2017), September 2017.
22. **Governa P.***, Giachetti D., Biagi M., Manetti F., De Vico L. 2016. "Hypothesis on *Serenoa repens* (Bartram) Small extract inhibition of prostatic 5 α -reductase through an *in silico* approach on 5 β -reductase x-ray structure". *PeerJ* (2016), 4: e2698.
23. Biagi M., Pecorari R., Appendino G., Miraldi E., Magnano AR., **Governa P.**, Cettolin G., Giachetti D. "Herbal Products in Italy: The Thin Line between Phytotherapy, Nutrition and Parapharmaceuticals; A Normative Overview of the Fastest Growing Market in Europe". *Pharmaceuticals* (2016), 9(4): 65.
24. Tsioutsiou EE., Giachetti D., Miraldi E., **Governa P.**, Magnano AR., Biagi M. "Phytotherapy and skin wound healing". *Acta Vulnologica* (2016), 14(3): 126-139.
25. **Governa P.**, Miraldi E., De Fina G., Biagi M. "Effectiveness of 5-pyrrolidone-2-carboxylic acid and copper sulfate pentahydrate association against drug resistant *Staphylococcus* strains". *Natural Product Communications* (2016), 11(4): 453-455.

°Co-first authors; *Corresponding author

APPENDIX II

Conferences participation

1. **Governa P.**, Biagi M., Manetti F., Forli S. “Structure-based identification of P-glycoprotein inhibitors from natural sources” EFMC-ISMC & EFMC-YMCS Virtual Poster Session. 9 September 2020.
2. **Governa P.**, Biagi M., Manetti F., Forli S. “Structure-based identification of P-glycoprotein inhibitors from natural sources”. Italian Young Medicinal Chemistry Virtual Meeting. 22-24 June 2020.
3. **Governa P.**, Biagi M., Manetti F. “*In vitro* gastrointestinal bioaccessibility as a model for exploring the pharmacokinetics properties of natural products”. I Bio.Natural Meeting 2019. Lisbona 27-28 September 2019.
4. Rigillo G., Borgonetti V., Benatti C., **Governa P.**, Tascetta F., Biagi M. “Cannabidiol-enriched *Cannabis sativa* L. extract modulates inflammatory-induced human peripheral mononuclear cells response”. 67° International Congress and Annual Meeting of the Society of Medicinal Plant and Natural Product Research. Innsbruck, 1-5 September 2019.
5. **Governa P.**, Manetti F., Miraldi E., Biagi M. “Stability and bioaccessibility of *Cannabis sativa* L. extracts under *in vitro* simulated gastrointestinal digestion”. XVI Congress of the Italian Society of phytochemistry jointly with 2nd International Congress on Edible, Medicinal and Aromatic Plants. Alghero, 19-21 June 2019.
6. **Governa P.**, Borgonetti V., Manetti F., Biagi M. “*In Vitro* Neuroprotective Effect of a CBD-enriched Non-psychotropic *Cannabis sativa* L. Extract”. 1st International Conference on Neuroprotection by Drugs, Nutraceuticals and Physical Activity. Rimini, 6-7 June 2019.
7. Borgonetti V., **Governa P.**, Biagi M., Galeotti N. “A Standardized Extract of *Zingiber officinale* Roscoe is More Effective Than its Main Constituents in Reducing Neurotoxicity *In Vitro* and Shows Anti-Nociceptive Activity in a Mice Model of Neuropathic Pain”. 1st International Conference on Neuroprotection by Drugs, Nutraceuticals and Physical Activity. Rimini, 6-7 June 2019.

8. Borgonetti V., **Governa P.**, Biagi M., Galeotti N. “Neuroprotective effects of a standardized extract of *Zingiber officinale* Roscoe in an *in vitro* model of neurotoxicity”. XXVII Congresso Nazionale di Fitoterapia jointly with IX SYRP: S.I.Fit. Young Researchers Project. Reggio Emilia, 24-26 May 2019.
9. **Governa P.**, Biagi M., Manetti F. “Evaluation of the pharmacokinetic properties of natural products: focus on bioaccessibility”. VIII SYRP: S.I.Fit. Young Researchers Project - Experimental models for the study of natural products. Imola, 14 January 2019.
10. Carullo G.[°], **Governa P.**[°], Biagi M., Manetti F., Aiello F. “Lipo-pinocembrin derivatives as new tools in wound healing drug development”. VIII SYRP: S.I.Fit. Young Researchers Project - Experimental models for the study of natural products. Imola, 14 January 2019.
11. Rigillo G., Borgonetti V., Benatti C., **Governa P.**, Tascetta F., Biagi M. “Effect of non-psychotropic *Cannabis sativa* L. extract on LPS-induced microglial response”. VIII SYRP: S.I.Fit. Young Researchers Project - Experimental models for the study of natural products. Imola, 14 January 2019.

[°]Co-first authors; *Corresponding author